UNIVERSITÀ DEGLI STUDI DI PADOVA

UNIVERSITA' DEGLI STUDI DI PADOVA

Dipertimento di Ingengeria Industriale DII

Corso di laurea in Ingegneria dell'Energia Elettrica

P.E.E.C. modelling of large-scale fusion reactor magnets

Riccardo Torchio

Matricola 1090348

Relatore:
Prof. Paolo Bettini
Correlatore:
Prof. Piergiorgio Alotto

Anno Accademico 2015/2016

Abstract e Sommario

Sommario

Il metodo *Partial Element Equivalent Circuit* (P.E.E.C.) utilizza il Metodo dei Momenti (*Method of Moments*, M.o.M.) interpretandolo come circuito elettrico equivalente.
Questa interpretazione permette lo studio e la modellizzazione di una vasta gamma di dispositivi elettromagnetici (come gli induttori per macchine a fusione) e permette di considerare nello stesso sistema elementi a parametri concentarti e elementi a "coefficienti parziali" (che discretizzano le strutture sotto analisi).
Scopo del progetto è sviluppare due codici numerici (uno "per filamenti" e uno "volumico") in grado di analizzare il comportamento di dispositivi elettromagnetici nel dominio del tempo e della frequenza.
Inizialmente è stato elaborato un procedimento generale ed efficiente per il calcolo dei coefficienti determinanti i legami elettromagnetici tra gli elementi che discretizzano l'oggetto studiato.
I codici implementati sono stati utilizzati per l'analisi di antenne e i risultati ottenuti sono stati confrontati con un metodo agli elementi finiti (F.E.M.), per dimostrare e testare la loro capacità di analizzare dispositivi che lavorano ad alta frequenza.
I codici sono stati poi applicati allo studio in frequenza del comportamento elettromagnetico delle Bobine di Campo Magnetico Toroidale per il reattore JT-60SA.
Tali strumenti così elaborati possono essere facilmente "accoppiati" ad un software CAD per la generazione della mesh. Scopo ultimo del lavoro è stato quello di aumentare l'efficienza e le performance da un punto di vista di costo computazionale.

Abstract

My thesis deals with the modelling and analysis of large scale electromagnetic devices, such as fusion reactor magnets, using a numerical code based on the *Partial Element Equivalent Circuit* (P.E.E.C.) method, which derives from *Method of Moment* (M.o.M.) and is an interpretation of M.o.M. as an electrical equivalent circuit.
The purpose of the project was to develop two numerical codes (a "filamentary" code and a "volume" code) able to analyse many types of electromagnetic devices, in the time and frequency domain.
During the first phase of the work my aim was to investigate about a general and efficient method for the evaluation of the coefficients, concerning the electromagnetic couplings between the elements of the mesh, in order to use non-orthogonal cells that allow to discretize complex electromagnetic objects in a more accurate way.
After the implementation, my goal was to use the codes for the analysis of antennas and to make a comparison with F.E.M. method, in order to test the capability of the codes to analyse devices which work at high frequency.
Secondly, the codes have been used for the analysis of the Toroidal field coils of the fusion reactor JT-60SA that, because of their complexity, lend themselves to be a subject for study and analysis in the time and frequency domain. The codes have been developed with the aim to be easily joined to a CAD software for the generation of the mesh, in order to facilitate their use.
In a second phase, my goal was to make the codes more efficient and performing from computational cost point of view.

Sommario Esteso

Obiettivi del Progetto di Tesi

Scopo della tesi è di implementare un codice numerico basato sul metodo *Partial Element Equivalent Circuit* (PEEC) per analizzare e studiare una grande varietà di dispositivi elettromagnetici, in particolare gli induttori utilizzati per la produzione dei campi magnetici necessari al confinamento del plasma nelle macchine da fusione.
Il Metodo PEEC si basa su una interpretazione circuitale del Metodo dei Momenti (MoM) e fornisce una soluzione numerica delle equazioni di Maxwell scritte in formulazione integrale.
Durante il lavoro sono stati sviluppati due codici basati su tale metodo: uno "per filamenti" e uno "volumico". Il primo considera come elementi primari "sottili" conduttori cilindrici, attraversati da corrente distribuita uniformemente sulla sezione normale; il secondo invece utilizza, come elementi base, celle esaedriche a facce piane quadrilatere .
Nella prima fase di lavoro si sono studiati metodi generali ed efficienti per la valutazione dei coefficienti parziali che determinano i legami elettromagnetici tra i vari elementi che discretizzano gli oggetti analizzati.
Tale studio è stato fatto con l'intento di elaborare un metodo che permetta di studiare dispositivi elettromagnetici di struttura complessa, utilizzando celle non-ortogonali che offrono una maggiore libertà durante la fase di discretizzazione.
Dopo l'implementazione, il codice "per filamenti" è stato utilizzato per l'analisi di antenne e i risultati sono stati confrontati con quelli ottenuti da un metodo agli elementi finiti (FEM) e un approccio analitico. Ciò è stato fatto al fine di testare la capacità del codice di studiare e simulare il funzionamento di dispositivi che lavorano ad alta frequenza, prerogativa del metodo PEEC.
Successivamente, entrambi i codici sono stati utilizzati per l'analisi nel dominio del tempo e della frequenza degli induttori di Campo Magnetico Toroidale del reattore JT-60SA.
Tale dispositivo, pur lavorando in DC, si presta ad analisi in frequenza e time-domain. In effetti risulta interessante studiare come il potenziale elettrico si distribuisce lungo i conduttori della bobina durante la scarica rapida della stessa nei circuiti di protezione (scarica necessaria per proteggere la macchina durante fenomeni di instabilità del plasma o altre problematiche).
Si teme infatti che l'onda di tensione, provocata dalla scarica rapida della bobina, possa indurre distribuzioni di tensione potenzialmente pericolose per l'isolante interposto tra le spire della bobina.
I codici sono stati sviluppati con l'intento di essere facilmente "accoppiati" ad un software "CAD" per la generazione della mesh, al fine di facilitarne l'utilizzo.
Scopo ultimo del lavoro è stato quello di aumentare l'efficienza di tali strumenti, diminuendo il tempo richiesto dalle simulazioni e il costo computazionale.

Attività Svolta

L'attività di lavoro svolta durante la tesi può essere riassunta in queste fasi:

- *Ricerca Bibliografica*: Mediante la consultazione di libri e articoli in letteratura è stata studiata ed approfondita la teoria relativa al metodo PEEC. Ciò è stato fatto per conoscere i diversi possibili approcci al metodo e per ottenere una visione globale dell'argomento.
- *Implementazione e Validazione del codice "per filamenti"*: $\mathbf{PEEC}_F$. Durante questa seconda fase è stato implementato in MATLAB il codice per filamenti che, data la più semplice natura degli elementi primari considerati, si è ritenuto essere di più facile elaborazione rispetto a quello "volumico". Tutte le varie parti del codice riguardanti la valutazione dei coefficienti parziali sono state validate passo per passo, confrontando i valori dei coefficienti ottenuti dal codice con quelli forniti da formule analitiche riportate in letteratura.
  Tali formule permettono di calcolare i coefficienti parziali tra elementi che stanno in qualche particolare posizione mutua (elementi allineati, paralleli, complanari ecc.) e che quindi non possono essere utilizzate per un metodo generale.
  Il metodo numerico implementato nel codice invece permette di calcolare tali coefficienti mutui tra

qualsiasi coppia di elementi posti in qualsiasi posizione nello spazio.
Le validazioni hanno dimostrato la correttezza del metodo utilizzato e successivamente, come ulteriore test, il codice è stato utilizzato per il calcolo dell'auto induttanza di semplici geometrie, per le quali esistono formule analitiche utili per il confronto.
Per quanto riguarda la validazione del metodo implementato per il calcolo dei coefficienti di potenziale (che descrivono gli accoppianti elettrici tra gli elementi) si sono confrontati i risultati in termini di "Matrici di Capacità di Maxwell", ottenuti come post-processing dal codice PEEC, con quelli ottenuti dal codice Open-Source *FarsterCap*.
Successivamente il codice è stato utilizzato per l'analisi nel dominio del tempo e della frequenza di semplici dispositivi elettromagnetici, quali linea bifilare, piastre e spire a sezione circolare.

- *Applicazione del Codice a Strutture Complesse*. Dopo l'implementazione e validazione, il codice "per filamenti" è stato utilizzato per l'analisi di due tipi di disposizioni di antenne. Grazie a questi studi sono stati messi in evidenza i punti di forza e di debolezza del codice ed è stata testata la capacità dello stesso di analizzare dispositivi funzionanti ad alta frequenza. I risultati sono stati confrontati con un metodo analitico e con un FEM; tale studio è stato raccolto in due contributi, [52] , [53].

- *Implementazione e Validazione del Codice "Volumico"*: $\mathbf{PEEC}_V$. In questa fase ci si è occupati dell'implementazione del codice PEEC avente come elementi primari celle esaedriche. Come per il codice "per filamenti", durante la fase di implementazione tutti i metodi numerici utilizzati per la valutazione dei coefficienti parziali sono stati validati attraverso confronti con formule analitiche presenti in letteratura (che permettono il calcolo dei coefficienti tra elementi che stanno in qualche particolare posizione mutua). Come ulteriore validazione sono stati confrontati i valori di auto induttanza e i coefficienti di capacità di qualche struttura a geometria semplice, che presentano formule analitiche utili per il confronto.
Anche per questo codice è stato fatto qualche confronto con il software Open-Source *FasterCap* (estrattore di coefficienti di induttanza e capacità).
Infine, anche in questo caso, il codice è stato impiegato per l'analisi di semplici dispositivi elettromagnetici, quali linee bifilari, piastre, spire circolari ecc. ; per le quali è possibile conoscere a priori il comportamento elettromagnetico e quindi verificare i risultati ottenuti dal codice.

- *Applicazione dei Codici agli Induttori di Campo Magnetico Toroidale del Reattore JT-60SA*. I codici sono stati utilizzati per l'analisi nel dominio del tempo e della frequenza delle bobine di campo magnetico toroidale del reattore JT-60SA.
Sono stati prodotti due modelli della macchina: uno "per filamenti" e uno "volumico", in modo da poter utilizzare entrambi i codici sviluppati e permettere così dei confronti.
Sono stati estratti i valori di auto e mutua induttanza delle spire e in particolare è stata valutata l'impedenza equivalente vista dall'alimentazione al variare della frequenza.
Tali risultati sono in parte stati confrontati con quelli ottenuti da un team di ricerca che lavora in Germania per "Fusion for Energy".
Ciò è stato solo in parte attuabile in quanto, nel modello PEEC, non è stato possibile considerare la presenza del materiale dielettrico interposto tra le spire della bobina di Campo Magnetico Toroidale di JT-60SA.
Nell'ultima parte del lavoro si è ragionato su come estendere il metodo PEEC e il modello utilizzato al fine di considerare anche la presenza del materiale dielettrico.
Al momento si è riusciti ad inserire nel codice le "celle dielettriche" (che permettono la discretizzazione del materiale dielettrico) e si sta considerando come modificare il modello delle bobine di JT-60SA valutandone l'effettiva complessità, senza però incrementare troppo il costo computazionale richiesto dal codice nel calcolo dei coefficienti e nell'inversione del sistema.
Alcune delle analisi fatte su tale dispositivo sono raccolte in due contributi, [50], [51].

- *Ottimizzazione*: Dopo le varie fasi di implementazione si è cercato di rendere più efficienti e performanti i due codici. In particolare il codice "volumico" è stato in parte riscritto in FORTRAN e parallelizzato. Ciò ha permesso di ottenere uno speed-up di un fattore 10000.

Contents

Chapter 1

P.E.E.C. THEORY AND FORMULATION

1.1 Introduction

The rapid growth of electrical modelling and analysis of electromagnetic and electronic systems is due to the increasing importance to have instruments which allow to foresee the behaviour of these devices in normal or particular working conditions. The electromagnetic nature with the geometric complexity of these objects call for efficient electromagnetic methodologies and computer-aided design tools, which allow a full-wave analysis of 3D structures characterized by inhomogeneous materials and complex geometries.
The three most popular computational methods which are usually adopted in computational electromagnetic are the finite element method (F.E.M.), the finite difference time domain (F.D.T.D.) technique, and the method of moments (M.o.M.). It is known that the first two approaches are essentially based on the partial differential equation from of Maxwell's equations and result into powerful techniques that have been widely used for a variety of Electromagnetic problems.
The Method of Moments is based on an integral formulation of Maxwell's equations. Among all the different integral equation based techniques this thesis focuses on the *Partial Element Equivalent Circuit* method. Stemming from the pioneering works by Ruehli, [1], [2], [3].
The main difference of P.E.E.C. method with other integral equation based techniques resides in the fact that it provides a circuit interpretation of the electric field integral equation, (1.24), in terms of partial elements, namely resistances, partial inductances and coefficients of potential. Thus, the resulting equivalent circuit can be studied by the Tableau analysis method or by means of Spice-like circuit solvers in both time and frequency domain. Furthermore, once the P.E.E.C. model for an electromagnetic system has been developed, a systematic procedure can be used to reduce its complexity, taking into account the electrical size of the structure under analysis. For example, if the characteristic time of the excitation is such that useful wavelengths are much larger than the spatial extent of the system, all retardation effects can be neglected.
Integral equation methods are very effective for electromagnetic modelling, interference and compatibility purpose. The first step of any integral equation-based method is the development of an integral formulation of Maxwell's equation. The most popular integral equation is the electric field integral equation (E.F.I.E.) which is obtained by enforcing the electric field at a point in the structure as the superposition of fields due to all electric currents and charges in the system.
Compared with differential equation based methods, the matrices resulting from Integral equation based techniques solutions are smaller in size and dense. The reason for the reduced size is that the unknowns are represented by electric currents flowing through the volumes of conductors dielectrics and charges on their surfaces; the reason for the density of matrices arising from Integral Equation solutions is that each element describes the electromagnetic interaction (electric and magnetic) between the discrete currents or charges in the structures.

1.2 Introduction to PEEC

The behaviour of an electric system can be often simulated using only the basic circuit theory (*lumped element model*). This way of proceeding is suitable only when the electric system under analysis is small compared to the wavelength of the frequency involved in the analysis. We can say that when the bigger geometric dimension is smaller than a tenth of the wavelength ($L \ll \frac{\lambda}{10}$).

When this condition doesn't subsist the study of the circuit with *lumped element model* it is no longer enough and we have to start to consider the system's analysis also from an electromagnetic point of view. Objects behave like antennas radiating or receiving electromagnetic energy, so we have to include in our analysis also the *Maxwell's Equation* in order to consider the effects of radiation and the electric and magnetic coupling.

Maxwell's equations

Differential form	Integral form
$\nabla \times \vec{H} = \vec{J} + \frac{\partial \vec{D}}{\partial t}$	$\oint_L \vec{H} \cdot d\vec{l} = \int_S (\vec{J} + \frac{\partial \vec{D}}{\partial y}) \cdot d\vec{S}$
$\nabla \times \vec{E} = -\frac{\partial \vec{B}}{\partial t}$	$\oint_L \vec{E} \cdot d\vec{l} = -\int_S \frac{\partial \vec{B}}{\partial t} \cdot d\vec{S}$
$\nabla \cdot \vec{D} = \rho_v$	$\oint_S \vec{D} \cdot d\vec{S} = \int_v \rho_v dv$
$\nabla \cdot \vec{B} = 0$	$\oint_S \vec{B} \cdot d\vec{S} = 0$

The terms in the *Maxwell's equations* are:

- $\vec{E}$ - Electric field intensity, $[\frac{V}{m}]$;
- $\vec{D}$ - Electric flux density, $[\frac{C}{m^2}]$;
- ρ_v - Volume charge density, $[\frac{C}{m^3}]$;
- ε - Capacitivity of the medium, $[\frac{F}{m}]$;
- $\vec{H}$ - Magnetic field intensity, $[\frac{A}{m}]$;
- $\vec{B}$ - Magnetic flux density, $[\frac{W}{m^2}]$;
- $\vec{J}$ - Electric current density, $[\frac{A}{m^2}]$;
- μ - Inductivity of the medium, $[\frac{H}{m}]$.

In addiction to the *Maxwell's equations* there are the three constitutive laws express in (1.1).

$$\begin{aligned} \vec{D} &= \varepsilon \vec{E} \\ \vec{B} &= \mu \vec{H} \\ \vec{J} &= \sigma \vec{E} \end{aligned} \tag{1.1}$$

An analytical approach can not often be used for effective interest problems; fortunately, electromagnetic problems can be solved using numerical techniques, the most popular methods are:

- Finite difference methods (FDM);
- Finite elements methods (FEM);
- The method of moments (MoM);
- The partial element equivalent circuit (PEEC).

These four methods are different in the basic mathematical approach so it is convenient to choose one of them according to the class of problem that we want to solve.

PEEC method is suitable to solve problems such as:

- Electrical interconnect packaging analysis;
- Printed circuit board simulations (mixed circuit and electromagnetic problem);
- Coupling mechanism characterization.

These problems require different kinds of analysis in terms of:

- Requested solution domain (time and/or frequency);
- Requested solution variables:
  - Circuit variables (currents and/ or voltages);
  - Field variables (electric and/or magnetic fields).

The numerical techniques used for the electromagnetic simulation can be also classified depending on which formulations of Maxwell's equations are considered. Using one of the two formulation produces a different approach in terms of *discretization of the structure* and *solution variables*.

By choosing the *differential formulation* we have to discretize the complete structure including the air, by doing this the method delivers the solution in field variables.
Indeed, this kind of formulation is suitable to analyse scattering problems that involve antennas or electromagnetic fields excited structures.
Instead, by choosing *integral formulation* only the materials need to be discretized and the method delivers the solution in terms of circuit variables.
For both two formulations, to obtain the solution in terms of electromagnetic fields (*for the integral formulation*) and in terms of circuit variables (*for the differential formulation*) post-processing is needed.

PEEC method is characterized by using the *integral formulation* of Maxwell's laws. The solutions delivered by the method are *circuit variables* and the solution domain can be in *time or frequency*. The main feature with PEEC method is the combined circuit and electromagnetic solution, that is performed with the *same equivalent circuit* in both time and frequency domain.

1.3 Moment Method

In this section we want shortly discuss about the main mathematical concepts concerning the Moment Method (or Method of Moments, M.o.M.), [43].
Given a deterministic problem of $\mathcal{L}(f) = g$, we must identify the operator $\mathcal{L}$, its domain (the functions f on which it operates), and its range (the functions g resulting from the operation). Furthermore, we usually need an inner product $\langle f, g \rangle$, which is a scalar defined to satisfy:

$$\begin{aligned} \langle f, g \rangle &= \langle g, f \rangle \\ \langle \alpha f + \beta g, h \rangle &= \alpha \langle f, h \rangle + \beta \langle g, h \rangle \\ \langle f^*, f \rangle &> 0 \quad \text{if } f \neq 0 \\ \langle f^*, f \rangle &= 0 \quad \text{if } f = 0 \end{aligned} \tag{1.2}$$

where α and β are scalars and "$*$" denotes the complex conjugate. We sometimes need the *adjoint operator* $\mathcal{L}^a$ and its domain, defined by: $\langle \mathcal{L}f, g \rangle = \langle f, \mathcal{L}^a g \rangle$ for all f in the domain of $\mathcal{L}$. An operator is *self-adjoint* if $\mathcal{L}^a = \mathcal{L}$ and the domain of $\mathcal{L}^a$ is that of $\mathcal{L}$. Properties of the solution depended upon properties of the operator. An operator is *real* if $\mathcal{L}f$ is *real* whenever f is *real*.

An operator is *positive define* if $\langle f^*, \mathcal{L}f \rangle > 0$ for all $f \neq 0$ in its domain. It is *positive semidefinite* if $>$ is replaced by $\geq$, it is *negative definite* if $>$ is replaced by $<$.
If the solution to $\mathcal{L}(f) = g$ exists and is unique for all g, then the *inverse operator* $\mathcal{L}^{-1}$ exists such that:

$$f = \mathcal{L}^{-1}(g) \tag{1.3}$$

If g is known, then (1.3) represents the solution to the original problem. However, (1.3) is an inhomogeneous equation for g if f is known, and its solution is $\mathcal{L}(f) = g$. Hence $\mathcal{L}$ and $\mathcal{L}^{-1}$ form a pair of operators, each of which is the inverse of the other.

We now discuss a general procedure for solving linear equations, called *Method of Moments*.
Consider the inhomogeneous equation:

$$\mathcal{L}(f) = (g) \tag{1.4}$$

where $\mathcal{L}$ is a linear operator, g is known, and f is to be determined. Let f be expanded in a series of functions $f_1, f_2, f_3, ...$ in the domain of $\mathcal{L}$ as:

$$f = \sum_n \alpha_n f_n \tag{1.5}$$

where the α_n are constants. We shall call the f_n *expansion functions* or *basis functions*. For exact solutions, (1.5) is usually an infinite summation and the f_n form a complete set of basis functions. For approximate solutions, (1.5) is usually a finite summation. Substituting (1.5) in (1.4), and using the linearity of $\mathcal{L}$, we have:

$$\sum_n \alpha_n \mathcal{L}(f_n) = g \tag{1.6}$$

It is assumed that a suitable inner product $\langle f, g \rangle$ has been determined for the problem. Now we define a set of *weighting functions*, or *testing functions*, $w_1, w_2, w_3, ...$ in the range of $\mathcal{L}$, and take the inner product of (1.6) with each w_m. The result is:

$$\sum_n \alpha_n \langle w_m, \mathcal{L}f_n \rangle = \langle w_m, g \rangle \tag{1.7}$$

for $m = 1, 2, 3, ...$. This set of equations can be written in matrix form as:

$$[l_{mn}][\alpha_n] = [g_m] \tag{1.8}$$

where

$$[l_{mn}] = \begin{bmatrix} \langle w_1, \mathcal{L}f_1 \rangle & \langle w_1, \mathcal{L}f_2 \rangle & ... \\ \langle w_2, \mathcal{L}f_1 \rangle & \langle w_2, \mathcal{L}f_2 \rangle & ... \\ ... & ... & ... \end{bmatrix} \tag{1.9}$$

and

$$[\alpha_n] = \begin{bmatrix} \alpha_1 \\ \alpha_2 \\ ... \end{bmatrix} \qquad [g_n] = \begin{bmatrix} \langle w_1, g \rangle \\ \langle w_2, g \rangle \\ ... \end{bmatrix} \tag{1.10}$$

If matrix $[l]$ is non-singular its inverse $[l^{-1}]$ exists. The α_n are then given by:

$$[\alpha_n] = [l^{-1}_{mn}][g_m] \tag{1.11}$$

and the solution for f is given by (1.5).

This solution may be exact or approximate, depending upon the choice of the f_n and w_n. The particular choice $w_n = f_n$ is known as *Galerkin's method*. If the matrix $[l]$ is of infinite order, it can be inverted only in special cases, for example if it is diagonal. The classical eigenfunction method leads to a diagonal matrix, and can be though of as a special case of the method of moments. If the sets f_n and w_n are finite, the matrix is of finite order, and can be inverted by known methods.
One of the main tasks in any particular problem is the choice of the f_n and w_n. The f_n should be linearly independent and chosen so that some superposition (1.5) can approximate f reasonably well. The w_n should also be linearly independent and chosen so that the products $\langle w_n, g\rangle$ depend on relatively independent properties of g. Some additional factors which effect the choice of f_n and w_n are :

- the accuracy of solution desired,
- the ease of evaluation of the matrix elements,
- the size of the matrix that can be inverted,
- the realization of a well-conditioned matrix $[l]$.

P.E.E.C. method uses M.o.M method to solve approximately the EFIE equation, (1.24) and the basis functions f_n are "rectangular" functions. The derivation of P.E.E.C. formulation is discussed in the next section.

1.4 PEEC Formulations

In this section we want to report shortly the theoretical derivation of the PEEC method.
First we have to find a suitable integral equation which can be solved by means the Method of Moments. To do that we have to express the total electric field in terms of vector magnetic potential, $\vec{A}$, and the scalar electric potential, V, at generic point of observation $\vec{r}$ (1.12).

$$\vec{E}(\vec{r},\omega) = -j\omega\vec{A}(\vec{r},\omega) - \nabla V(\vec{r},\omega) \tag{1.12}$$

where $\vec{A}$, [14], is given by (1.13).

$$\vec{A}(\vec{r},\omega) = \mu \int_{v\prime} G(\vec{r},\vec{r\prime})\vec{J}(\vec{r\prime},\omega)dv\prime \tag{1.13}$$

where $\vec{J}$ is the volume current density at a source point $\vec{r\prime}$ and G is the free-space Green's function (1.14).

$$G(\vec{r},\vec{r\prime}) = \frac{e^{-j\beta|\vec{r}-\vec{r\prime}|}}{4\pi|\vec{r}-\vec{r\prime}|} \tag{1.14}$$

The scalar potential V, [14], is given by (1.15).

$$V(\vec{r},\omega) = \frac{1}{\varepsilon}\int_{v\prime} G(\vec{r},\vec{r\prime})q(\vec{r\prime},\omega)dv\prime \tag{1.15}$$

where $v\prime$ is the volume of the conductor and q is the charge density at the conductor.

Now, if we substitute (1.13) and (1.15) in (1.12) we obtain an expression for the electric field in the unknown variables $\vec{J}$ and q (1.16).

$$\vec{E}(\vec{r},\omega) = -j\omega\mu\int_{v\prime} G(\vec{r},\vec{r\prime})\vec{J}(\vec{r\prime},\omega)dv\prime - \frac{\nabla}{\varepsilon}\int_{v'} G(\vec{r},\vec{r\prime})q(\vec{r\prime}\omega)dv\prime \tag{1.16}$$

Finally equation (1.16) is solved by expanding each unknown, $\vec{J}$ and q, into a series of pulse basis functions with unknown amplitude. These pulse basis functions are also selected for the weighting functions resulting in a Galerkin method. This leads to apply a special discretization for the structures: an

inductive and a capacitive partition; so each part of (1.16) can be considered as circuit element in this sense:

- $\left[\vec{E}(\vec{r},\omega)\right]$ is concerning to the voltage drop over a conducting volume cell.
- $\left[-j\omega\mu\int_{v\prime} G(\vec{r},\vec{r\prime})\vec{J}(\vec{r\prime},\omega)dv\prime\right]$ is concerning to the inductive voltage drop over the volume cell. It can be interpreted as the summation of the voltage drops over the partial inductance between the nodes (*self partial inductance*) and the mutual partial inductance of the volume cells (*representing the magnetic filed coupling, the mutual partial inductance*).
- $\left[-\frac{\nabla}{\varepsilon}\int_{v'} G(\vec{r},\vec{r\prime})q(\vec{r\prime}\omega)dv\prime\right]$ is concerning to the difference between the potentials of two nodes of the current volume cell. This term can be also written using the partial capacitance of each node (*self partial capacitance*) and the mutual partial capacitance of the surface cells (*representing the electric field coupling*).

In figure (1.1) is represented a cell with all the *partial elements* previously discussed and also the partial resistance of the element.

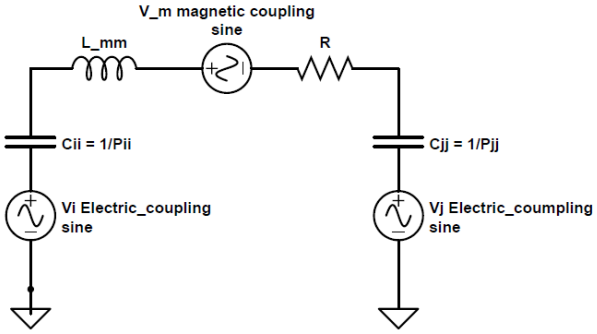

Figure 1.1: *PEEC model for a volum cell*

Now we can start the theoretical derivation with the expression of the *total electric field* in free space (1.17).

$$\vec{E_T}(\vec{r},t) = \vec{E_i}(\vec{r},t) - \frac{\partial\vec{A}(\vec{r},t)}{\partial t} - \nabla V(\vec{r},t) \tag{1.17}$$

where $\vec{E_i}$ is an applied external electric field (which can also be not present).

When the point $\vec{r}$ is on the surface of a conductor we can write the equation (1.18).

$$\vec{E_T}(\vec{r},t) = \frac{\vec{J}(\vec{r},t)}{\sigma} \tag{1.18}$$

where $\vec{J}$ is the current density in a conductor and σ is the conductivity of conductor.

Combining the last two equations we can write (1.19).

$$\vec{E_i} = \frac{\vec{J}(\vec{r},t)}{\sigma} + \frac{\partial\vec{A}(\vec{r},t)}{\partial t} + \nabla V(\vec{r},t) \tag{1.19}$$

Now we have to use the expression of the vector magnetic potential, $\vec{A}$, and electric scalar potential, V, shown in (1.20) and (1.23) respectively.

$$\vec{A}(\vec{r},t) = \sum_{k=1}^{N} \mu \int_{v_k} G(\vec{r},\vec{r\prime}) \vec{J}(\vec{r\prime},t_d) dv_k \tag{1.20}$$

where the summation is over N conductors and μ is the permeability of the medium, G is the *Green's function* define in (1.21), $\vec{J}$ is the current density at source point $\vec{r\prime}$, and t_d is the retardation time between the observation point $\vec{r}$ and the source point defined in (1.22).

$$G(\vec{r},\vec{r\prime}) = \frac{1}{4\pi} \frac{1}{|\vec{r} - \vec{r\prime}|} \tag{1.21}$$

$$t_d = t - \frac{|\vec{r} - \vec{r\prime}|}{c} \tag{1.22}$$

where c is equal to $3 \cdot 10^8 m/s$.

The electrical scalar potential at observation point $\vec{r}$ is shown in (1.23).

$$V(\vec{r},t) = \sum_{k=1}^{N} \frac{1}{\varepsilon_0} \int_{v_k} G(\vec{r},\vec{r\prime}) q(\vec{r\prime},t_d) dv_k \tag{1.23}$$

where ε_0 is the permittivity of free space, q is the charge density at the source point and the summation is over N conductors.

Now we can combine (1.19), (1.20) and (1.23) to obtain the *electric field integral equation* (EFIE), (1.24) .

$$\begin{aligned} \hat{n} \times \vec{E}_i(\vec{r},t) = \hat{n} \times & \Big[\frac{\vec{J}(\vec{r},t)}{\sigma} \Big] \\ & + \hat{n} \times \Big[\sum_{k=1}^{N} \mu \int_{v_k} G(\vec{r},\vec{r\prime}) \frac{\partial \vec{J}(\vec{r\prime},td)}{\partial t} dv_k \Big] \\ & + \hat{n} \times \Big[\sum_{k=1}^{N} \frac{\nabla}{\varepsilon_0} \int_{v_k} G(\vec{r},\vec{r\prime}) q(\vec{r\prime},t_d) dv_k \Big] \end{aligned} \tag{1.24}$$

where $\hat{n}$ is the surface normal to the body surfaces.

Finally, we have to transform the EFIE into a PEEC formulation and we start by expanding the current and the charge densities.

In the PEEC method the EFIE is discretized using a method of moments process, [43], interpreted as an equivalent circuit and solved using circuit theory. The solution obtained are the current in the material ($I = Ja$, where a is the cross sectional area normal to the current flow) and the node potential v in the materials.

With post-processing is possible to obtain the electromagnetic fields, so all the quantities in Maxwell's laws can be calculated. We can start to transform the EFIE equation into PEEC formulation by expanding the total current density $\vec{J}$ in $\vec{J}_c$ and $\vec{J}_p$, that are respectively the conduction current density and the polarization current density due to the dielectric material properties (1.25).

$$\begin{aligned} & \vec{J} = \vec{J}_c + \vec{J}_p \quad \textit{Where...} \\ & \vec{J}_c = \sigma \vec{E} \\ & \vec{J}_p = \varepsilon_0 (\epsilon_r - 1) \frac{\partial \vec{E}}{\partial t} \end{aligned} \tag{1.25}$$

For perfect conductors $\vec{J}$ is equal to the conducting component, while for perfect dielectrics the total current density coincides with the polarization term.

By using this expression for the total current density we can write the *Ampere-Maxwell law* in differential form, like in (1.26).

$$\nabla \times \vec{H} = \vec{J_c} + \varepsilon_0(\varepsilon_r - 1)\frac{\partial \vec{E}}{\partial t} + \varepsilon_0 \frac{\partial \vec{E}}{\partial t} \tag{1.26}$$

In this way we can study separately the displacement current (due to the bound charges for the dielectric materials that have $\varepsilon_r > 1$) from the conduction currents due to the free charges, [44].

By ending, we can rewrite the EIFE equation in a PEEC formulation (where q_T is the total charge due to q_F, the free charge, and q_B the bound charge) (1.27).

$$\begin{aligned}
\hat{n} \times \vec{E_i}(\vec{r}, t) = \hat{n} \times & \Big[\frac{\vec{J_c}(\vec{r}, t)}{\sigma}\Big] \\
& + \hat{n} \times \Big[\sum_{k=1}^{N} \mu \int_{v_k} G(\vec{r}, \vec{r\prime}) \frac{\partial \vec{J_c}(\vec{r\prime}, td)}{\partial t} dv_k\Big] \\
& + \hat{n} \times \Big[\sum_{k=1}^{N} \varepsilon_0(\varepsilon_r - 1)\mu \int_{v_k} G(\vec{r}, \vec{r\prime}) \frac{\partial^2 \vec{E}(\vec{r\prime}, td)}{\partial t^2} dv_k\Big] \\
& + \hat{n} \times \Big[\sum_{k=1}^{N} \frac{\nabla}{\varepsilon_0} \int_{v_k} G(\vec{r}, \vec{r\prime}) q_T(\vec{r\prime}, t_d) dv_k\Big]
\end{aligned} \tag{1.27}$$

Now we can analyse this general expression for conductors and dielectric materials first excluding the external applied field $\vec{E_i}$ and finally the more general case including it.

1.4.1 Conductors

For a perfect conductor, by don't taking into account the external field and the "dielectric term", the general expression (1.27) becomes (1.28).

$$\begin{aligned}
0 = \hat{n} \times & \Big[\frac{\vec{J_c}(\vec{r}, t)}{\sigma}\Big] \\
& + \hat{n} \times \Big[\sum_{k=1}^{N} \mu \int_{v_k} G(\vec{r}, \vec{r\prime}) \frac{\partial \vec{J_c}(\vec{r\prime}, td)}{\partial t} dv_k\Big] \\
& + \hat{n} \times \Big[\sum_{k=1}^{N} \frac{\nabla}{\varepsilon_0} \int_{v_k} G(\vec{r}, \vec{r\prime}) q_T(\vec{r\prime}, t_d) dv_k\Big]
\end{aligned} \tag{1.28}$$

In this system of equations we have two unknowns that are the $\vec{J_c}$ and q_F, so to solve it we can use the following procedure:

- The current densities are discretized into volume cells by defining rectangular pulse functions $P_{\lambda nk}$ that are equal to one inside the volume cell nk and zero elsewhere (where λ are the current components of the cell n in the k conductor).
- The charge densities are descretized into surface cells over the corresponding volume cell by defining rectangular pulse function p_{mk} that are equal to one inside the surface cell and zero elsewhere (where m is the charge density in the surface cell of the k conductor).

So, by using the pulse functions, it is possible to write the current and the charge densities as (1.29) and (1.30).

$$J_C^{\vec{\lambda}k}(\vec{r\prime}, t_d) = \sum_{n=1}^{N_\lambda k} P_{\lambda nk} J_{\lambda nk}(\vec{r}_{\lambda nk\prime}, t_{\lambda nk}) \tag{1.29}$$

$$q_T^k(\vec{r\prime}, t_d) = \sum_{m=1}^{M_k} p_{mk} q_{mk}(\vec{r\prime}_{mk\prime}, t_{mk}) \tag{1.30}$$

where

$$t_{\lambda nk} = t - \frac{|\vec{r} - r_{\vec{\lambda bk\prime}}|}{v}$$

$$t_{mk} = t - \frac{|\vec{r} - r_{\vec{mk\prime}}|}{v}$$

In the equations $\vec{r}_{\lambda nk\prime}$ and $\vec{r\prime}_{mk\prime}$ represent the source position vectors for volume and surface cells; the two summations are over all the volume cells and over all the surface cells in the conductor k respectively.

By using (1.29) and (1.30) in (1.28) we can obtain (1.31).

$$\begin{aligned} 0 = \hat{n} \times & \left[\frac{\vec{J}_c(\vec{r}, t)}{\sigma}\right] \\ & + \hat{n} \times \left[\sum_{k=1}^{K}\sum_{n=1}^{N_{\lambda k}} \mu \int_{v\prime}\int_{v_{\lambda nk}} G(\vec{r}, r_{\vec{\lambda nk\prime}}) \frac{\partial P_{\lambda nk} J_{\lambda nk}(\vec{r}_{\lambda nk\prime}, t_{\lambda nk})}{\partial t}\, dv_{\lambda nk} dv\prime\right] \\ & + \hat{n} \times \left[\sum_{k=1}^{K}\sum_{n=1}^{M_k} \frac{\nabla}{\varepsilon_0} \int_{v_m k} G(\vec{r}, r_{\vec{mk\prime}}) p_{mk} q_{mk}(\vec{r}_{mk}\prime, t_{mk}) dv_{mk}\right] \end{aligned} \tag{1.31}$$

that is the basic discretized form of the EIFE equations for the PEEC method from which it is possible obtain the expression for the partial element calculation, that are:

- *Partial inductances*; the basic expression can be derived from the second term of (1.31). By using the free space Green's function and the expression $I_{\lambda m} = J_{\lambda m} a_m$ for the total current through a cross sectional area a_m we can obtain:

$$\sum_{k=1}^{K}\sum_{n=1}^{N_{\lambda k}} \frac{\mu_0}{4\pi} \frac{1}{a_{v\prime} a_{v_{\lambda nk}}} \int_{v\prime}\int_{v_{\lambda nk}} \frac{\frac{\partial}{\partial t} I_{\lambda nk}(\vec{r}_{\lambda nk\prime}, t_{\lambda nk})}{|\vec{r} - \vec{r\prime}|} dv_{\lambda nk} dv\prime \tag{1.32}$$

  that can be seen as the inductive voltage drop over the volume cell. Using the expression of partial inductance of [4] defined by (1.33):

$$Lp_{\alpha\beta} = \frac{\mu}{4\pi} \frac{1}{a_\alpha a_\beta} \int_{v_\alpha}\int_{v_\beta} \frac{\vec{u}_\alpha \cdot \vec{u}_\beta}{|\vec{r_\alpha} - \vec{r_\beta}|} dv_\alpha dv_\beta \tag{1.33}$$

  we can write (1.32) as:

$$v_L = \sum_{k=1}^{K}\sum_{n=1}^{N_{\lambda k}} Lp_{v\prime\lambda nk} \frac{\partial}{\partial t} I_{\lambda nk}(t - \tau_{v\prime v_{\lambda nk}}) \tag{1.34}$$

  where $\tau_{v\prime v_{\lambda nk}}$ is the center to center delay between the volume cell $v\prime$ and $v_{\lambda nk}$.

  The interpretation of (1.32) as an inductive voltage drop leads to assume the concept of *self partial inductance* for each volume cell (when in (1.33) $\alpha = \beta$) and a *mutual inductive coupling* of each volume cell with all the others, with the concept of *mutual partial inductance* (when in (1.33) $\alpha \neq \beta$). All the inductive couplings of a cell with all the others can be combined as in (1.35).

$$V_m^L(t) = \sum_{\forall n, n \neq m} L_{pmn} \frac{\partial i_n(t - \tau_{mn})}{\partial t} \tag{1.35}$$

In this way each cell can be modelled (from a magnetic point of view) such as a partial inductance in series with a voltage source, as shown in figure (1.1).

- *Coefficient of Potential*; the basic expression can be derived from the third term of (1.31) and, by considering that the charges only reside on the surface of the volumes, we can convert the volume integral in a surface integral, (1.36), [4].

$$\sum_{k=1}^{K} \sum_{m=1}^{M_k} \left[q_{mk}(t_{mk}) \frac{1}{4\pi\varepsilon_0} \int_{S_{mk}} \frac{1}{|\vec{r}_i^{+} - \vec{r}\prime_j|} ds\prime - q_{mk}(t_{mk}) \frac{1}{4\pi\varepsilon_0} \int_{S_{mk}} \frac{1}{|\vec{r}_i^{-} - \vec{r}\prime_j|} ds\prime \right] \tag{1.36}$$

where $\vec{r}^{+}$ and $\vec{r}^{-}$ are respectively associated with the positive and negative end of the cell.

In analogy with the analysis of *Partial inductance*, we can consider (1.36) such as a capacitive voltage drop, v_C, and we can introduce the *partial coefficient of potential* as (1.37).

$$p_{ij} = \frac{1}{4\pi\varepsilon_0} \frac{1}{S_i S_j} \int_{S_i} \int_{S_j} \frac{1}{|\vec{r_i} - \vec{r_j}|} dS_i dS_j \tag{1.37}$$

so the capacitive voltage drop can be written as (1.38).

$$v_C = \sum_{k=1}^{K} \sum_{m=1}^{M_k} Q_{mk}(t - t_{mk}) [p^{+}_{i(mk)} - p^{-}_{i(mk)}] \tag{1.38}$$

The interpretation of (1.36) as a capacitive voltage drop leads to assume the concept of *pseudo-capacitances*, that connect each cell to infinity. The *mutual capacitive couplings* of each surface cell with all the others can be combine as in (1.39).

$$V_i^C(t) = \sum_{\forall j, j \neq i} \frac{P_{ij}}{P_{jj}} V_{C_j}(t - \tau_{ij}) \tag{1.39}$$

where $V_{C_j}(t - \tau_{ij})$ is the voltage over the pseudo-capacitance $\frac{1}{P_{jj}}$ of the node j at an earlier instance.

In this way each surface cell (*node*) can be modelled (from an electric point of view) such as a self partial pseudo-capacitance in series with a voltage source V_i^C, as shown in figure (1.1).

- *Partial Resistance*; This term is referred to the first term of (1.31), that can be interpreted as a resistive voltage drop over the volume cell. So, by assuming a constant current density in the volume cell, we can easily obtain the expression of the *partial resistance* (1.40), that appears in figure (1.1).

$$R_\lambda = \frac{l_\lambda}{a_\lambda \sigma_\lambda} \tag{1.40}$$

where l_λ is the length of the volume cell.

1.4.2 Dielectric Materials

A dielectric cell can be modelled in the same way of the conductor cell, [44]. The only difference is the addition of the *excess capacitance* in parallel with the partial resistance (as shown in figure (1.2)) calculated from the geometrical data and the relative permittivity of the cell m as in (1.41).

$$C_m^+ = \frac{\varepsilon_0(\varepsilon_m - 1)a_m}{l_m} \tag{1.41}$$

where ε_m is the relative permittivity, a_m is the cross sectional area of the dielectric cell and l_m is the length in the current direction.
In this thesis the capacitive cells have not been deepened.

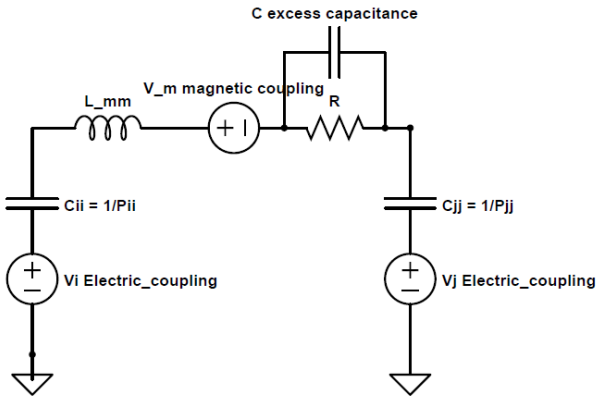

Figure 1.2: *Dielectric cell.*

1.4.3 Inclusion of External Applied Fields

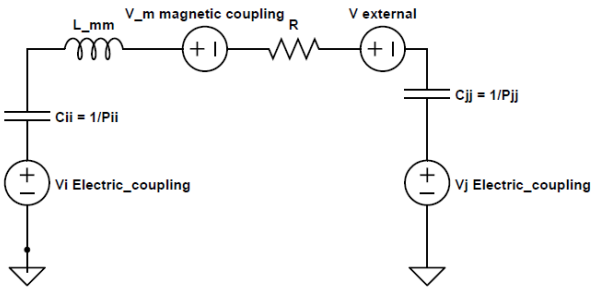

Figure 1.3: *Cell excited by an external Electric field.*

In a PEEC model can be used voltage and current sources, but it is also possible to simulate the excitation of an object by an external electric field (an incident field). This is done by adding to the circuit cell of the object an equivalent voltage source (as shown in figure (1.3)) calculated as in (1.42).

$$V_{P_m}(t_m) = \frac{1}{a_m}\int_{a_m}\int_{l_m} \vec{E}\prime(\vec{r}, t_m)dadl \tag{1.42}$$

In this thesis the inclusion of external applied field has not been considered.

Chapter 2

PARTIAL ELEMENT, FILAMENT

In this chapter we discuss about the PEEC method with filamentary partial elements. We report:

- The method and formulas adopted for the evaluation of the partial coefficients, with some validation;
- The used method to assembly the system (that must be solved to reach the solution in terms of currents and/or node potentials) by explaining how to obtain the matrices that compose it;
- Some results and comparisons with analytical approach for some given geometry.

It is convenient using Filamentary PEEC-Code when the geometry gives a privileged direction for the current flow, such as transmission lines and antennas.

2.1 Partial Inductance Coefficient Evaluation

From the second term of (1.31) we can derive a general expression, (2.1), for the partial inductance of an element.

$$Lp_{\alpha\beta} = \frac{\mu}{4\pi}\frac{1}{a_\alpha a_\beta}\int_{v_\alpha}\int_{v_\beta}\frac{\vec{u}_\alpha \cdot \vec{u}_\beta}{|\vec{r_\alpha} - \vec{r_\beta}|}dv_\alpha dv_\beta \tag{2.1}$$

where a_α and a_β are the cross sections area normal to the current flow, v_α and v_β are the volumes of the elements and $\vec{r_\alpha}$ and $\vec{r_\beta}$ are the distances of the points in the two volumes from the origin of the reference system. $\vec{u}_\alpha$ and $\vec{u}_\beta$ are the unit vectors which give the direction of the density current vectors.

For a one dimensional problem the partial elements are thin wire carrying the current, so, for this particular case, the general expression (2.1) can be elaborated to find an *easy* and *general* method for the calculation of the coefficient. In literature it is possible to find analytical formulas that allow the calculation of the self and mutual partial inductance coefficient of two wires in particular position (parallel, aligned, coplanar etc.) or in arbitrary position, [11], [16].

These analytical expressions allow to achieve a good accuracy but they are usable only for particular and easy case (for example when the elements are parallel to each other). Indeed, they become more complicated to use for a general case, because they are related to a particular reference system and often present some singularity if we try to use them when the filaments are in some particular position.

For our purpose we are interest in the general case of straight filaments in arbitrary position in the space. So, to avoid this problem, we have decided to use a numerical method based on *Gauss-Legendre quadrature*, in order to solve the second volume integral in (2.1).

In order to obtain the mutual inductance coefficient, we can calculate the line integral of vector magnetic potential, $\vec{A}$, produced by one of the two filaments (carrying a unitary current) along the other wire.

$$Lp_{\alpha\beta} = \frac{\Phi_B}{I} = \frac{\int_S \vec{B} \cdot \vec{n} dS}{I} = \frac{\int_{l_\beta} \vec{A} dl}{I} \tag{2.2}$$

where l_β is the second wire and for the evaluation of $\vec{A}$ (that is the vector magnetic potential generated by the first wire in a general point in the space), it is possible to find an analytical expression by solving the note integral equation (2.3). Equation (2.3) allows to compute the vector magnetic potential generated by an arbitrary distribution of current in the space.

$$\begin{aligned}
\vec{A}(P) &= \int_V \frac{\mu \vec{J}(\vec{r_q})}{4\pi |\vec{r_p} - \vec{r_q}|} dv \qquad \text{for a volume current density J} \\
\vec{A}(P) &= \int_S \frac{\mu \vec{G}(\vec{r_q})}{4\pi |\vec{r_p} - \vec{r_q}|} dS \qquad \text{for a surface current density G} \\
\vec{A}(P) &= \int_l \frac{\mu \vec{I}(\vec{r_q})}{4\pi |\vec{r_p} - \vec{r_q}|} dl \qquad \text{for a line current I}
\end{aligned} \tag{2.3}$$

By applying (2.3) to our problem, we obtain the expression (2.4), referring to figure (2.1).

$$\vec{A}(P) = \frac{\mu I}{4\pi} \ln \frac{R_i + R_f + L_\alpha}{R_i + R_f - L_\alpha} \tag{2.4}$$

where L_α is the length of the wire and R_i & R_f are the distances of the point from the two endpoints of the wire.

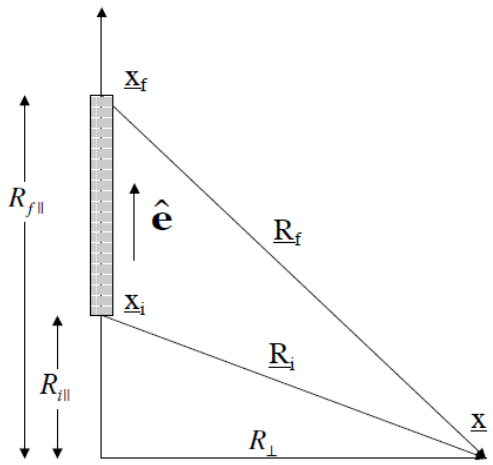

Figure 2.1: *$\vec{A}$ and V produced by stick conductor crossed by current, geometrical entities.*

Now we have to integrate (2.4) along the second wire l_β, in order to find the value of the *mutual partial coefficient* $L_{\alpha\beta}$. As saying above, we have decided to solve this problem in a numerical way using *Gauss-Legendre quadrature* method:

$$
\begin{aligned}
Lp_{\alpha\beta} &= \frac{\int_{l_\beta} \vec{A} dl}{I} \\
&= \frac{\mu_0}{4\pi} \int_{l_\alpha} \int_{l_\beta} \frac{1}{|\vec{r_p} - \vec{r_q}|} d\vec{l}_\beta d\vec{l}_\alpha \\
&= \cos(\theta) \frac{\mu_0}{4\pi} \int_{l_\alpha} \ln \frac{R_i + R_f + L_\alpha}{R_i + R_f - L_\alpha} dl_\alpha \\
&\approx \cos(\theta) \frac{\mu}{4\pi} \frac{l_\alpha}{2} \sum_{i=1}^{n} w_i f(P_i)
\end{aligned}
\tag{2.5}
$$

where θ is the angle formed by the direction of the two wires, $f(\bullet)$ is the logarithmic term in (2.4), w_i and P_i are respectively the weights and Gauss points (with n the number of the Gauss points used) and $\frac{l_\alpha}{2}$ is the Jacobian.

The same result of (2.5) can be reached also starting from (1.33), considering the case of the cylinder with the cross section radius which tends to zero.

This approach allows to write a general code that evaluates the mutual partial coefficient between two arbitrary position wires. We have to specify that this method doesn't work for "two coincident wires". This happends when we are evaluating the *self partial coefficient* $L_{\alpha\alpha}$, so to calculate it we use an analytic expression for the self inductance of a thin wire found in literature: (2.6), [12], [13].

$$
Lp_{\alpha\alpha} = \frac{\mu_0}{4\pi}\, 2l \left[\ln\left(\frac{l}{r_w} + \sqrt{\left(\frac{l}{r_w}\right)^2 + 1} \right) - \sqrt{1 + \left(\frac{r_w}{l}\right)^2} + \frac{r_w}{l} + \frac{1}{4} \right] \tag{2.6}
$$

where l is the length of the cylindrical wire and r_w is the radius of the cross section of the conductor.

Another possibility for the evaluation of the self coefficient can be derived from the discussion in section (3.1.1).

2.2 Method Validation for Partial Inductance Coefficients

In this section we are going to validate the method used to compute the *partial inductance coefficients* by making comparisons with analytical approach and by evaluating the self inductance of circular and square loops (which have analytical expressions).

2.2.1 Comparison between G-L and formulas in the literature

In order to validate the numerical method used for the evaluation of the *partial inductance coefficients* we have first compared the results obtained by our "semi-numerical" approach with "MATEMATICA". Then we have also compared the values obtained with the numerical approach with those obtained from the analytic formulas found in literature for some particular case, like parallel, aligned or complanar wires, [11].

In the tables we report some result obtained from the different methods, in case of aligned wires (*Table, Aligned Wires*) and parallel wires (*Table, Parallel Wires*).

Table, Aligned Wires, N Coefficient

Distance [m]	Clayton Aligned	Clayton Coplanar	Gauss-Legender	Mathematica
0.0000	2.7716	NaN	2.7696	2.77259 (*numeric*)
0.0030	2.7521	2.7522	2.7516	2.7521
0.0190	2.6781	2.6782	2.6781	2.6781
0.0200	2.6742	2.6742	2.6742	2.6742

where $N = \frac{L_{\alpha\beta}}{\frac{\mu_0}{4\pi}}$.

Table, Parallel Wires, N Coefficient

Distance [m]	Clayton Parallel	Gauss-Legendre	Mathematica
0.0000	47.5968	NaN	NaN
0.0200	17.2311	17.2331	17.2332
0.1400	9.6844	9.6847	9.6847
0.4000	5.9704	5.9705	5.9705

In figure (2.2) the values of N coefficient evaluated by Gauss-Legendre (G-L) method are compared with Clayton's formula for aligned wires: (2.7), while in figure (2.3) are compared with Clayton's formula for coplanar wires: (2.8) (used for the particular case of aligned wire), [11].

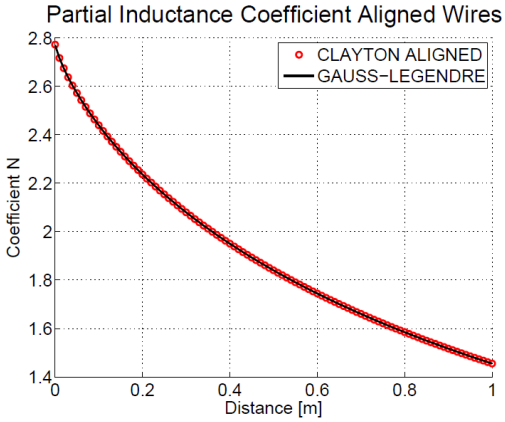

Figure 2.2: *N coefficient, comparison between Gauss-Legender and Clayton's formula* (2.7)

$$\begin{aligned} Lp_{\alpha\beta} = \frac{\mu_0}{4\pi}\Bigg[&(l+s+m)\sinh^{-1}\frac{l+s+m}{r_w} - (m+s)\sinh^{-1}\frac{m+s}{r_w} \\ &- (l+s)\sinh^{-1}\frac{l+s}{r_w} + s\sinh^{-1}\frac{s}{r_w} - \sqrt{(l+s+m)^2+r_w^2} \\ &+ \sqrt{(m+s)^2+r_w^2} + \sqrt{(l+s)^2+r_w^2} - \sqrt{s^2+r_w^2}\Bigg]. \end{aligned} \tag{2.7}$$

where l is the length of the upper wire, m is the length of the lower wire, s is the distance between the endpoints and r_w is the radius of the wires.

$$\begin{aligned} Lp_{\alpha\beta} = \frac{\mu_0}{4\pi}\ \cos(\theta)\ \Bigg[&(\alpha+l)\ln\frac{R_1+R_2+m}{R_1+R_2-m} + (\beta+m)\ln\frac{R_1+R_4+l}{R_1+R_4-l} \\ &- \alpha\ln\frac{R_3+R_4+m}{R_3+r_4-m} - \beta\ln\frac{R_2+R_3+l}{R_2+R_3-l}\Bigg]. \end{aligned} \tag{2.8}$$

where l and m are the length of the two wires and the other terms $R_1, R_2, R_3, R_4, \alpha$ and β are represented in the figure (2.3).

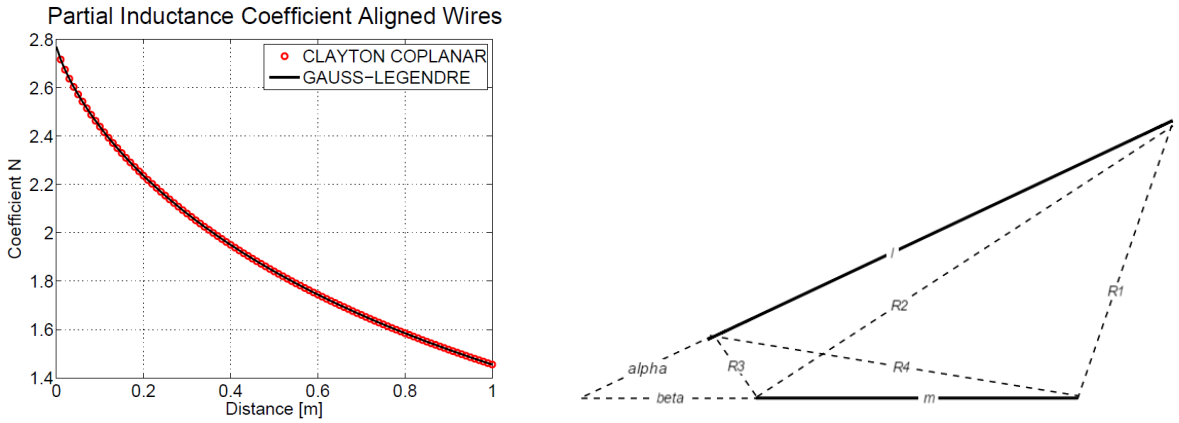

Figure 2.3: *Left: N coefficient, comparison between Gauss-Legender and Clayton's formula* (2.8). Right: *Reference system Clayton's formula* (2.8).

Instead, in figure (2.4) are compared the values of N coefficient obtained by G-L and Clayton's formula for parallel wires: (2.9). In the two cases both wires are *2m* long. For the aligned wires it does vary the distance between the two ends of the segments from zero (*consecutive segments*) to *1m*; instead for parallel wires it does vary the distance between the two parallel segments from zero (*coincident segments*) and *1m*.

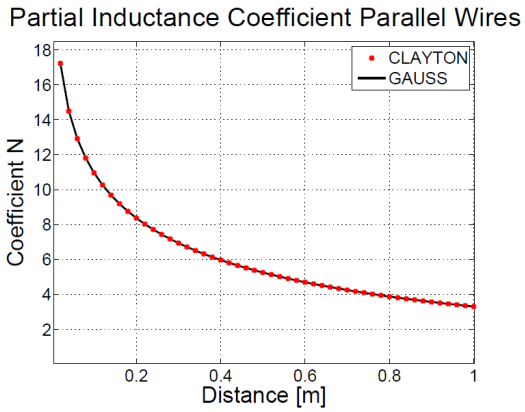

Figure 2.4: *N coefficient, comparison between Gauss-Legender and Clayton's formula* (2.9)

$$Lp_{\alpha\beta} = \frac{\mu_0}{4\pi}\, 2l \left[\ln\left(\frac{l}{d+r_w} + \sqrt{\left(\frac{l}{d+r_w}\right)^2 + 1} \right) - \sqrt{1 + \left(\frac{d+r_w}{l}\right)^2} + \frac{d+r_w}{l} \right]. \tag{2.9}$$

where l is the length of the two wires, r_w is the radius of the conductors and d is the distance.

As we can see in the figures and in the tables, the results obtained by G-L method are thoroughly validated by the values reached from analytical methods.

2.2.2 Circular and Square Loops

As second verification of the numerical method used, we have evaluated the self inductance of a circular coil and a square coil. So we want to compare the results obtained by G-L method with the analytical formulas found in literature for the self inductance of these particular loops, [12], [14].

For the evaluation of the self inductance by using G-L method, we have discretized the coil in many stick conductors and for each of them we have computed all the mutual partial inductance coefficients between the other sticks (*using G-L*) and the self partial inductance coefficients (*by using equation (2.1)*).

In this way we have found the *Matrix of Partial Inductance Coefficient* $\mathbf{L}$, that is a $N_e \times N_e$ matrix (with N_e the numbers of elements) where the diagonal terms are the self partial inductance coefficients and the off-diagonal terms are the mutual coefficients. So, by summing all the entrances of the matrix, we have obtained the self inductance of the coil under analysis.

About the geometrical entities of the circular coil, we have considered a radius of *10m* for the loop and a radius of *0.001m* for the conductor. For the square coil we have considered the same radius for the conductor and a side of *10m*. We have done the calculation by using different numbers of elements and the results are reported in the *Table Circular Coil* and in the *Table Square Coil*.

Table, Circular Coil

Number of elements	Gauss-Legendre [H]	Analytical Formula [H]	Relative Error
10	3.7179e-05	3.8159e-05	0.0257
20	3.7899e-05		0.0068
40	3.8089e-05		0.0018
60	3.8127e-05		0.0008

Table, Square Coil

Elements, each side	Gauss-Legendre [H]	Analytical Formula [H]	Relative Error
1	2.2120e-05	2.2120e-05	0
4	2.2118e-05		9.5243e-05
10	2.2119e-05		5.2149e-05
20	2.2121e-05		5.4235e-05

About analytical formulas, we have used equation (2.10) for the circular coil and equation (2.11) for the square coil (*in all the calculations we have obviously considered a current uniformly distributed in the cross section*).

$$L_{self} = \mu_0 R \left(\ln \frac{8R}{a} - \frac{7}{4} \right) \tag{2.10}$$

where R is the radius of the loop and a is the radius of the circular cross section of the conductor.

$$L_{self} = \frac{\mu_0}{4\pi} \left(4L_1 - 4M \right) \quad where... \tag{2.11}$$

$$L_1 = 2l \left[\ln \frac{a + \sqrt{l^2 + a^2}}{a} - \sqrt{1 + \frac{a^2}{l^2}} + \frac{1}{4} + \frac{a}{l} \right] \tag{2.12}$$

$$M = 2l \left[\ln \frac{l + \sqrt{2\ l^2}}{l} - \sqrt{2} + 1 \right] \tag{2.13}$$

where l is the side of the square coil and a is the radius of the circular cross section of the conductor.

As example, we report here the $\mathbf{N}$ matrix obtained for the square coil in figure (2.5) with four elements for each side (*to reach the* $\mathbf{L}$ *matrix we have just to multiply the entrances by the coefficient* $\frac{\mu_0}{4\pi}$).

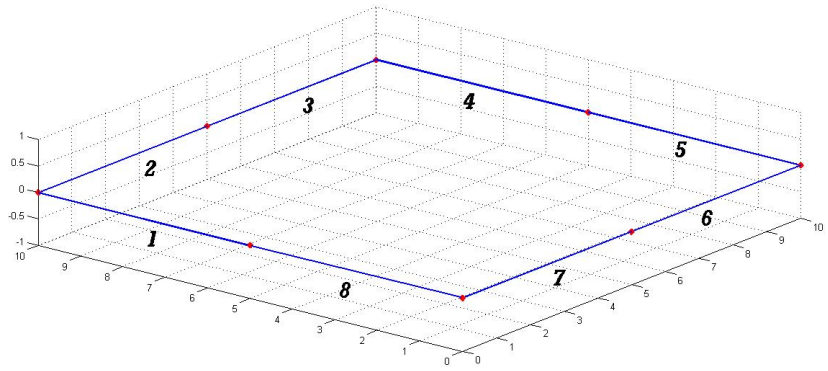

Figure 2.5: *Square coil with four elements for each side.*

$$\begin{bmatrix}
84.6054 & 0 & 0 & -2.4514 & -2.2202 & 0 & 0 & 6.9240 \\
0 & 84.6054 & 6.9240 & 0 & 0 & -2.2202 & -2.4514 & 0 \\
0 & 6.9240 & 84.6054 & 0 & 0 & -2.4514 & -2.2202 & 0 \\
-2.4514 & 0 & 0 & 84.6054 & 6.9240 & 0 & 0 & -2.2202 \\
-2.2202 & 0 & 0 & 6.9240 & 84.6054 & 0 & 0 & -2.4514 \\
0 & -2.2202 & -2.4514 & 0 & 0 & 84.6054 & 6.9240 & 0 \\
0 & -2.4514 & -2.2202 & 0 & 0 & 6.9240 & 84.6054 & 0 \\
6.9240 & 0 & 0 & -2.2202 & -2.4514 & 0 & 0 & 84.6054
\end{bmatrix}$$

By analysing the results reported in the two tables, we see that the numerical method adopted gives very good results in terms of relative error respect the values provided by the analytical formulas.

In particular, we observe that, for the circular coil, with the increasing of the numbers of elements the accuracy of the estimation of the self inductance improves, while, for the square loop, we have an error equal to zero when we take only one element for each side (*just because in this case the calculation of the partial inductance coincides with the equations of* L_1 *and* M *reported in (2.11)*), then, with the increasing of the number of elements, the relative error has the trend shown in figure (2.6).

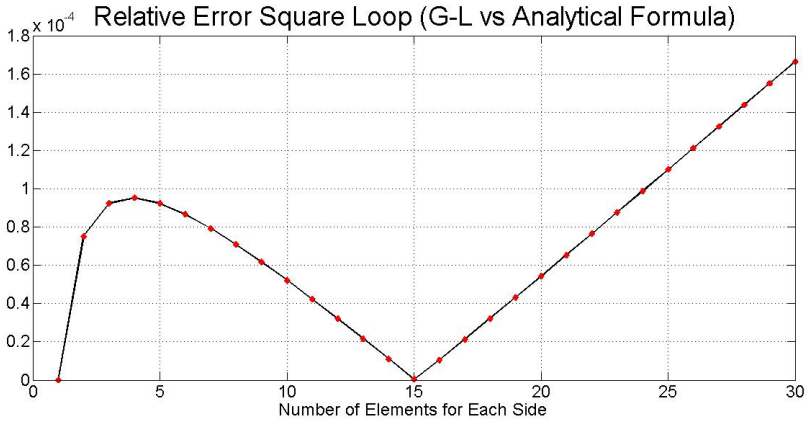

Figure 2.6: *Relative Error of Self Inductance of a Square Coil Varying the Number of Elements.*

The trend of figure (2.6) is caused by the fact that with the increasing of the number of elements their length decreases, so the numerical errors growths (the formulas used for the calculation of the partial

inductance give a good accuracy when $l \gg r$, where l and r are respectively the length and the radius of the cross section of the stick conductors).

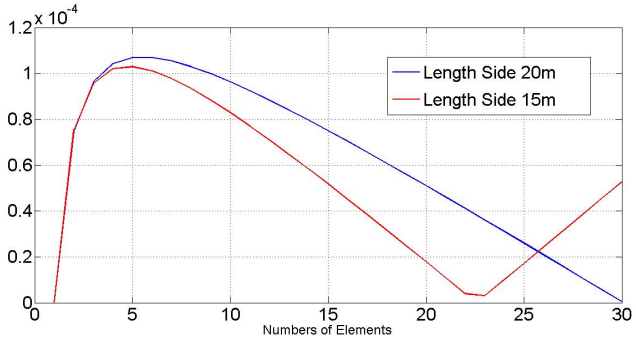

Figure 2.7: *Relative Error of Self Inductance of two Square Coil (15m and 20m Side) Varying the Number of Elements.*

Indeed, with the increasing of the length of the side, the trend of the relative error changes as we can see in figure (2.7).

The same graphics reported in figure (2.6) has been produced for the circular loop in figure (2.8).

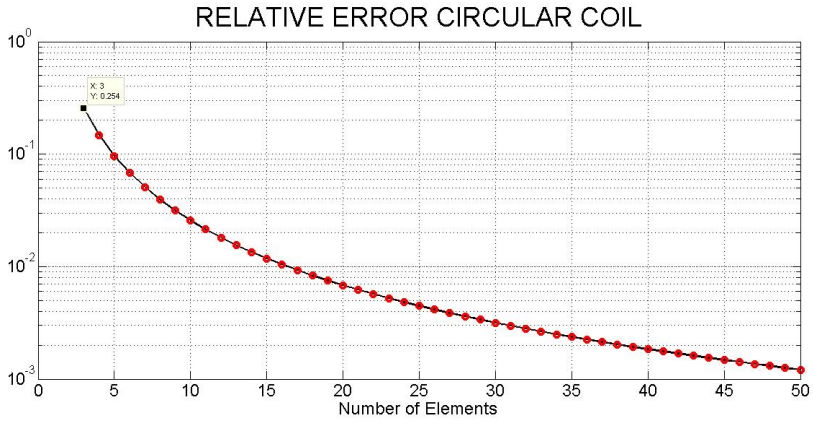

Figure 2.8: *Relative Error of Self Inductance of a Circular Coil Varying the Number of Elements.*

In agreement with what previously said, we observe that (*at least until the largest value used for the number of elements*) the relative error always decreases with the increasing of the number of elements.

But, if we have considered a coil with a smaller ration between the radius of the loop and the radius of the cross section of the conductor, we will have the same phenomenon discussed above for the square loop.

2.3 Partial Coefficient of Potential Evaluation

In this section, in analogy with what we have done in section (2.1), we are going to discuss about the calculation of the *Partial Coefficient of Potential*.

From the third term of (1.31) we can derive a general expression (2.14) for the partial coefficient of potential of an element.

$$p_{ij} = \frac{1}{4\pi\varepsilon_0}\frac{1}{S_i S_j}\int_{S_i}\int_{S_j}\frac{1}{|\vec{r_i} - \vec{r_j}|}dS_i dS_j \tag{2.14}$$

where S_i and S_j are charged surface and $\vec{r}_i$ and $\vec{r}_j$ are the vector distances of the points in the surfaces from the center of the reference system.

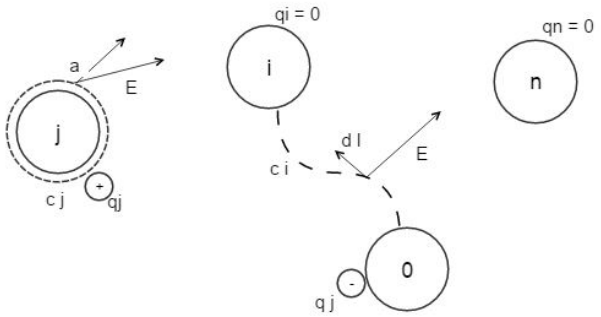

Figure 2.9: *Coefficient of Potential.*

The expression (2.14) is referred to a three dimensional element, where the charge is uniformly distributed in the surface, so in the expression is present a surface integral.

In this chapter we consider a one dimensional elements so, in analogy with what we have done for *partial inductance coefficients*, we can say that, in order to obtain the mutual potential coefficients, we have to solve the line integral of electric field $\vec{E}$ as in (2.15), [23].

$$\begin{aligned} p_{ij} &= \left.\frac{V_i}{q_j}\right|_{q_1=\cdots=q_{j-1}=q_{j+1}=\cdots=q_n=0} \\ &= \frac{-\int_{c_i} \vec{E}_t \cdot d\vec{l}}{\varepsilon \oint_{c_j} \vec{E}_t \cdot \vec{a_n} dl} \end{aligned} \tag{2.15}$$

where the geometrical entities are shown in figure (2.9).

The p_{ij} coefficient is equal to the potential in the element i when the charge in null in all the elements, except for the element j and infinity.

$$V(P) = \int_S \frac{\rho(\vec{r_q})}{4\pi\varepsilon_0 |\vec{r_p} - \vec{r_q}|} dl \tag{2.16}$$

Starting from (2.14), it is possible to obtain an expression for the 1D problem by considering the case of two cylinders with cross section radius which tends to zero:

$$\begin{aligned} p_{ij} &= \frac{1}{4\pi\varepsilon_0} \frac{1}{l_i l_j} \int_{l_i} \int_{l_j} \frac{1}{|\vec{r}_i - \vec{r}_j|} dl_j dl_i \\ &= \frac{1}{4\pi\varepsilon_0} \frac{1}{l_i l_j} \int_{l_i} \ln \frac{R_i + R_f + L_i}{R_i + R_f - L_i} dl_i \end{aligned} \tag{2.17}$$

where L_i is the length of the wire and R_i & R_f are the distances of the points from the two endpoints of the wire.

Now we have to integrate (2.17) along the second element l_i, in order to find the value of the *mutual partial coefficient* p_{ij}. As we have done for the mutual partial inductance coefficient, we have decided to solve this problem numerically, by using *Gauss-Legendre quadrature* method.

$$p_{ij} \approx \frac{1}{l_i l_j} \frac{1}{4\pi\epsilon_0} \frac{l_i}{2} \sum_{i=1}^{n} w_i f(P_i) \tag{2.18}$$

where $f(\bullet)$ is the logarithmic term in (2.17), w_i and P_i are respectively the weights and Gauss points (with n the number of the Gauss points used) and $\frac{l_i}{2}$ is the Jacobian.

This approach allows to write a general code that evaluates the mutual partial coefficient of potential of two arbitrary position wires. We have to specify that this method doesn't work for "two coincident wires", that is when we are evaluating the self partial coefficient p_{ii}, so, to perform the calculation, we have used an analytic expression for the self partial coefficient of potential of a thin cylindrical wire found in the literature, (2.19), [13].

$$p_{ii} = \frac{1}{4\pi\epsilon_0} \frac{2}{l} \left[\ln\left(\frac{l}{r_w} + \sqrt{\left(\frac{l}{r_w}\right)^2 + 1} \right) - \sqrt{1 + \left(\frac{r_w}{l}\right)^2} + \frac{r_w}{l} \right] \tag{2.19}$$

where l is the length of the cylindrical wire and r_w is the radius of the cross section of the conductor.

Another possibility to reach the self coefficient can be derived from the discussion in (3.1.1).

Now we have to specify how we have considered the *"capacitive elements"* for the calculation of the partial coefficients of potential in the case of a 1D problem. Considering for example a circular loop: first we have divided it in a certain number of *"inductive elements"* (for example 10) for which we have found the middle points. By doing this, we have identified the *"capacitive elements"* which have their middle points coincident with the endpoints of the inductive elements, so we have determined a number of capacitive elements equal to the number of nodes of the descretized object (figure (2.10)). Indeed, the analytical and numerical integral in equations (2.17) and (2.18) have been divided in two parts respectively. In this way we can work with a more general case, with thin elements formed by two non-aligned segments.

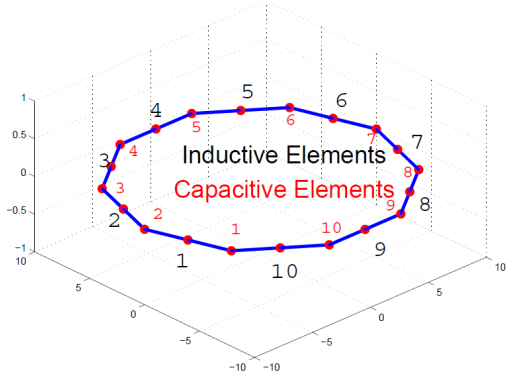

Figure 2.10: *Inductive and Capacitive Elements in a Circular Loop.*

By using this approach the *branch elements* are straight conductors while the *nodal elements* are divided in two straight conductors. Obviously also the dual approach can be used.

2.4 Method Validation for Partial Coefficients of Potential

In this section we are going to validate the method used for the evaluation of the *partial coefficients of potential*. To do this we have first calculated the capacitance respect to the infinite of a circular and thin conductor and we have compared the results with *FastCap* (*FastCap* and *FastHenry*, from Massachusetts Institute of Technology, are two free parasitics extractor tolls for capacitance, inductance and resistance).

Secondly, we have computed the Maxwell Capacitance Matrix, [42], of two thin cylindrical conductors comparing the results with *FastCap* and the analytical formula found in literature for this kind of geometry, [14].

For the first validation we have considered a single thin cylindrical conductor *10m* long and with a circular cross section of radius *0.01m*. We have first considered it as the only partial element forming the conductor, so in this way we have validated the expression used for the *self partial coefficient of potential*, (2.19). The value of capacitance can be easily obtained by the inverse of p_{ii}, $c_{ii} = \frac{1}{p_{ii}}$.

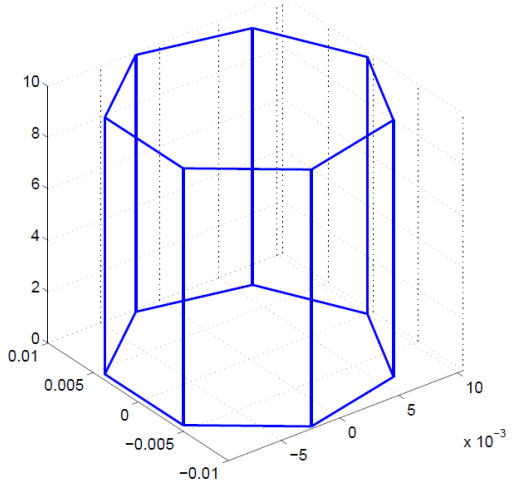

Figure 2.11: *Cylindrical conductor discretized by 7 rectangular panels.*

To model the geometry with *FastCap* we have considered the lateral surface of the cylindrical conductor formed by a certain number of rectangular panels (*the geometry files have been created with* MATLAB); for example in figure (2.11) is represented the geometry obtained by using seven panels for the lateral surface.

The results obtained by the comparison are shown in *Table, Thin Cylindrical Conductor.*

Table, Thin Cylindrical Conductor

Number of panels	FasterCap [pF]	FastCap [pF]	Our Code [pF]
5	83.9804	78.81	
5 *reduced tollerance*	83.6575	83.52	84.4323 *1 element*
6	84.3822	79.32	
7	84.2370	79.63	
8	84.4243	79.84	
9	84.5674		
15	84.8141		84.4591 *10 elements*
16	84.8819		
17	84.7734		

Then, we have done the same calculation dividing the conductor in many partial elements, so, by doing this, we have validated also the numerical method used to compute the *partial mutual coefficients of potential* (2.18). Afterwards, we have calculated the $\mathbf{P}$ matrix of the object (a $n \times n$ matrix where n is the number of the nodes, or the number of *capacitive elements*, of the object).

$\mathbf{C}$ matrix has been obtained by the inversion of $\mathbf{P}$ matrix, $\mathbf{C} = \mathbf{P}^{-1}$; finally we have reached the value of capacitance by summing all the entrances of $\mathbf{C}$ matrix. As we can see from the table, the results obtained are very similar, so we can consider correct the numerical method used.

For the second analysis we have considered two parallel cylindrical thin wires $10m$ long, with a circular cross section of radius $0.01m$. Each conductor was first divided in 29 partial inductive elements and then we have computed the **P** matrix for the 30 capacitive elements. By the inversion of **P**, we have reached **C** (a 60×60 matrix, indeed for each conductor we have 30 nodes and then 30 partial capacitive elements). Then, considering the four blocks, $\mathbf{C}= \begin{pmatrix} C_{ii_{30\times30}} & C_{ij_{30\times30}} \\ C_{ji_{30\times30}} & C_{jj_{30\times30}} \end{pmatrix}$, by summing all the terms for each of the four blocks we can obtain the Maxwell Capacitance Matrix of the two objects that can be compared with the matrix obtained by *FasterCap* using 9 panels for the discretization of the two cylindrical conductors. The results are shown here in $[F]$.

$$C_{FasterCap} = \begin{bmatrix} +1.20243 \cdot 10^{-10} & -6.53036 \cdot 10^{-11} \\ -6.52966 \cdot 10^{-11} & +1.20234 \cdot 10^{-10} \end{bmatrix}$$

$$C_{OurCode} = \begin{bmatrix} +1.20069 \cdot 10^{-10} & -6.52214 \cdot 10^{-11} \\ -6.52214 \cdot 10^{-11} & +1.20069 \cdot 10^{-10} \end{bmatrix}$$

2.5 Matrices and Global System

2.5.1 Matrices

In this section we discuss about the matrices that compose the system which we have to solve in order to obtain the solution in terms of node potentials and branch currents.

Matrix of Inductances, L

The *Matrix of Inductances*, **L**, is a $l \times l$ matrix where l is the number of the inductive elements (sides) that discretize the objects. The diagonal entrances are the *self partial inductances* and the off-diagonal entrances are the *mutual partial inductances* between the partial elements. An example for a square coil has been reported in section (2.2). In this example a lot of off-diagonal entrances are null because the relative partial elements are perpendicular but in general **L** is a full and symmetric matrix. The entrances can be evaluated as explained in section (2.1) by using the numerical method; analytical formulas can be used only for some particular geometry. In this thesis we use the numerical method (2.5) for the mutual inductances and the analytical formula (2.6) for the self partial inductances. The matrix represents the magnetic coupling of the partial elements and can be used to obtain the self inductance of an object by summing all the entrances off the matrix.

Matrix of Coefficients of Potential, P

The *Matrix of Coefficients of Potential*, **P**, is a $n \times n$ matrix, where n is the number of nodes (capacitive elements) that are the endpoints of the inductive elements, (from the standpoint of the electrical equivalent circuit). The diagonal entrances are the *self partial coefficients of potential* (between the element i and the infinity) and the off diagonal entrances are the *mutual partial coefficients of potential* between the partial elements.

As example, we report here the **P** matrix for a circular wire ($10m$ radius and with the radius of cross section equal to $1mm$) divided by 8 capacitive elements as in figure (2.12), (the matrix entrances are express in $[10^{10}\ F^{-1}]$).

$$\begin{bmatrix} 2.0283 & 0.1677 & 0.0697 & 0.0521 & 0.0479 & 0.0521 & 0.0697 & 0.1677 \\ 0.1677 & 2.0283 & 0.1677 & 0.0697 & 0.0521 & 0.0479 & 0.0521 & 0.0697 \\ 0.0697 & 0.1677 & 2.0283 & 0.1677 & 0.0697 & 0.0521 & 0.0479 & 0.0521 \\ 0.0521 & 0.0697 & 0.1677 & 2.0283 & 0.1677 & 0.0697 & 0.0521 & 0.0479 \\ 0.0479 & 0.0521 & 0.0697 & 0.1677 & 2.0283 & 0.1677 & 0.0697 & 0.0521 \\ 0.0521 & 0.0479 & 0.0521 & 0.0697 & 0.1677 & 2.0283 & 0.1677 & 0.0697 \\ 0.0697 & 0.0521 & 0.0479 & 0.0521 & 0.0697 & 0.1677 & 2.0283 & 0.1677 \\ 0.1677 & 0.0697 & 0.0521 & 0.0479 & 0.0521 & 0.0697 & 0.1677 & 2.0283 \end{bmatrix}$$

The entrances can be evaluated as explain in section (2.3). In this thesis we have used the numerical method (2.18) for the mutual coefficients and the analytical formula (2.19) for the self partial coefficients. The matrix represents the electric coupling of the partial capacitive elements.

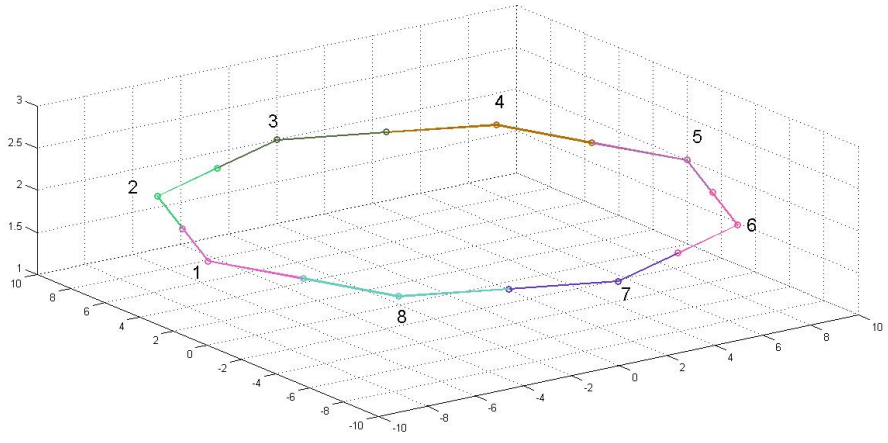

Figure 2.12: *Cyrcular wire, capacitive elements.*

Maxwell Capacitance Matrix, C

The *Maxwell Capacitance Matrix*, **C**, is a $n \times n$ matrix where n is the number of nodes (capacitive elements) that are the endpoints of the inductive elements. This matrix can be reached by the inversion of the **P** matrix and can be used to obtain the capacitance of the object or the Maxwell Capacitance Matrix for more objects (a $o \times o$ matrix, where o is the number of objects considered).

Matrix of Resistances, R

The *Matrix of Resistances*, **R**, is a $l \times l$ diagonal matrix (where l is the number of the sides of the objects, inductive elements). Every branch resistance can be obtained by the formula (1.40), where it is necessary to consider the partial element like a thin cylinder with a non-zero radius for the cross section, so l_λ is the length of the thin cylinder, a_λ is the area of the cross section and σ_λ is the conductivity of the partial element.

Incidence Matrix, A

The *Incidence matrix*, **A**, is a $n \times l$ sparse matrix that describes the topology of the electrical equivalent circuit formed by partial elements. The Incidence matrix is obtained from the *complete incidence Matrix* **Ac**, which entrances are created using the following rules:

- Each row corresponds to one node (capacitive element);
- Each column corresponds to one inductive element;
- The entry -1 at the row i and column j indicates that the current direction in the inductive element j is from the node i;
- The entry 1 at the row i and column j indicates that the current direction in the inductive element j is into the node i.

It is useful to specify that in this problem the infinity must be considered as a node and also all the voltage sources and loads must be considered like sides which add up to the *objects sides* (the inductive elements that descerize the objects).

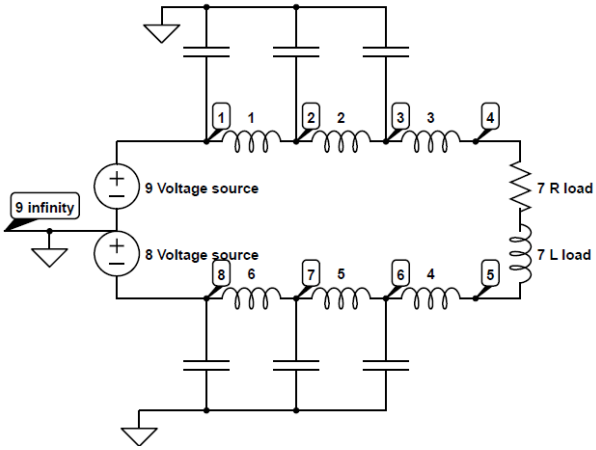

Figure 2.13: *Two wire line, in this representation, for semplicity, we don't have inserted the partial resistances and the voltage soruces of each side and of each node concerning the magnetic and electric coupling.*

In this way the **Ac** matrix has a number of rows equal to the number of capacitive elements plus the number of nodes formed by the voltage sources and loads considering also the *infinity node*. The number of column is equal to the number of inductive elements (objects sides) plus the number of voltage sources and loads considered in the problem. So, l is the total number of sides and n is the total number of nodes, considering also the infinity node. The **A** matrix can be easily obtained by the elimination of one row from the **Ac** matrix (for example the one relative to the *infinity node*), in this way the Kirchoff's laws (that we will write subsequently) will be linearly independent. This is true if we consider a model where there are no fluctuating objects. If some fluctuated objects is present the incidence matrix will not be linearly independent but the linearly independence of the system will be insured by the electric coupling between the objects, expressed by the **P** matrix.

As example, referring to figure (2.13), the **Ac** matrix has nine rows and nine columns (six object sides, two voltage sources and one load) so **A** matrix is a 8×9 matrix:

$$\begin{bmatrix} -1 & 0 & 0 & 0 & 0 & 0 & 0 & 0 & +1 \\ +1 & -1 & 0 & 0 & 0 & 0 & 0 & 0 & 0 \\ 0 & +1 & -1 & 0 & 0 & 0 & 0 & 0 & 0 \\ 0 & 0 & +1 & 0 & 0 & 0 & -1 & 0 & 0 \\ 0 & 0 & 0 & -1 & 0 & 0 & +1 & 0 & 0 \\ 0 & 0 & 0 & +1 & -1 & 0 & 0 & 0 & 0 \\ 0 & 0 & 0 & 0 & +1 & -1 & 0 & 0 & 0 \\ 0 & 0 & 0 & 0 & 0 & +1 & 0 & -1 & 0 \end{bmatrix}$$

Matrix of Admittance, Y

The *Matrix of Admittance*, **Y**, is a $n \times n$ matrix, where n is the number of nodes. Its entrances represent a possible connection between two arbitrary nodes of the problem through an element with a certain admittance Y_{ij}. The diagonal entrances off the matrix are null.

Matrix of Pseudo-Capacitance, F

The *Matrix of Pseudo-Capacitance*, **F**, is a $n \times n$ diagonal matrix, where the entrances represent the admittances of the pseudo-capacitance. The matrix can be easily obtained by the diagonal terms of **P**

matrix:

$$F_{ii} = \frac{1}{P_{ii}} \tag{2.20}$$

Matrix of Normalized Partial Coefficients of Potential, S

The *Matrix of Normalized Partial Coefficients of Potential*, **S**, is a $n \times n$ matrix that can be obtained easily by the **P** matrix:

$$S_{ij} = \frac{P_{ij}}{P_{jj}} \tag{2.21}$$

It contains the retarded electric field couplings between elements (if considered) and the normalized coefficients.

Vector of Sources, Source

The *Vector of Source* is the vector containing the values of the voltage and current sources. It is a $(n+l)\times 1$ vector formed by the vector of voltage source, **Vs**, (a $l \times 1$ vector) and the vector of current sources, **Is**, (a $n \times 1$ vector).

$$Source = \begin{bmatrix} V_{s_{l\times 1}} \\ I_{s_{n\times 1}} \end{bmatrix}$$

Indeed, the voltage sources are added to the problem as *appended elements*. So the addition of a voltage source increases the number of sides then the matrices **L** and **R** become larger: we have to add a row and a column for each voltage source and load appended to the problem and in the diagonal entrances we have to write the value of the resistance and inductance of the load and of the voltage source (null if is a ideal voltage source). In the off-diagonal entrances it is possible to write the value of mutual inductance between the appended element and the partial elements, if it is useful and easily to evaluate it, otherwise the off diagonal entrances in the rows and columns of appended elements are nulls. The current source can be added to the problem without the insertion of appended sides but they have to be seen as currents injected in the related nodes.

Vector of Unknowns, X

The *Vector of Unknowns* is the vector containing the potentials of the nodes respect to the infinity node and the branch currents. It is a $n + l \times 1$ vector formed by the vector of node potentials, **V**, (a $n\times$ 1 vector) and the vector of branch currents, **I**, (a $l \times 1$ vector).

$$X = \begin{bmatrix} V_{n\times 1} \\ I_{l\times 1} \end{bmatrix}$$

As already said, the results are obtained in terms of potentials and currents; in order to reach electric and magnetic field post-processing is required.

2.5.2 Dimension of the Matrices

For clarity we report here a table with the dimension of the matrices. l is the total number of sides including the objects sides (inductive elements) and the appended elements (loads and voltage sources). n is the total number of nodes including the nodes referred to the endpoints of inductive elements (capacitive elements) and the possible nodes formed by two loads and/or voltage sources (*added nodes*) but excluding the infinity node. For the *added nodes* it is necessary to insert 1 in the diagonal entrance of the **S** matrix and 0 for all the other "*nodal matrices*".

Matrix dimension

Matrix	Number of rows	Number of columns
L	l	l
R	l	l
P	n	n
C	n	n
F	n	n
S	n	n
Ac	$n+1$	l
A	n	l
Vs	l	1
Is	n	1
V	n	1
I	l	1

2.5.3 Solution Strategy

The problem that we want to solve has $n+l$ unknowns (n node potentials and l side currents) so we want to write $n+l$ linearly independent equations in the searching unknowns. The circuit equations are obtained from Kirchoff's laws:

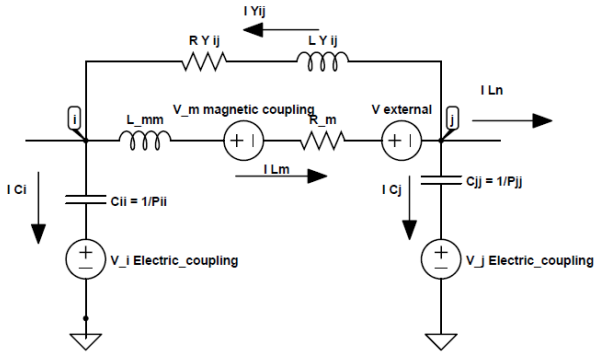

Figure 2.14: *One PEEC cell for the derivation of Kirchoff's laws.*

- Kirchoff's voltage law applied to the inductive branch gives:

$$V_i + j\omega Lp_{mm} I_{Lm} - \sum_{b=1, b\neq m}^{M} -R_m I_{Lm} - V_j = 0 \tag{2.22}$$

that written in matrix form becomes:

$$\text{-}\mathbf{A}^T\mathbf{V} - (\mathbf{R} + j\omega\mathbf{L})\mathbf{I} = \mathbf{Vs} \tag{2.23}$$

- Kirchoff's current law applied to each node gives:

$$I_{Lm} = I_{Ln} + I_{Y_{ij}} + I_{Cj} \tag{2.24}$$

that becomes:

$$I_{Lm} = I_{Ln} + (V_j - V_i)Y_{ij} + j\omega C_{jj} V_{C_j} \tag{2.25}$$

that written in matrix form becomes:

$$\mathbf{Y}_L\mathbf{V} + j\omega\mathbf{F}\mathbf{V}_c - \mathbf{A}\mathbf{I} = \mathbf{Is} \tag{2.26}$$

- The node potentials are expressed using its constituents parts, for example for node j:

$$V_j = V_{C_j} + \sum_{a=1, a\neq j}^{N} \frac{P_{ja}}{P_{aa}} V_{C_a} \tag{2.27}$$

that written in matrix form become:

$$\text{-}\mathbf{V} + \mathbf{S}\mathbf{V}_c = 0 \tag{2.28}$$

The matrix equations (2.23), (2.26) and (2.28) gives the system of $n+l$ equations reported in (2.29).

$$\begin{bmatrix} -\mathbf{A}^T & -(\mathbf{R} + j\omega\mathbf{L}) \\ j\omega\mathbf{P}^{-1} + \mathbf{Y}_L & -\mathbf{A} \end{bmatrix} \begin{bmatrix} \mathbf{V} \\ \mathbf{I} \end{bmatrix} = \begin{bmatrix} \mathbf{Vs} \\ \mathbf{Is} \end{bmatrix} \tag{2.29}$$

To solve this system it is necessary to invert the $\mathbf{P}$ matrix; this operation could be heavy from a computational point of view because $\mathbf{P}$ matrix is in general a very full matrix.

It is possible to obtain a different system that doesn't require the inversion of $\mathbf{P}$ matrix by using the following properties, [4].

$$\begin{aligned} \mathbf{P}^{-1} &= \mathbf{F}\mathbf{S}^{-1} \\ &= {\mathbf{S}^{-1}}^T\mathbf{F} \end{aligned} \tag{2.30}$$

So, by multiplying to the left the transpose of $\mathbf{S}$ matrix we obtain:

$$\mathbf{S}^T\mathbf{P}^{-1} = \mathbf{F} \tag{2.31}$$

So, from (2.29), we can write a different system that doesn't contain the the inverse of $\mathbf{P}$ matrix (2.32):

$$\begin{bmatrix} -\mathbf{A}^T & -(\mathbf{R} + j\omega\mathbf{L}) \\ j\omega\mathbf{F} + \mathbf{S}^T\mathbf{Y}_L & -\mathbf{S}^T\mathbf{A} \end{bmatrix} \begin{bmatrix} \mathbf{V} \\ \mathbf{I} \end{bmatrix} = \begin{bmatrix} \mathbf{Vs} \\ \mathbf{S}^T\mathbf{Is} \end{bmatrix} \tag{2.32}$$

Another possibility to avoid the inversion of $\mathbf{P}$ matrix is given by [28]. The second line of (2.29) is multiplied to the left by $\mathbf{P}$, in this way we obtain:

$$\begin{bmatrix} -\mathbf{A}^T & -(\mathbf{R} + j\omega\mathbf{L}) \\ j\omega\mathbf{1} + \mathbf{P}\mathbf{Y}_L & -\mathbf{P}\mathbf{A} \end{bmatrix} \begin{bmatrix} \mathbf{V} \\ \mathbf{I} \end{bmatrix} = \begin{bmatrix} \mathbf{Vs} \\ \mathbf{P}\mathbf{Is} \end{bmatrix} \tag{2.33}$$

This method becomes useful when the system becomes very large, so it requires an hight computational cost to be solved (the dimension of the systems (2.29), (2.32) and (2.33) is $N_l + N_n \times N_l + N_n$, where N_l is the number of sides and N_n is the number of nodes of the electrical equivalent circuit).

Indeed, considering for simplicity $\mathbf{Y}_L$ as null matrix, we can obtain (2.34) from the second matrix equation of the system.

$$\mathbf{V} = \frac{1}{j\omega}\mathbf{P}\mathbf{Is} + \frac{1}{j\omega}\mathbf{P}\mathbf{A}\mathbf{I} \tag{2.34}$$

Equation (2.34) can be substituted in the first matrix equation of (2.33), so we can obtain a matrix equation containing only the vector of unknowns $\mathbf{I}$:

$$(\mathbf{R} + j\omega\mathbf{L} + \frac{1}{j\omega}\mathbf{A}^T\mathbf{P}\mathbf{A})\mathbf{I} = -\mathbf{Vs} - \frac{1}{j\omega}\mathbf{A}^T\mathbf{P}\mathbf{I}_S \tag{2.35}$$

In this way, the vector of unknowns $\mathbf{V}$ can be reached by post-processing from (2.34) and the dimension of system to solve is $N_l \times N_l$, where N_l is the number of sides.

2.6 Two-wire line

In this section we report the results obtained by the simulation of two-wire line by using the PEEC method. The results have been compared with the ones obtained by using the analytical approach discussed in literature for this problem, [23], [15] [31].

We have considered a two-wire line $10m$ long with the cross section radius of $0.01m$ (that is required for the calculation of the p_{ii} coefficient) and separated by $0.2m$. Each one of the two conductors has been divided in 29 inductive elements and 30 nodes (or capacitive elements). Referring to figure (2.13), we have appended two voltage sources (each one $50[V]$) in the left side of the line, each one is connected to one of the extreme of the line and the infinity node; in the right side we have appended the load that is connected to the two extremes of the line. We have studied it in the time and frequency domain. For the time domain we have implemented the *theta method*.

2.6.1 Two-wire line values

The first results that we can obtain by the PEEC code is the numerical evaluation of the inductance and capacitance of the line. For each one of the two conductors it is possible to evaluate the self and the mutual coefficients of inductance and potential. Indeed, we can find the four matrix L_{ij} and the four matrix P_{ij}, where $i, j = 1, 2$ refer to the two conductors. By summing all the terms of the L_{ij} we can find the self and the mutual inductance of the conductors and by summing all together this four term we reach the value of the self inductance of the line. This value obtained numerically can be compared with the expression (2.36) found in [15].

$$l_{self} = \frac{\mu_0}{\pi} \cosh^{-1}\left(\frac{s}{2r_w}\right) \tag{2.36}$$

where s is the center to center distance of two conductors and r_w is the radius of the two conductors.

The obtained results are:

$$\mathbf{L}_{ij} = \begin{bmatrix} L_{11} & L_{12} \\ L_{21} & L_{22} \end{bmatrix} = \begin{bmatrix} 13.256\ [\mu H] & -7.2501\ [\mu H] \\ -7.2501\ [\mu H] & 13.256\ [\mu H] \end{bmatrix}$$

So we obtain:

$$\begin{aligned} l_{self\ numerically} &= 12.013\ [\mu H] \\ l_{self\ analitycally} &= 11.973\ [\mu H] \end{aligned} \tag{2.37}$$

In order to obtain the Maxwell Capacitance Matrix of the elements of the line it is necessary to invert the global $\mathbf{P}$ matrix (that is a 60×60 matrix) to obtain the global $\mathbf{C}$ matrix. Then, this matrix can be divided in four matrices, C_{ij} (each one is a 30×30 matrix), that allow to built a 2×2 matrix by summing all the terms all together. This matrix is called the Maxwell Capacitance Matrix of the objects and it can be compared with the matrix of capacitance obtained by *FasterCap*, as done in the previous section (2.4).

This matrix is reported here:

$$\mathbf{C} = \begin{bmatrix} C_{11} & C_{12} \\ C_{21} & C_{22} \end{bmatrix} = \begin{bmatrix} +1.2001\ [10^{-10}\ F] & -6.5224\ [10^{-11}\ F] \\ -6.5224\ [10^{-11}\ F] & +1.2001\ [10^{-10}\ F] \end{bmatrix}$$

Instead, by means of the analytical formulas in [15] and reported in (2.38), it is possible to evaluate the capacitance of the Two-wire line.

$$c = \frac{\pi \varepsilon_0}{\cosh^{-1}(\frac{s}{2r_w})} \tag{2.38}$$

The result obtained by this analytical formula is:

$$c_{self\ analitycally} = 92.93\ [pF] \tag{2.39}$$

2.6.2 Frequency domain

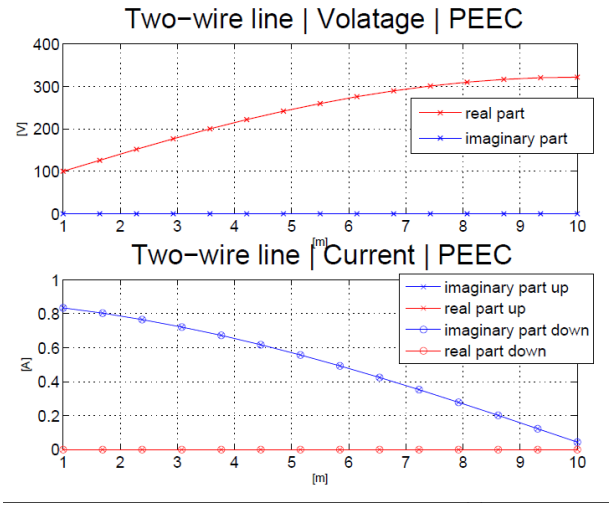

Figure 2.15: *Node potentials and branch Currents along a two-wire line at the frequency of* 6 $[MHz]$ *compute by PEEC-Code.*

Then it is possible to study the case of open line, that has been well analysed in literature, [31]. First we have done a study in the frequency domain varying the value of frequency, in order to observe the different behaviour of the line. From the theory of the transmission ideal line (without resistive term) we expect that the line seems like a capacitor when is length is lower than a quarter of the wavelength and it seems like an inductance when is length is between a quarter and an half of wavelength. If the line length is lower than $\lambda/4$ we will expect that the voltage increases along the line, from the voltage source to the open circuit.

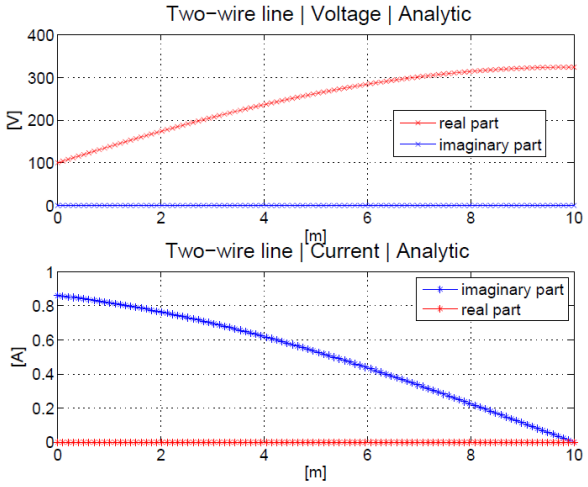

Figure 2.16: *Node potentials and branch Currents along a two-wire line at the frequency of* 6 $[MHz]$ *compute analycally.*

In figure (2.15) we report the results in terms of voltage potentials and branch currents obtained for the analysed line when the frequency is 6 $[MHz]$, so λ is equal to $\lambda = \frac{c}{f} = 80m$ and $d_{line} = 10m < \frac{\lambda}{4} = 11.67m$, where d_{line} is the length of the line.
The analysis has been done by using both (2.29) and (2.32) and the results have been obviously the same.

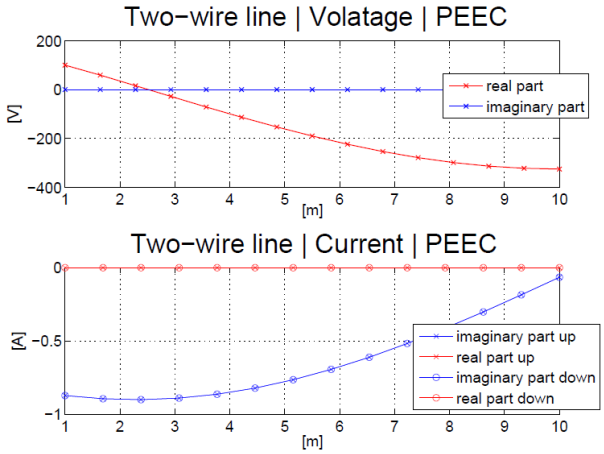

Figure 2.17: *Node potentials and branch Currents along a two-wire line at the frequency of* 9 $[MHz]$ *compute by PEEC-Code.*

To validate the results obtained by the PEEC-Code we have also studied the same problem by an analytical point of view by using the transmission matrix for the two-line wire, [31], [15]. With this "analytical method" we have studied the same line $10m$ long with a value of l_{self} and c_{self} equal to the one computed numerically by the PEEC-Code. The results in terms of node potentials and branch currents are reported in figure (2.16).

The same figure have been obtained by using a different frequency for which the line, seen from the beginning, becomes an inductance. With a frequency of 9 $[MHz]$ we have that the wavelength becomes $\lambda = 31.1m$, so $\frac{\lambda}{4} = 7.78m < d_{line} < 15.56m = \frac{\lambda}{2}$.

The numerically results are reported in figure (2.17) and the analytical results are reported in figure (2.18).

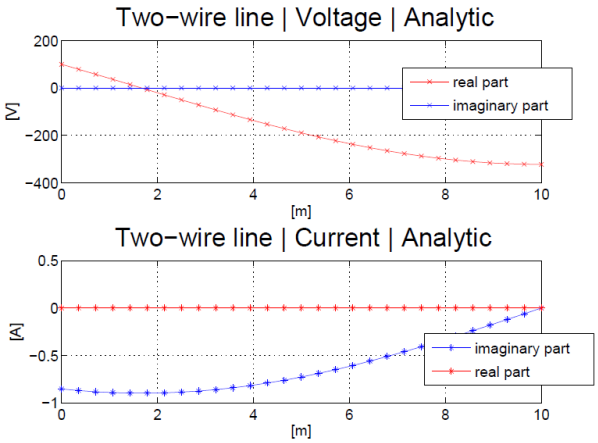

Figure 2.18: *Node potentials and branch Currents along a two-wire line at the frequency of* 9 $[MHz]$ *compute analycally.*

To conclude the analysis of the two-wire line open, we report here the value of the imaginary part of the impedance seen from the elements along the line when the frequency is 30$[MHz]$. With this value of frequency the wavelength is about $10m$, so we can see a complete voltage wave along the line.

In figure (2.19) are reported the values obtained for the imaginary part of the impedance and in figure (2.20) is reported, as done for the previously studies, the trend of voltage potentials and branch currents of the nodes and inductive elements respectively.

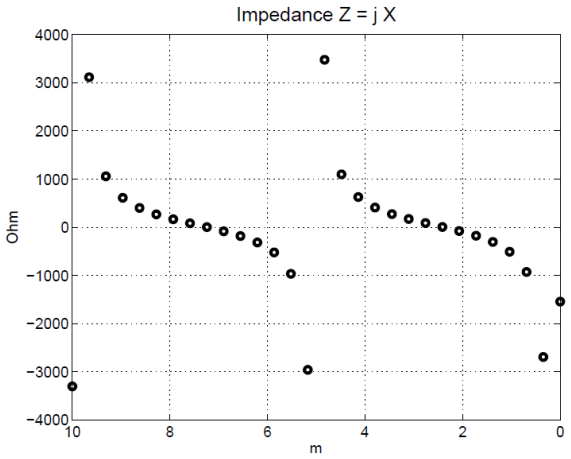

Figure 2.19: *Impedance of the two-wire line seen from the 30 nodes along the line at the frequency of* 30 $[MHz]$, *compute by PEEC-Code.*

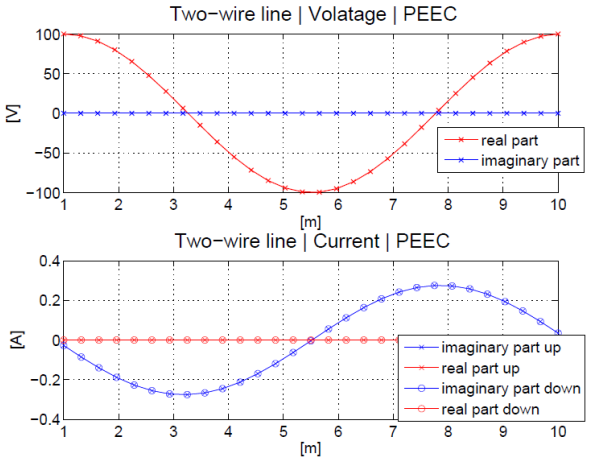

Figure 2.20: *Node potentials and branch Currents along a two-wire line at the frequency of* 30 $[MHz]$ *compute by PEEC-Code.*

The analysis can be done also imposing a certain value of resistivity to the conductors. That involves a resistive voltage fall along the conductor. In this way $\mathbf{R}$ matrix becomes a diagonal matrix (for the ideal line it was a null matrix). In figure (2.21) we report the results obtained for the line powered at $6[MHz]$ with a resistivity of the conductor equal to $7 \cdot 10^{-3}[\Omega m]$ (the value has been chosen for emphasize the resistive voltage fall).

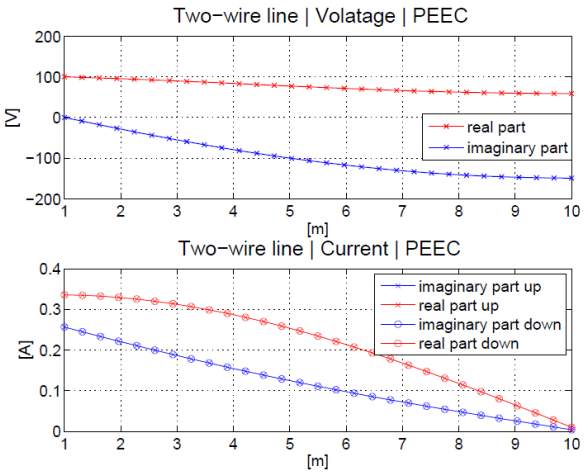

Figure 2.21: *Node potentials and branch Currents along a two-wire line at the frequency of* 6 $[MHz]$ *and with a resistivity of* $7 \cdot 10^{-3}[\Omega m]$ *compute by PEEC-Code.*

2.6.3 Time domain

The matrices obtained by the PEEC-Code can be also used to study time domain problems.

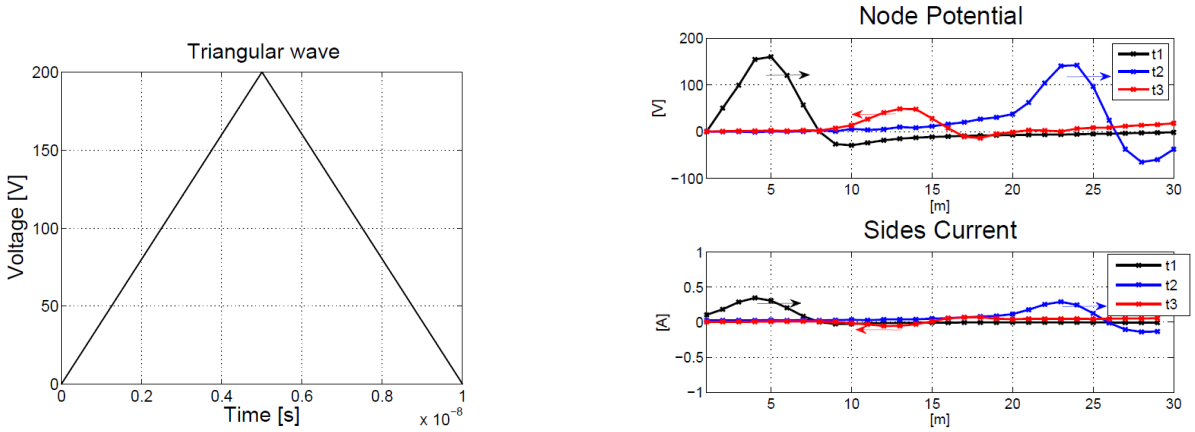

Figure 2.22: *Triangular wave applied to the two wire line for a time domain analysis and triangular wave propagation.*

The problem that we want to solve can be expressed in terms of matrix equation as in (2.40)

$$\begin{bmatrix} -\mathbf{A}^T & -\mathbf{R} \\ \mathbf{S}^T\mathbf{Y}_L & -\mathbf{S}^T\mathbf{A} \end{bmatrix} \begin{bmatrix} \mathbf{V} \\ \mathbf{I} \end{bmatrix} + \begin{bmatrix} \mathbf{0} & -\mathbf{L} \\ \mathbf{F} & \mathbf{0} \end{bmatrix} \begin{bmatrix} \frac{d}{dt}\mathbf{V} \\ \frac{d}{dt}\mathbf{I} \end{bmatrix} = \begin{bmatrix} \mathbf{Vs} \\ \mathbf{S}^T\mathbf{Is} \end{bmatrix} \tag{2.40}$$

and in a compressed way in (2.41).

$$\mathbf{M}_1 x + \mathbf{M}_2 \dot{x} = \mathbf{s} \tag{2.41}$$

We can apply the theta method to expression (2.41) obtaining (2.42).

$$(\theta\mathbf{M}_1 + \frac{1}{\Delta t}\mathbf{M}_2)x_{n+1} = (-(1-\theta)\mathbf{M}_1 + \frac{1}{\Delta t}\mathbf{M}_2)x_n + \theta s_{n+1} + (1-\theta)s_n \tag{2.42}$$

Where the term to the left side that multiplies the vector of unknowns x at the time step $n+1$, x_{n+1} is the preassembled system that we have to invert and the term to the right is the known term that has to be update for each step.

With this code we have studied the two-wire line excited by a singular voltage triangular wave. For this analysis, the line has been closed with a load of 300Ω.

The obtained result is an animated plot that shows the propagation and the reflection of the wave along the line. The chosen value for Δt is 10^{-11} $[s]$ and the period of the triangular wave applied is 10^{-8} $[s]$.

2.7 Antenna array

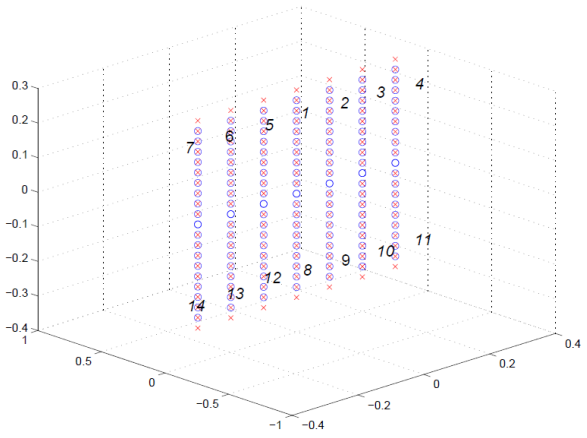

Figure 2.23: *Geometry of the antenna*

In this section we report the results obtained by the simulation of an array of filaments forming an antenna. The geometry of the objects is shown in figure (2.23).

Each wire is formed by two equal stick conductors those are excited by a current source of $2[A]$ in the middle, as shown in figure (2.24).

In figure (2.24), for simplicity, we have not represented the voltage sources due to magnetic and electrical coupling of each element with all the others.

In this problem we have considered 7 wires (each one divided in two conductors) $0.6m$ long and the distance from two consecutive wires is $0.1m$. The gap between the two parts of the conductors is $0.1mm$ and the radius of each conductor is $0.5mm$. The frequency of the system is $1[G\ Hz]$ and each of the two parts of the wire has been divided in 10 inductive elements. In this way each inductive element is about $\frac{\lambda}{10}$ long, where λ is $\lambda = \frac{c}{f} = 0.3m$.

Due to the high value of frequency, in this simulation the effect of the propagation time has be necessarily considered, while in the analysis of the Two-wire line has been neglected.

In order to consider it we have introduced the evaluation of the center to center element distances in the routines which compute the mutual partial inductance and the mutual partial coefficient of potential.

The two formulas for the partial coefficients have been modified by introducing the complex term relative to the retard:

$$\begin{aligned} L_{\alpha\beta} \approx & e^{-j\beta\Delta r}\cos(\theta)\ \frac{\mu}{4\pi}\ \frac{l_\alpha}{2}\ \sum_{i=1}^{n} w_i f(P_i) \\ p_{ij} \approx & \ e^{-j\beta\Delta r}\frac{1}{l_i l_j}\frac{1}{4\pi\varepsilon_0}\frac{l_i}{2}\sum_{i=1}^{n} w_i f(P_i) \end{aligned} \tag{2.43}$$

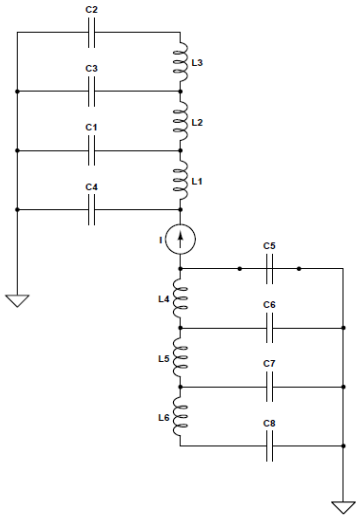

Figure 2.24: *Electrical representation of one wire of the array that forms the antenna, in this figure each of the two part of the wire has been divided in three partial inductive elements.*

where $e^{-j\beta\Delta r}$ is the term related to the retard, Δr is the center to center distance, β is the constant of propagation equal to $\beta = \frac{\omega}{c}$ and c is the speed of light.

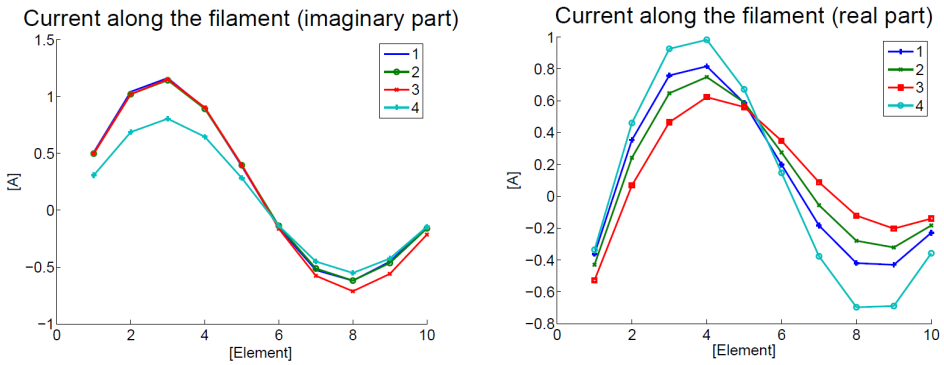

Figure 2.25: *Imaginary and Real part of the current in each element of conductors 1,2,3 and 4.*

To test the PEEC-Code we have first analysed the results in terms of branch currents of the inductive elements.

Without considering the effect of retardation due to propagation time we will achieve the wrong solution where the current remains completely real along the inductive elements of the conductors.

In the left figure (2.25) is shown the value of the imaginary part of the branch currents of conductors 1, 2, 3 and 4 while in the right figure (2.25) is shown the real part.

The conductors have been numbered as shown in figure (2.23).

To show that the solution satisfies the obvious symmetries we report in the left figure of (2.26) the values of the current obtained for the inductive elements of conductors 2 and 5, and in the right figure (2.26) the values of the current obtained for the inductive elements of conductors 1 and 8.

The values of currents along the wire have been used to compare the analytical results reached by a simplified analytical solution for this kind of "antenna problem" that, as opposed to PEEC-Code, doesn't taking into account the electromagnetic coupling between the wires.

With post-processing we have obtained the plots of the directivity of the antenna that are reported here. For clarity we show the results relative to a single wire (divided in two conductors) while the array

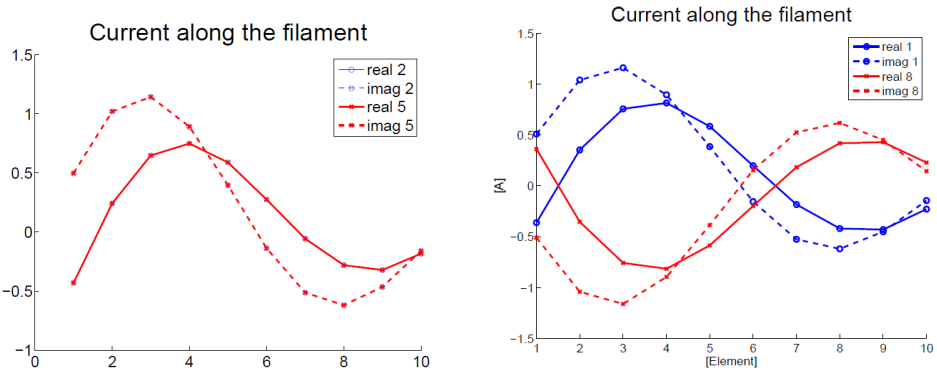

Figure 2.26: *Left: Real and imaginary part of the current for conductors 2 and 5. Right: Real and imaginary part of the current for conductors 1 and 8.*

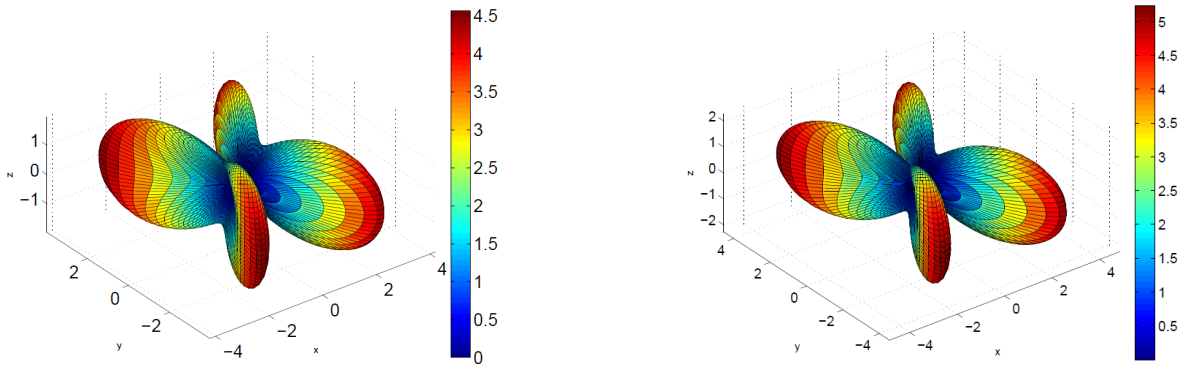

Figure 2.27: *3D directivity obtained from PEEC-Code (left) and Analytical solution (right).*

is formed by three wires.

In this simulation the frequency is $1[GHz]$, the two conductors that form the wire are $\frac{\lambda}{2}$ long where $\lambda = \frac{c}{f} = 0.3m$, the gap between the two conductors is $10^{-4}m$, the diameter is $10^{-3}m$ and the distance between two consecutive wire is equal to λ.

In figure (2.27) is reported the three dimensional directivity relative to one wire, obtained by PEEC-Code and analytical solution.

In figure (2.28) are compared the results obtained form PEEC-Code and Analytical solution in terms of directivity in plane $x-y$, while in figure (2.29) and in figure (2.30) are shown the results of directivity in plane $x-z$ and $y-z$ respectively.

The results have been also compared with the ones obtained by a Finite Elements Method (FEM) and the comparisons have been collected in two contributions, [52], [53].

PEEC-Code has shown a good capability to analyse this kind of objects and, respect to FEM, the computational time has been dramatically reduced just because PEEC method is based on the integrals formulation and it does not require the discretization of the non-active parts, while FEM method, that is based on the differential formulation, needs to discretize also the air. Minor errors of 1% have been shown in the majority of the analyses. On the other hand, PEEC-Code (filamentary) has shown its limitation when the parallel conductors have been considered very close to each other, just because the current is considered uniformly distributed in the cross section, so the skin effect and the proximity effect can not be considered. Furthermore, where the two aligned wires are considered very close to each other, the capacitive effect due to the electric coupling of the two circular surfaces of the two closer cylindrical elements becomes non negligible while, in the filament model used for the PEEC method, these surfaces have not been considered.

In order to consider also these effects a "planar" PEEC-Code (where the primary elements are conducting surfaces) should be implemented.

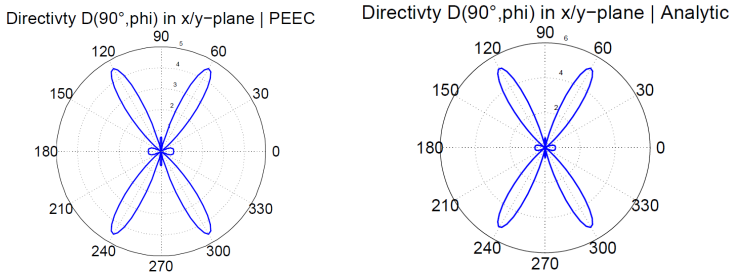

Figure 2.28: *Directivity in x-y plane obtained from PEEC-Code and Analytical solution.*

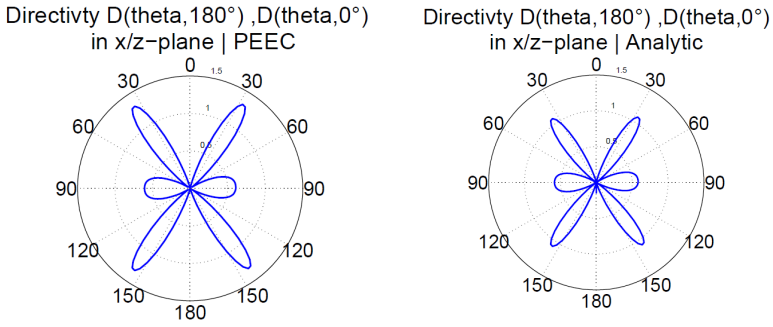

Figure 2.29: *Directivity in x-z plane obtained from PEEC-Code and Analytical solution.*

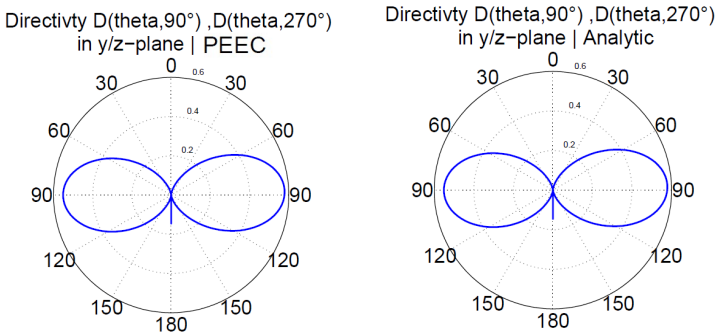

Figure 2.30: *Directivity in y-z plane obtained from PEEC-Code and Analytical solution.*

Chapter 3

PARTIAL ELEMENT, VOLUME

In this chapter we discuss about the PEEC method with hexahedral cells as primary elements. We report:

- The method and the formulas adopted for the evaluation of the partial coefficients, with some validation;
- Mesh construction method for the PEEC model;
- Discussions concerning "Special Attention";
- Some results and comparisons with analytical approach for some given geometry.

3.1 Partial Inductance Coefficient Evaluation

The general expression for the partial inductance (self or mutual) of an element is given by (1.33), that is shown here for clarity.

$$L_{p\alpha\beta} = \frac{\mu_0}{4\pi}\frac{1}{a_\alpha a_\beta}\int_{v_\alpha}\int_{v_\beta}\frac{\vec{u}_\alpha \cdot \vec{u}_\beta}{|\vec{r}_\alpha - \vec{r}_\beta|}dv_\beta dv_\alpha \tag{3.1}$$

In this chapter we consider hexahedral elements that, as opposed to filamentary case, in general allow the flow of current in any direction.
From now on, with the term "hexahedron" we mean a polyhedron with six quadrilateral faces.
In literature it is possible to find formulas that compute the self and mutual partial inductance of parallelepipeds crossed by current which flows in a given direction, normal to two opposed faces, [4], [5], [11]. Unfortunately, as for the filamentary case, these formulas are given only for elements placed in some mutual particular position, so they became of little use for the study of problems with complex geometries. Furthermore, these formulas are given for parallelepipeds and not for hexahedra, so, for these reasons, in this thesis they are not be used for the evaluation of the partial coefficients, except for the self partial inductance. The problem related to the evaluation of the coefficients is given by the fact that doesn't exist an analytical solution of the double volume integral of $\frac{1}{|\vec{r}_\alpha - \vec{r}_\beta|}$, where $|\vec{r}_\alpha - \vec{r}_\beta|$ is the distance between two generic points in the two considered volumes.
So, in order to overcome this problem, we have to adopt a numerical method for the evaluation of the coefficients, as done for the filamentary case.

3.1.1 Evaluation of 1/R Integral

The evaluation of the double volume integral shown in (3.1) is the main problem that must be addressed. As already said, it doesn't exist an analytical solution for the double integral, instead it is possible to solve analytically one volume integral of $\frac{1}{R}$, where R is the function that gives the distance between a given point and a general point inside the considered volume. In [19] it is explained how to compute analytically the the Magnetic vector Potential, $\vec{A}$, produced by a uniform current density inside an arbitrary polyhedron.

$$\vec{A}(\vec{r}) = \frac{\mu_0 \vec{J}}{4\pi} \int_V \frac{d^3 r\prime}{|\vec{r} - \vec{r}\prime|} \tag{3.2}$$

In (3.2) it is clearly shown the dependence of $\vec{A}$ from the volume integral of $\frac{1}{R}$, so we can use the approach explained in [19] in order to solve exactly one of the two volume integrals in (3.1). Here we report briefly the steps.

We can introduce the identity (3.3) following [40], where the "prime" on ∇ refers to its evaluation in points $\vec{r}\prime$.

$$\frac{1}{|\vec{r} - \vec{r}\prime|} = \nabla\prime \cdot \left(\frac{\vec{r} - \vec{r}\prime}{2|\vec{r} - \vec{r}\prime|} \right) \tag{3.3}$$

Applying Gauss's theorem and (3.3) in (3.2) we can obtain (3.4).

$$\vec{A}(\vec{r}) = \frac{\mu_0 \vec{J}}{8\pi} \sum_{S_f \in \partial V} \int_{S_f} \frac{(\vec{r}\prime - \vec{r}) \cdot \vec{n}_f}{|\vec{r} - \vec{r}\prime|} d^2 r\prime \tag{3.4}$$

where ∂V is the boundary of the polyhedron and $\vec{n}_f$ is the outgoing normal unit vector which is constant over each polygonal face $S_f \in \partial V$. In a plane face the quantity $(\vec{r}\prime - \vec{r}) \cdot \vec{n}_f$ is constant, so we can bring it outside the integral and compute its value in an arbitrary points r_f of the face. In this way we can reach:

$$\vec{A} = \frac{\mu_0 \vec{J}}{8\pi} \sum_{S_f \in \partial V} (\vec{r}_f - \vec{r}) \cdot \vec{n}_f W_f(\vec{r}) \tag{3.5}$$

where:

$$W_f(\vec{r}) = \int_{S_f} \frac{d^2 r\prime}{|\vec{r} - \vec{r}\prime|} \tag{3.6}$$

Now the problem is the evaluation of W_f and we need to introduce the identity (3.7).

$$\frac{1}{|\vec{r} - \vec{r}\prime|} = \vec{n}_f \cdot \nabla\prime \times \left(\vec{n}_f \times \frac{\vec{r}\prime \vec{r}}{|\vec{r} - \vec{r}\prime|} \right) - \frac{[(\vec{r}\prime - \vec{r}) \cdot \vec{n}_f]^2}{|\vec{r}\prime - \vec{r}|^3} \tag{3.7}$$

Considering that the quantity $(\vec{r}\prime - \vec{r}) \cdot \vec{n}_f$ is constant over the face and substituting it with $(\vec{r}_f - \vec{r}) \cdot \vec{n}_f$, where $\vec{r}_f$ is an arbitrary point of the face, we can obtain (3.8).

$$W_f(r) = \oint_{\partial S_f} \frac{\vec{n}_f \times (\vec{r}\prime - \vec{r}) \cdot d\vec{r}\prime}{|\vec{r}\prime - \vec{r}|} - [(\vec{r}_f - \vec{r}) \cdot \vec{n}_f] \int_{S_f} \frac{(\vec{r}\prime - \vec{r} \cdot \vec{n}_f}{|\vec{r}\prime - \vec{r}|^3} d^2 r\prime \tag{3.8}$$

Where ∂S_f is the boundary of the face S_f formed by $l_e \in S_f$. The second integral of (3.8) is the solid angle subtended by the polygon S_f, $\Omega(\vec{r})$.

Now we can obtain (3.9):

$$W_f(\vec{r}) = \sum_{l_e \in \partial S_f} \int_{l_e} \vec{n}_f \times \frac{\vec{r}\prime - \vec{r}}{|\vec{r}\prime - \vec{r}|} \cdot \vec{u}_e dr\prime - [(\vec{r}_f - \vec{r}) \cdot \vec{n}_f] \Omega(\vec{r}) \tag{3.9}$$

Where u_e is the unit vector along one edge of the face which orientation is given in according to $\vec{n}_f$. In analogy with what we have done previously we can bring out from the integral the quantity $\vec{n}_f \times (\vec{r}\prime - \vec{r}) \cdot \vec{u}_e$, that is constant at the relative edge, so it can be replaced by $\vec{n}_f \times (\vec{r}_e - \vec{r}) \cdot \vec{u}_e$, where $\vec{r}_e$ is an arbitrary fixed point of the edge.

Now we can define (3.10), that is the same integral that we have found in the evaluation of the partial coefficients in PEEC filamentary method.

$$w_e(\vec{r}) = \int_{l_e} \frac{dr\prime}{|\vec{r}\prime - \vec{r}|} \tag{3.10}$$

This integral has the analytical solution given by (3.11)

$$w_e(\vec{r}) = ln\left(\frac{|\vec{r}_2 - \vec{r}| + |\vec{r}_1 - \vec{r}| + |\vec{r}_2 - \vec{r}_1|}{|\vec{r}_2 - \vec{r}| + |\vec{r}_1 - \vec{r}| - |\vec{r}_2 - \vec{r}_1|}\right) \tag{3.11}$$

Where $\vec{r}_1$ and $\vec{r}_2$ are the endpoints of the edge. (3.11) shows a singularity when $\vec{r}$ belongs to the edge l_e, but it is completely removed in (3.13) by $\vec{n}_f \times (\vec{r}_e - \vec{r}) \cdot \vec{u}_e$. So, to avoid the numerical singularities, it is possible to modify (3.11) by substituting the norm with (3.12).

$$|\vec{r}\prime - \vec{r}| = \sqrt{|\vec{r}\prime - \vec{r}|^2 + \epsilon^2} \tag{3.12}$$

So the final expression of W_f is (3.13).

$$W_f(\vec{r}) = \sum_{l_e \in \partial S_f} \vec{n}_f \times (\vec{r}_e - \vec{r}) \cdot \vec{u}_e w_e(\vec{r}) - [(\vec{r}_f - \vec{r}) \cdot \vec{n}_f]\Omega(\vec{r}) \tag{3.13}$$

About the evaluation of the solid angle $\Omega(\vec{r})$, it is convenient to split the faces in triangles. Indeed, for triangular faces exist the analytical expression for the solid angle subtended by the point $\vec{r}$, (3.14).

$$\begin{aligned} \Omega_T(\vec{r}) &= 2Arctan[\frac{(\vec{r}_1 - \vec{r}) \cdot (\vec{r}_2 - \vec{r}) \times (\vec{r}_3 - \vec{r})}{D} \\ D &= |\vec{r}_1 - \vec{r}||\vec{r}_2 - \vec{r}||\vec{r}_3 - \vec{r}| \\ &+ |\vec{r}_3 - \vec{r}|(\vec{r}_1 - \vec{r}) \cdot (\vec{r}_2 - \vec{r}) \\ &+ |\vec{r}_2 - \vec{r}|(\vec{r}_1 - \vec{r}) \cdot (\vec{r}_3 - \vec{r}) \\ &+ |\vec{r}_1 - \vec{r}|(\vec{r}_2 - \vec{r}) \cdot (\vec{r}_3 - \vec{r}) \end{aligned} \tag{3.14}$$

Then, following the steps explained above, it is possible to obtain the exact value of Magnetic vector Potential, $\vec{A}$, produced by a uniform current density inside an arbitrary polyhedron in any point of the space. Moreover it is easy to reach also an expression for the integral of $\frac{1}{R}$, (3.15).

$$I_v(\vec{r}) = \frac{1}{2} \sum_{S_f \in \partial V} (\vec{r}_f - \vec{r}) \cdot \vec{n}_f W_f(\vec{r}) \tag{3.15}$$

By using (3.15) in (3.1) it is possible to reach (3.16).

$$L_{p\alpha\beta} = \frac{\mu_0}{4\pi} \frac{\vec{J}_\alpha \cdot \vec{J}_\beta}{a_\alpha a_\beta} \int_{v_\alpha} I_v(\vec{r})\, dv_\alpha \;=\; \frac{\mu_0}{4\pi} \frac{\vec{J}_\alpha \cdot \vec{J}_\beta}{a_\alpha a_\beta}\, I_{2v} \tag{3.16}$$

Where the current densities $\vec{J}_\alpha$ and $\vec{J}_\beta$ have been bring out from the integral, because they are uniform inside the volumes.

Now we can evaluate the second volume integral in (3.16) using Gauss-Legendre, in analogy with the filamentary case.

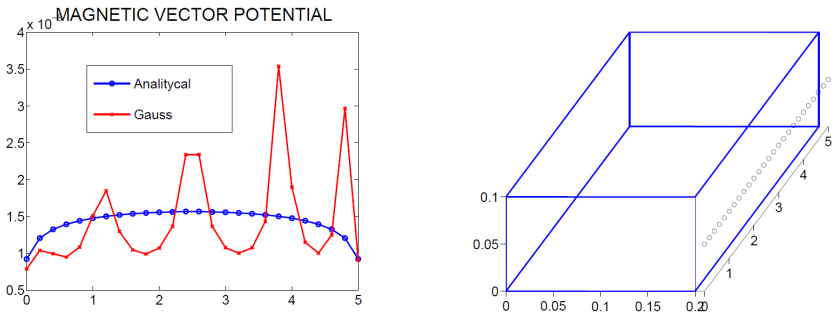

Figure 3.1: *Comparison Analytical method* [19] *and Gauss-Legendre method*

In this way by defining I_{2v} as the integral of $I_v(\vec{r})$ in the volume v_α, we can obtain (3.17).

$$I_{2v} = \sum_{i=1}^{N} I(P_i) w_1(P_i) w_2(P_i) w_3(P_i) J_{3D} \tag{3.17}$$

Where P_i, with $i = 1 \cdots N$, are the Gauss points inside the volume, w_1, w_2 and w_3 are the weights related to the Gauss points in the three directions and J_{3d} is the Jacobian of the transformation.
By doing this, we can obtain a general expression for the partial inductance coefficient, which can be implemented in the code. Obviously, the evaluation of the double volume integral can be done also using the Gauss-Legendre method for both the volume integral (with two different orders of Gauss for the evaluation of the self coefficient, in order to avoid numerical singularities). This pure numerical approach gives good results when the two hexahedra are quite distant from each other, while it shows more significant errors when the two volumes are close to each other.

In figures (3.1) and (3.2) it is reported the value of Magnetic vector Potential produced by a uniform current that cross the shown hexahedron. The values have been evaluated by the analytical method presented in [19] (and reported above) and by the numerical method; the amplitude of $\vec{A}$ has been evaluated in in the black points.

We can see that the two methods give similar results when the points are quite distant from the hexahedron, while the numerical errors are more relevant for the evaluation of the Magnetic vector Potential in points very close to the solid. The degree of Gauss-Legendre used for the numeric integration is five (for all the three direction).

For this reason we have decided to use the analytical approach for the evaluation of the first $\frac{1}{R}$ integral; the only drawback is that this approach seems quite expensive from a computational cost point of view.

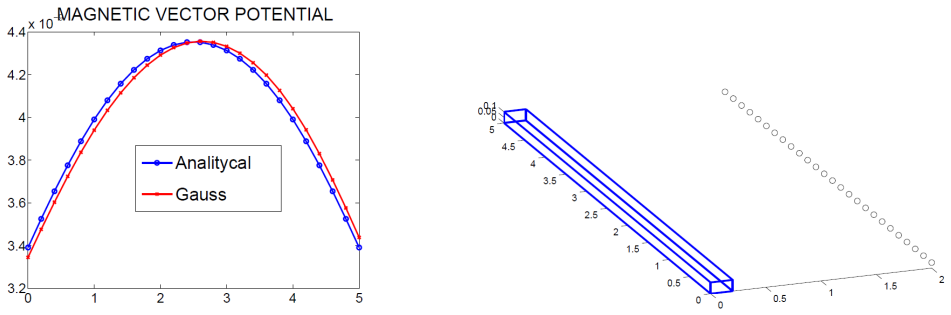

Figure 3.2: *Comparison Analytical method* [19] *and Gauss-Legendre method*

3.1.2 Current Density

The other relevant term in (3.1) is the dot product between the two unitary and uniform current densities which flow in the two hexahedra.
For our purpose, we will consider hexahedra crossed by current density that enters the volume from a given face and goes out from the opposite face; the direction of the current density must give no flow on the four lateral faces.

For the simply case of parallelepipeds, the direction of vector $\vec{J}$ that satisfies this goal is given by the line normal to the opposed faces crossed by the current, but this is not valid for the more general case of hexahedral elements.

In order to satisfy this goal, we follow [35], where it is reported a method which allows to find the correct direction of the current density vector. For our purpose this expression is given by (3.18).

$$\vec{J} = \frac{C_{F_{out}} - C_{F_{in}}}{|C_{F_{out}} - C_{F_{in}}|} \tag{3.18}$$

Where $C_{F_{out}}$ and $C_{F_{in}}$ are the centroids of the outgoing face and incoming face, respectively.

3.1.3 Evaluation of self Partial Inductance Coefficient

The evaluation of the self partial inductance coefficient can be performed in the same way and with the same code used for the evaluation of the partial mutual inductance coefficient, just because the analytical method for the evaluation of the $\frac{1}{R}$ doesn't give any singularities for the Gauss points inside the volume itself.
As alternative, in literature we can find some analytical formulas for the evaluation of this coefficient. These formulas refer to parallelepipeds crossed by a uniform current, [5], [11], [16]. The formula in [5] is shown in (3.19).

$$\begin{aligned}\frac{L_{self}}{l} = \frac{2\mu_0}{\pi}\Bigg\{ & \frac{\omega^2}{24u}\left[ln\frac{1+A_2}{\omega} - A_5\right] + \frac{1}{24u\omega}\left[ln(\omega + A_2) - A_6\right] \\ & + \frac{\omega^2}{60u}(A_4 - A_3) + \frac{\omega^2}{24}\left[ln\frac{u+A_3}{\omega} - A_7\right] + \frac{\omega^2}{60u}(\omega - A_2) + \frac{1}{20u}(A_2 - A_4) \\ & + \frac{u}{4}A_5 - \frac{u^2}{6\omega}tan^{-1}\frac{\omega}{uA_4} + \frac{u}{4\omega}A_6 - \frac{\omega}{6}tan^{-1}\frac{u}{\omega A_4} + \frac{A_7}{4} \\ & + \frac{1}{6\omega}tan^{-1}\frac{u\omega}{A_4} + \frac{1}{24\omega^2}\left[ln(u + A_1) - A_7\right] + \frac{u}{20\omega^2}(A_3 - A_4) \\ & + \frac{1}{60\omega^2 u}(1 - A_2) + \frac{1}{60u\omega^2}(A_4 - A_1) + \frac{u}{20}(A_3 - A_4) \\ & + \frac{u^3}{24\omega^2}\left[ln\frac{1+A_1}{u} - A_5\right] + \frac{u^3}{24\omega}\left[ln(\frac{\omega + A_3}{u}) - A_6\right] \\ & + \frac{u^3}{60\omega^2}\left[(A_4 - A_1) + (u - A_3)\right]\Bigg\}\end{aligned} \tag{3.19}$$

Where:

$$\begin{aligned} A_1 &= \sqrt{1+u^2} \quad A_2 = \sqrt{1+\omega^2} \\ A_3 &= \sqrt{\omega^2+u^2} \quad A_4 = \sqrt{1+\omega^2+u^2} \\ A_5 &= ln\frac{1+A_4}{A_3} \quad A_6 = ln\frac{\omega + A_4}{A_1} \\ A_7 &= ln\frac{u+A_4}{A_2} \quad u = \frac{l}{w} \quad \omega = \frac{t}{w} \end{aligned} \tag{3.20}$$

Where l is the length, t and w the height and base of the incoming face respectively (equal to the outgoing face).

This formula gives the correct result only for parallelepipeds but it could be also used as alternative to the numerical method, when the considered hexahedron is slightly distorted and it allows to find the parameters related to an "equivalent" parallelepiped.

However, the formula can be used in order to test the numerical approach proposed for the evaluation of the partial self coefficient of inductance of a parallelepiped. We report the results obtained for a parallelepiped with square cross section of $1m^2$ and $4m$ long: numerical approach gives $1.607856\ 10^{-6}[H]$ while equation (3.19) gives $1.60775\ 10^{-6}[H]$.

3.1.4 Cross section

The last two terms in equation (3.1) are the two cross section of the two elements crossed by the uniform current densities.

These two terms are outside the integral just because the formula refers to parallelepipeds, which obviously have constant cross section. The right expression of the *partial inductance coefficient* for a

non-orthogonal cell (like a irregular hexahedron) crossed by a uniform current would be more complex and it requires a pure numerically strategy for the evaluation. The expression is reported in [8] and in the same paper it is proposed a numerical method for the calculation.

For our purpose we will consider the "equivalent" cross section of the parallelepiped which has the same volume of the considered hexahedron and a length equal the the distance between the centroids of the two faces crossed by the current.

With this approach the formulation is not exact from a analytically point of view but it allows to consider the simplified expression of the *partial inductance coefficient* for orthogonal cells (which has got a more accurate method of evaluation) and gives good results also if applied to non-orthogonal cells "fairly" regular.

3.2 Method Validation for Partial Inductance Coefficients

In this section we are going to validate the method used for the evaluation of the *partial inductance coefficients* for hexahedral elements.
In analogy with what we have done for the filamentary case, we are going to evaluate the inductance of a circular loop with rectangular (or square cross section) and we are going to compare the results with a semi-analytical formula found in [16]. The loop has been divided in a certain number of elements (that correspond to the sides of equivalent electrical circuit) and each of them has been divided in two hexahedra, as shown in figure (3.2), where each element is represented with its unique color.

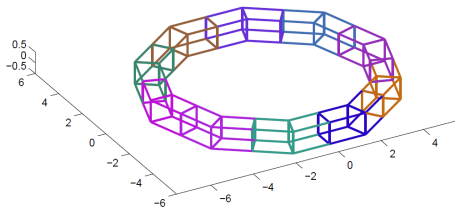

Figure 3.3: *Circular Loop with square cross section discretised by hexahedral mesh*

In this way, each self partial inductance coefficient of an element (that is formed by two hexahedra) must be calculated how shown in (3.21).

$$L_{self} = L_{11} + L_{12} + L_{21} + L_{22} \tag{3.21}$$

where the terms L_{ij}, with $i, j = 1, 2$, are the entrances of the local matrix of inductance, $\mathbf{L}_{local}$, related to the two hexahedra which form the elements: L_{ii} is the self partial local coefficient of inductance and L_{ij} is the mutual partial local coefficient of inductance (so, in general, we have $L_{ij} = L_{ji}$).

The mutual partial inductance coefficient is calculated in a similar way, how expressed in (3.22).

$$L_{mutual_{ij}} = L_{ac} + L_{ad} + L_{bc} + L_{bd} \tag{3.22}$$

where the subscript a, b, c and d are related to the two hexahedra which form the two elements: a and b are the two hexahedra of element i, c and d are the two hexahedra of element j.

The considered loop has a medium radius of 5 m and a square cross section of 1 m^2.
The self and mutual coefficients of the elements are the entrances of $\mathbf{L}$ matrix and, by the summation of all the entrances of the matrix, it is possible to achieve the value of the self inductance of the loop. The results obtained by the PEEC-method have been compared with the semi-analytical formula for this kind of loop given by [16] and also with a circular loop which has a circular cross section with the same area of square cross section.

Table, Inductance Circular Loop with Square Cross Section, $[\mu H]$

Number of elements	Analytic square	Analytic circular	PEEC
10	15.718	15.778	14.943
15			15.506
19			15.723

3.3 Partial Coefficient of Potential Evaluation

In this section we are going to discuss about the calculation of *Partial Coefficient of Potential* for the volume PEEC-Code.
The evaluation of these coefficients is quite simpler than the evaluation of the inductance coefficients, just because the charge hasn't the directional dependence, as opposed to the current. For clarity we report here the general expression of the coefficient.

$$p_{ij} = \frac{1}{4\pi\varepsilon_0 S_i S_j} \int_{S_i} \int_{S_j} \frac{1}{|\vec{r}_i - \vec{r}_j|} dS_i dS_j \tag{3.23}$$

In this chapter we are considering the volume PEEC method, so the partial elements of capacitance that we must consider are the free surfaces of the hexahedra. The problem of the evaluation of the partial coefficient of potential is one more time related to the evaluation of the $\frac{1}{R}$ surface integral (R is the distance from two points that belong to the two surfaces).
Also for this coefficient some analytical or semi-analytical formulas are present in literature but only for quadrilateral surfaces that are in some particular mutual position, [4], [5], [10]. Moreover, the particular case of self partial coefficient of potential is little discussed in literature, so, also for its evaluation, we have to use a numerical approach.
Such as for the evaluation of inductance coefficient, the adopted approach can be numeric only or based on the analytical method shown in subsection (3.1.1).

For the evaluation of the surface double integral of $\frac{1}{R}$ it is sufficient to solve (3.6), for the first integral, and to use the Gauss-Legendre numerical method for the second integral.

The final expression that it is possible to implement in the code is shown in (3.24).

$$p_{ij} = \frac{1}{4\pi\epsilon_0 S_i S_j} \sum_{k=1}^{N} I_S(P_k) w_1(P_k) w_2(P_k) w_3(P_k) J_{3D} \tag{3.24}$$

where $I_S(\bullet)$ is the one surface integral evaluated in the Guass points of the second surface, w_i are the Gauss weights, with $i = 1, 2, 3$, and J_{3D} is the Jacobian of the transformation.

About the self partial coefficient of potential, it has been evaluated with the same numerical method by introducing the modified normal (3.12), needed to remove the singularities.

The method described above allows to find the self and mutual coefficients between quadrilateral surfaces but, for our purpose, the capacitive elements associated to a node of the equivalent electric circuit in general are formed by many quadrilateral surfaces, which give the boundary of the hexahedron. As example, if we want to evaluate the mutual partial coefficient of potential between two hexahedra free in the space, we have to evaluate a local matrix, $\mathbf{P}_{local}$, which (in this particular case) is a 12×12 matrix, where the four blocks matrices 6×6 shown below are:

- $\mathbf{P}_{11}$ is related to the self and mutual partial coefficients of potential of the faces of hexahedron 1;
- $\mathbf{P}_{22}$ is related to the self and mutual partial coefficients of potential of the faces of hexahedron 2;
- $\mathbf{P}_{12} = \mathbf{P}_{21}$ is related to the mutual partial coefficients of potential between the faces of the two hexahedra.

$$\mathbf{P}_{local_{12\times12}} = \begin{bmatrix} P_{11_{6\times6}} & P_{12_{6\times6}} \\ P_{21_{6\times6}} & P_{22_{6\times6}} \end{bmatrix}$$

To reach the value of the mutual coefficient of potential it is necessary to invert the $\mathbf{P}_{local}$ matrix, in this way we obtain the local matrix of capacitance $\mathbf{C}_{local} = \mathbf{P}_{local}^{-1}$ and by summing all the terms together we can find the value of capacitance between the two hexahedra, $\mathbf{c}_{ij}$. The mutual partial coefficient of capacitance is finally obtained by the inversion of the coefficient of capacitance: $\mathbf{p}_{ij} = \mathbf{c}_{ij}^{-1}$.

3.4 Method Validation for Partial Coefficients of Potential

In this section we want to validate the method used for the evaluation of the *partial coefficients of potential* for the quadrilateral faces of hexahedra elements.
In analogy with what we have done for the filamentary case, we compare the results in terms of *Maxwell Capacitance Matrix*, obtained by our PEEC-Code, with the results obtained by the open source software *Fastercap*.

The geometry taken under analysis is the one shown in figure (3.4). We want to evaluate the matrix of capacitance related to the two elements (parallelepipeds). The smaller one is inside the other one and we are considering only the four lateral faces for both of them.

The bigger one is a parallelepiped $0.01 \times 0.001 \times 0.1m$. The smaller one is a parallelepiped $0.002 \times 0.002 \times 0.1m$ for the first case and $0.005 \times 0.005 \times 0.1m$ for the second case.

In the matrices below we report the results obtained from the two analyses, by comparing PEEC and *Fastercap* results. For the first case we have used a number of Gauss points in any direction equal to 3 and the objects have been divided in 5 elements, for the second case we have chosen a number of Gauss equal to 4 and we have divided the objects in 7 elements.

1) Case :

- *Fastercap* $10^{-11}[F]$

$$\mathbf{C} = \begin{bmatrix} +0.57214 & -0.3763 \\ -3.77346 & +3.8027 \end{bmatrix}$$

- *PEEC-Code* $10^{-11}[F]$

$$\mathbf{C} = \begin{bmatrix} +0.5746 & -0.3608 \\ -0.3608 & +0.3602 \end{bmatrix}$$

2) Case:

- *Fastercap* $10^{-11}[F]$

$$\mathbf{C} = \begin{bmatrix} +1.146 & -0.927 \\ -0.930 & +0.935 \end{bmatrix}$$

- *PEEC-Code* $10^{-11}[F]$

$$\mathbf{C} = \begin{bmatrix} +1.143 & -0.926 \\ -0.914 & +0.912 \end{bmatrix}$$

The matrix of capacitance $\mathbf{C}$ has been reached by post-processing after the evaluation of $\mathbf{P}$ matrix. $\mathbf{P}$ matrix has been inverted and the entrances of the four blocks of the inverted matrix has been summed all together, in order to obtain the 2×2 elements of the Maxwell Capacitance Matrix.

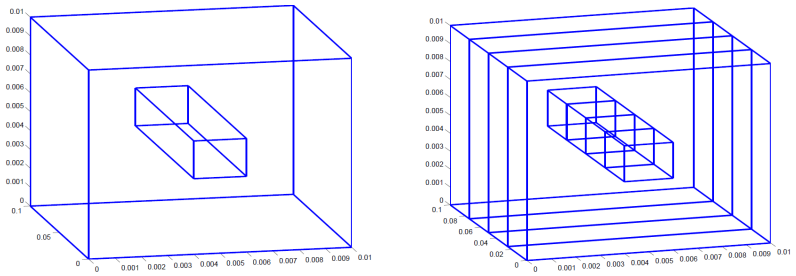

Figure 3.4: *Analized geometry (Left) and Discretization (Right) for the Validation of the Evaluation of Partial Coefficient of Potential Method.*

3.5 Partial Resistance Coefficient Evaluation

In this section we want shortly discuss about the evaluation of Partial Resistance Coefficient.
The general expression for the evaluation of this coefficient for a hexahedron is given by (3.25).

$$R_{\alpha\alpha} = \int_{l_\alpha} \frac{\rho_\alpha}{S_\alpha} dl_\alpha \tag{3.25}$$

where l_α is the the line which connects the two centroids of input and output faces, ρ_α is the resistivity of the element and S_α is the surface normal to the direction of l_α. In general, S_α varies along l_α while is a constant value only for parallelepipeds.

In this thesis the *partial inductance coefficients* have been evaluated exactly only for parallelepipeds and the "equivalent" parallelepiped has been considered for hexahedral cells.
Also for the evaluation of partial coefficient of resistance this approach has been used: the coefficient is evaluated exactly for parallelepipeds while for hexahedra the "equivalent" parallelepiped has been considered.
In this way the equation for the partial resistance coefficient becomes:

$$R_\alpha = \rho_\alpha \frac{l_\alpha}{S^*_\alpha} \tag{3.26}$$

where S^*_α is evaluated as: $S^*_\alpha = \frac{v_\alpha}{l_\alpha}$, and v_α is the volume of the hexahedron.

As done for the *partial inductance coefficient*, the *partial resistance coefficient*, which is evaluated for *branch elements*, is computed by considering the two hexahedra that compose the *branch element*. These two hexahedra in general can be made by different materials.

3.6 Meshing for PEEC volume model

In this section we are going to explain how to discretize the objects in three dimensions for the PEEC volume model.

3.6.1 Nodal mesh, Nodal hexahedron

First we have to define the *nodal discretization*, that consists to determine the hexahedra related to the nodes of the electrical equivalent circuit (which represents the analysed objects). Each of these *nodal hexahedron* represents a *capacitive element* and for each of them we have to compute the self and mutual coefficient of potential between all the others *capacitive elements* and the infinity (self coefficient).
These partial coefficients of potential are evaluated only considering the "free faces" of the elements, which are the unshared faces with the other *nodal hexahedra*.

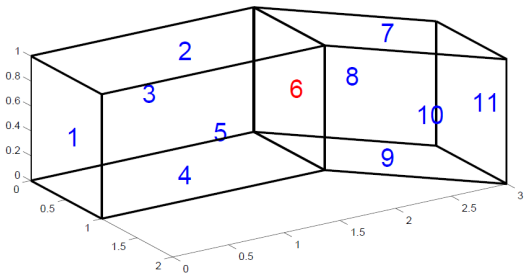

Figure 3.5: *"Free faces" (blue) and "Shared faces" (red) for two nodal hexahedra*

In this way, considering the example in figure (3.5), in order to evaluate the self coefficient of potential of the two hexahedra we have to compute the local matrix $\mathbf{P}_{local\ 5\times5}$ related to faces with blue ID while, for the mutual coefficient of potential between the two hexahedra, we have to compute $\mathbf{P}_{local\ 10\times10}$.

From the equivalent electrical circuit point of view, the two hexahedra can be seen like two nodes which are connected to the infinity node through the pseudo capacitance $\frac{1}{p_{ii}}$ (where p_{ii} is the self coefficient of potential) and through a voltage generator that represents the electrical coupling between the *nodal hexahedron* and all the others.

In our volume PEEC-Code every "appended" load and source generator is connected to a certain nodal hexahedron through a certain face, so also the face (or faces) of the hexahedron that are connected to some appended circuit element must be considered such as shared faces, so they are not taking into account for the evaluation of the coefficients (it is also possible to consider these faces like "free" and "shared" faces at the same time, if necessary).

3.6.2 Side mesh, Face hexahedron

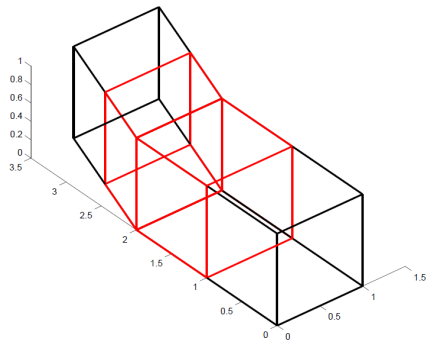

Figure 3.6: *Two* nodal hexahedra *(black) connected by a* face hexahedron *(red).*

After the construction of the *nodal mesh* it is automatically defined also the *side mesh*, that is the definition of the elements which connect two consecutive nodes. In literature the topic of meshing three dimensional structures for PEEC model has not been sufficiently treated yet. In this work we refer to [33] and [34].

In order to allow the curvature of the geometry, the *side elements* (or *face hexahedra*) are composed by two hexahedra, that have the middle face in common. The first hexahedron (that correspond to one of the two parts of the side) has the first face internal to the "start" *nodal hexahedron*: the four vertices which compose the face are obtained by the the average between the coordinates of the points of the considered shared face (the face that connects the "start" *nodal hexahedron* and the "end" *nodal hexahedron*) and the opposite face to the shared face in the "start" *nodal hexahedron*; the second face is the shared face.

The second hexahedron has the first face in common with the first hexahedron (the shared face) and the second face is obtained by the average of the vertices that form the shared face and the opposite face

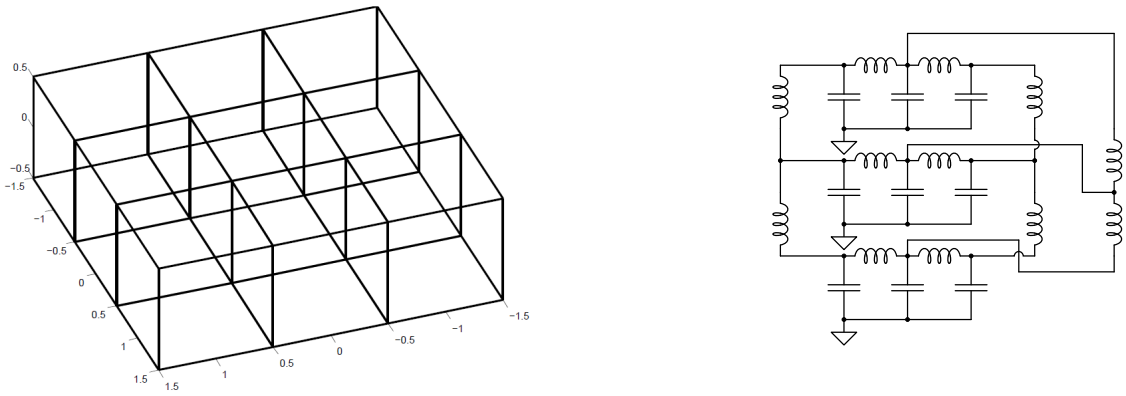

Figure 3.7: $3 \times 3 \times 1$ *plate and its electrical equivalent circuit.*

to the shared face in the "end" *nodal hexahedron*.

By doing this, each partial inductance coefficient must be evaluated considering these elements formed by two hexahedra, with the face which they refer in common. The current flows through the two hexahedra how explained in subsection (3.1.2): it goes from face one to face two and the partial inductance coefficient must be evaluated how explained in section (3.2).

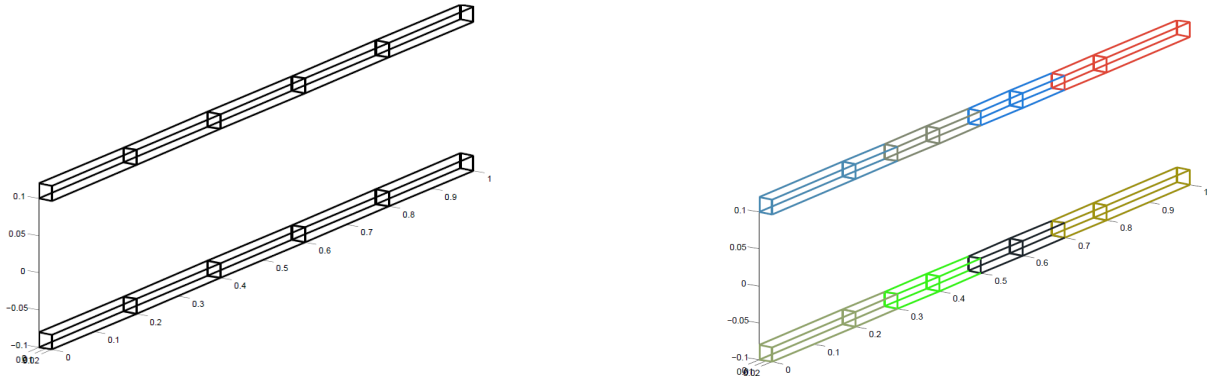

Figure 3.8: *Nodal and side dicretization for a Two-wire line* .

In general the code must consider objects discretized in three dimensions (like the plate in figure (3.7) that is disctetized by only one element in a direction and by three elements in the other two directions). It is easy to understand that in this general condition the *face hexahedra* related to the same *nodal hexaheron* could intersect. The "semi-numerical" method used for the evaluation of the partial inductance coefficient allows to evaluate the coefficient between two elements that intersect (if using the modified normal that avoids the numerical singularities).
Also, note that when the hexahedra are parallelepipeds these mutual coefficients are zeros just because the two hexahedra have the current density vectors perpendicular to each other.

In figure (3.7) it is represented a simple plate discretized by $3 \times 3 \times 1$ *nodal hexahedra* and its equivalent electrical circuit. For simplicity and clarity for each node and each side we have represented only a capacitance and an inductance, omitting the voltage sources that represent the mutual coupling between the elements.

The only exception in the *side meshing* must be done for the shared faces which have their relative opposite face, in the "start" or "end" *nodal hexahedron*, that is a free face. For these shared faces one of the hexahedron that composes the side element must extend until the free face, otherwise we don't consider correctly the boundary part of the disretized object. In figure (3.8) is shown the *nodal* and *side*

discretization performed for a two wire line, it is possible to see that the start and end sides are longer than the others for the reason explained above.

3.7 PEEC volume model: Special Attention

In this section we want to focus on some particular topic related to PEEC volume model.

3.7.1 Inductance Evaluation

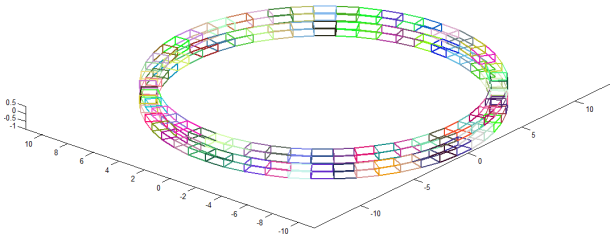

Figure 3.9: *Two loops geometry.*

In the previous chapters we have considered the possibility to reach the value of the inductance of an object simply by summing all the entrances of the **L** matrix.

This approach is not always applicable, for example if the loop analysed in section (3.2) was been discretized by more than one element in the cross section we should have compute the value of the inductance in a different way, because the presence of sides which connects two non-consecutive *nodal hexahedra* along the toroidal direction in the entrances of the **L** matrix.
These branches are not interested by current flow in normal condition.

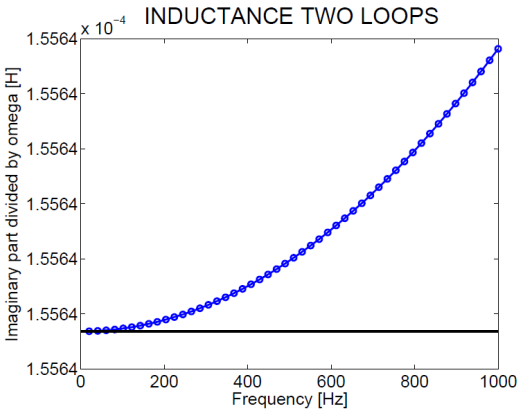

Figure 3.10: *Inductance values extracted from the imaginary part of the impedance (blue) vs Inductance value evaluated from* **L** *matrix (black).*

In general, in order to reach the equivalent inductance value of an object (at some given frequency), we have to evaluate the imaginary part of the impedance seen from the two nodes where the voltage source is connected.

Here we report results in terms of impedance and inductance of two circular loops with rectangular cross section fed by a voltage source connected to the ends of the two loops; the two loops are connected

to each other by an appended side with zero inductance and zero resistance. The medium radius of the loops is $10.5m$, the cross section is $0.5m \times 1m$ instead the distance between the loops is $1m$.

In figure (3.10) is shown the trend of the imaginary part of the impedance divided by $2\pi f$ considering ideal loops (zero resistivity) compared to the value obtained from the $\mathbf{L}$ matrix. Instead, in figure (3.11), it is shown the real and imaginary part of the impedance, considering an ideal (zero resistivity) and a real loop ($2\ 10^{-4}[\Omega m]$). The values have been evaluated in the frequency domain and it is possible to see the anti-resonance peak when it happens the transition form inductive to capacitive behaviour.

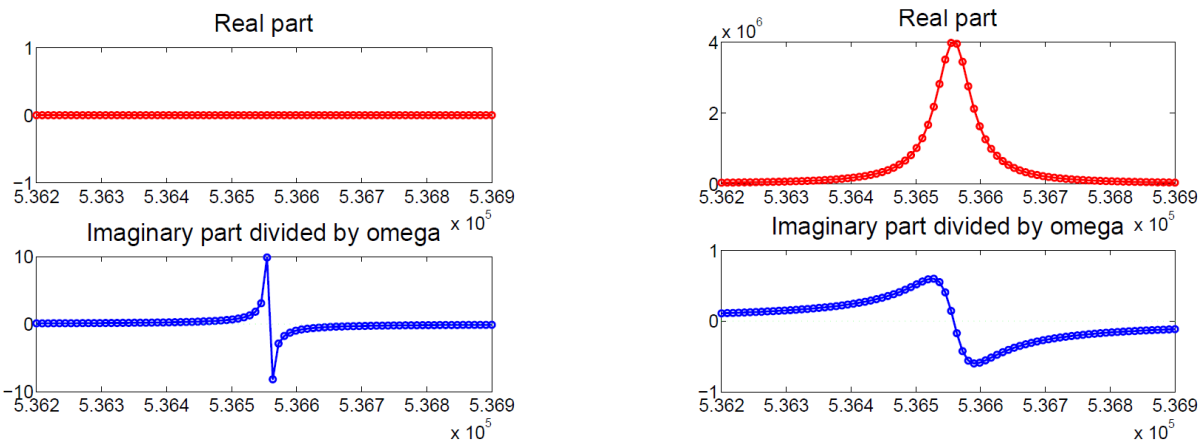

Figure 3.11: *Ideal and Real Conductor, Anti-Resonance Condition.*

3.7.2 Completely Embedded Nodal Hexahedron

In general, for a massive object, it is sometimes interesting to have a fine discretization in order to see the fields distribution inside the structure. So, it is necessary to know how to behave when an element is completely embedded by others elements (for example a cube divided in $3 \times 3 \times 3$ elements has the internal element (2,2,2) completely embedded by the other elements).

These elements don't have any free faces so they don't have any electrical coupling with the others. The related row and column in the $\mathbf{P}$ matrix must have "zero" in all the off diagonal entrances and "one" in the diagonal entrance.

Indeed the system that we have to solve must be slightly changed respect the one reported in subsection (2.5.3).

$$\begin{bmatrix} \mathbf{A}^T & (\mathbf{R} + j\omega\mathbf{L}) \\ j\omega\mathbf{1} & -\mathbf{PA} \end{bmatrix} \begin{bmatrix} \mathbf{V} \\ \mathbf{I} \end{bmatrix} = \begin{bmatrix} \mathbf{Vs} \\ \mathbf{PIs} \end{bmatrix} \tag{3.27}$$

The system shown in (3.27) must be changed in (3.28), where $\mathbf{1}^\star$ is the diagonal matrix with ones in the diagonal entrances related to *nodal hexahedra* that have at least one free face, and zeros in the diagonal entrances related to completely embedded elements.

$$\begin{bmatrix} \mathbf{A}^T & (\mathbf{R} + j\omega\mathbf{L}) \\ j\omega\mathbf{1}^\star & -\mathbf{PA} \end{bmatrix} \begin{bmatrix} \mathbf{V} \\ \mathbf{I} \end{bmatrix} = \begin{bmatrix} \mathbf{Vs} \\ \mathbf{PIs} \end{bmatrix} \tag{3.28}$$

By doing this, the rows of the system related to a completely embedded elements will have only the coefficients of the incidence matrix that give the Kirchoff's current law for the nodes.

3.7.3 Bad Conditioned System

The system shown in (3.28) can be always implemented but it can suffer of bad conditioned problem because of the big difference between the entrances related to the partial inductance and potential coefficients. This kind of problem is more significant for "electrically" large and complex objects, that require

a lot of elements for the discretization.
To improve the condition number of the system it is possible to apply a "pre multiplier" diagonal matrix, **B**, to the second matrix row of the system.
B matrix is a diagonal matrix which entrances are simply the inverse of the maximum entrances of the rows (or columns) of **P** matrix.
In this way the system becomes the one shown in (3.29).

$$\begin{bmatrix} \mathbf{A}^T & (\mathbf{R}+j\omega\mathbf{L}) \\ j\omega\mathbf{B1}^\star & -\mathbf{BPA} \end{bmatrix} \begin{bmatrix} \mathbf{V} \\ \mathbf{I} \end{bmatrix} = \begin{bmatrix} \mathbf{Vs} \\ \mathbf{BPIs} \end{bmatrix} \tag{3.29}$$

3.7.4 Retarded Potential

When the electrical dimension of the analysed objects is comparable to the wavelength (for example in the Antenna problem) it is necessary to consider the effect of retardation of electric and magnetic potential, as already done in section (2.7). To do this it is necessary to evaluate the mutual distance between the *nodal* and *side* elements and the expression for the partial coefficient of potential becomes:

$$\begin{aligned} L_{p\alpha\beta} &\approx e^{-j\beta\Delta r}\frac{\mu_0}{4\pi}\frac{1}{a_\alpha a_\beta}\int_{v_\alpha}\int_{v_\beta}\frac{\vec{J}_\alpha\cdot\vec{J}_\beta}{|\vec{r}_\alpha-\vec{r}_\beta|}dv_\beta dv_\alpha \\ p_{pij} &\approx e^{-j\beta\Delta r}\frac{1}{4\pi\varepsilon_0 S_i S_j}\int_{S_i}\int_{S_j}\frac{1}{|\vec{r}_i-\vec{r}_j|}dS_i dS_j \end{aligned} \tag{3.30}$$

where the symbol "$\approx$" is due to the fact that the exponential term should be evaluated inside the integral of volume or surface, β is the constant of propagation, $\beta = \frac{\omega}{c}$, and Δr is the center to center distance between the two considered elements.

In order to consider correctly the retardation we should impose that for all the *side* elements that have a *node* in common there must be no delay. This it is necessary to improve the time domain stability, [8].

3.8 PEEC-Code volume example application

In this section we want to report the results obtained by the PEEC volume Code for the simulations of some particular and easy structure.

3.8.1 Two-wire line

In analogy with PEEC filamentary code, we have considered a two-wire line with square cross section of $0.02 \times 0.02m$, $10m$ long and with a distance of $0.2m$ from the two conductors (in figure (3.8) is shown a coarse discretization of the object).

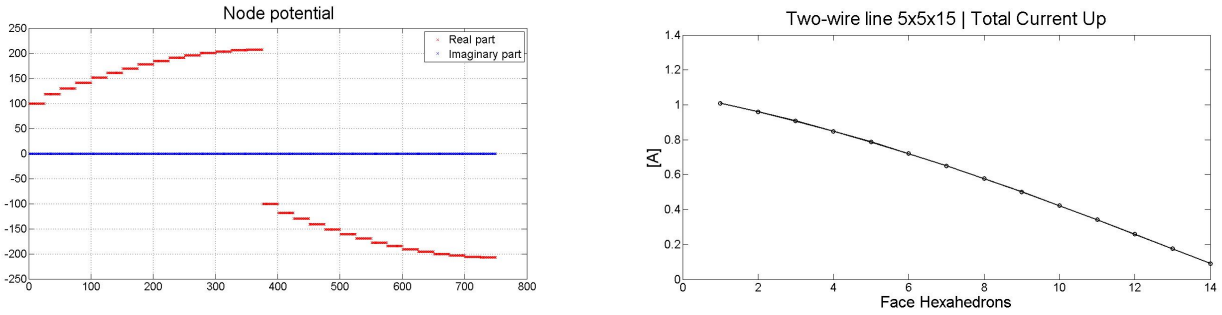

Figure 3.12: *Left: Potential of Nodal hexahedra. Right: Total current flowing in longitudinal direction.*

The simulation has been done how explained in section (2.6) for the filamentary case, considering a line symmetrically fed respect the infinity node by two voltage sources. The simulation has been done for different frequencies, considering an ideal and a real line (without or with some resistivity) and with a $1 \times 1 \times n$, $3 \times 3 \times 15$, $5 \times 5 \times 15$ and $6 \times 6 \times 10$ nodal disretization for each of two conductors.

The results obtained for the different frequencies are comparable with the ones reached with the filamentary code, thanks to the similarity of the two considered objects.

We report here, in figure (3.12), the results in terms of node potentials for the $5 \times 5 \times 15$ line. As we can see, the 25 *nodal hexahedra*, which give the transversal dimension of the object, are virtually at the same potential so, as expected, we will have a current flow mainly in the longitudinal direction.

In figure (3.12) is reported the total current flowing in longitudinal direction while in (3.13) is reported the current distribution in the 25 conductors that form the transversal discretization of the objects, along the longitudinal dimension.

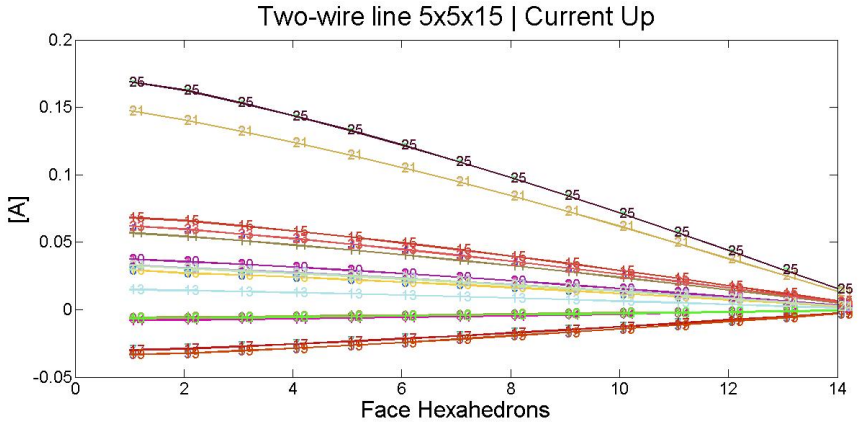

Figure 3.13: *Current distribution in the 25 elements that form the transversal section of the conductors along the longitudinal direction.*

The results in (3.13) show that the *nodal hexahedra* in the corners bring more current than the internal ones, furthermore, we see that in some conductor the current has an opposite value for the effect of the field distribution into the solid conductor.

3.8.2 Plate

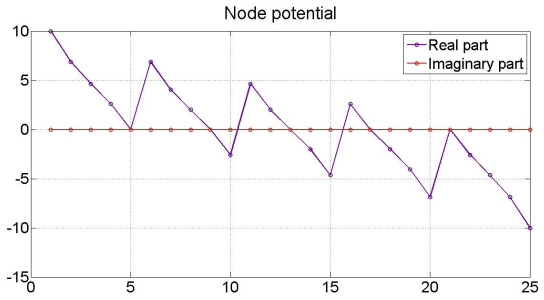

Figure 3.14: *Node potential.*

In this subsection we show the obtained results, in terms of potentials and current distribution, for a plate discretized by $5 \times 5 \times 1$ *nodal hexahedra*.
The dimensions of the plate are $1 \times 1 \times 0.25$ m and it is powered by two voltage sources connected to the opposite vertices and, both of them, to the infinity node.
For the first simulation we have considered an ideal plate (zero resistivity).

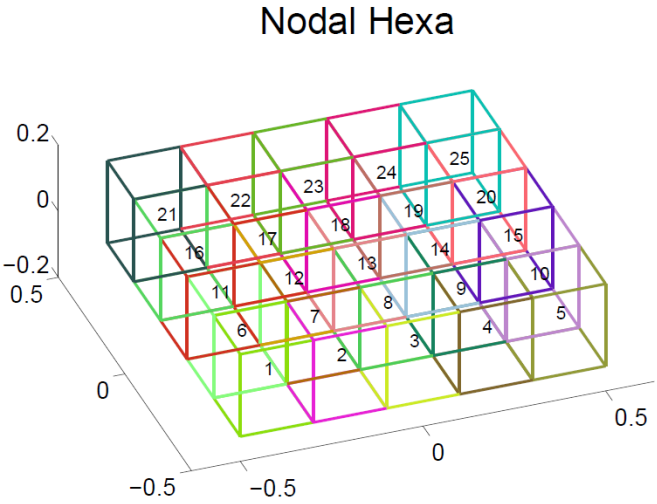

Figure 3.15: $5 \times 5 \times 1$ *plate nodal discretization.*

The results in terms of node potential are reported in (3.14), where the points refer to figure (3.15). The simulation was made at a frequency equal to $5 \cdot 10^6 [Hz]$.

For the second analysis we have considered a not homogeneous plate made by ideal material and "real" material, in order to see the change in the distribution of current flow.

The "super conductor" elements are the ones that connect the *nodal hexahedra* 1 and 25 along the diagonal (which are the supplied hexahedra) while the others are made by a material with high value of resistivity.

The results are reported in figure (3.16) where we can see that for the ideal and homogeneous plate the current flows mainly in the boundary of the object, while for the heterogeneous plate the current is forced to flow in the central hexahedra, that are "superconductors" elements.

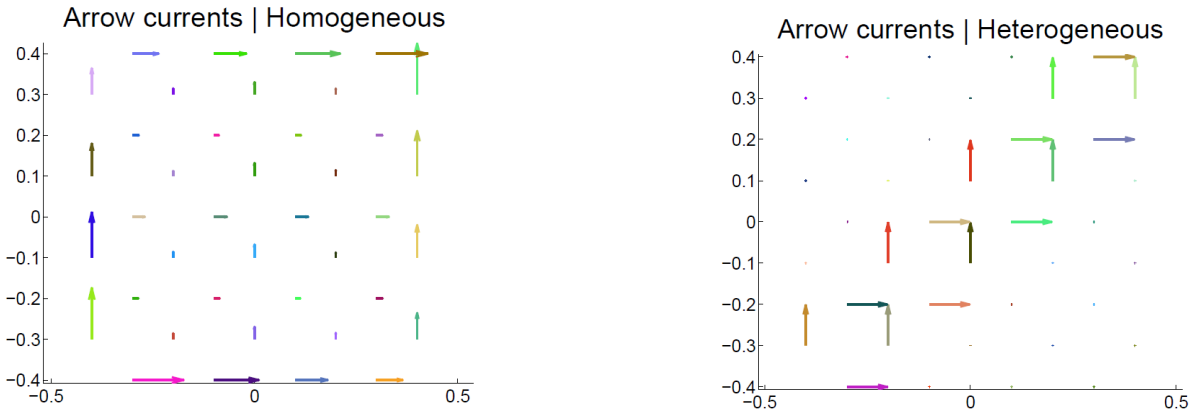

Figure 3.16: *Differnt current distributions in homogeneous and heterogeneous plate.*

3.8.3 Loops, Induction

In this subsection we want to analyse the case of two concentric loops where the bigger one is powered by two voltage sources (connected to the end points and infinity node) while the smaller is floating and closed on itself, as represented in figure (3.17).

Figure 3.17: *Current induction between two concentric loops; Left: Nodal discretization; Right: Current distribution.*

The voltage sources impose the potential of the starting and ending *nodal hexahedra* of the bigger loop at 1 $[V]$ and -1 $[V]$ respectively and the frequency is 500 $[Hz]$.

In figure (3.17) is shown the current flux in the two objects and the values of the currents are about 17.48 $[A]$ for the bigger one and -9.18 $[A]$ for the smaller one (completely imaginary).

The dimensions of the bigger loops are: $10m$ for the middle radius and a square cross section of $0.5 \times 0.5m$, the smaller one has the same cross section and a $8.4m$ middle radius.

Chapter 4

APPLICATION OF P.E.E.C. Method TO JT-60SA TF COILS

In this chapter we discuss about the application of PEEC filamentary and volume codes to the Toroidal Field Coils of the fusion reactor JT-60SA. We speak about:

- The tokamak devices;
- The role covered by JT-60SA related to the fusion research scenario;
- The description of the machine, focusing on the Toroidal Field Coils;
- The analyses performed by using PEEC filamentary and volume codes;
- General comments and considerations about the PEEC-model of the devices and some possible future developments.

4.1 Tokamak

The tokamak is an axisymmetric configuration with a large toroidal magnetic field and a DC toroidal current, [45]. Tokamaks have achieved stable operation at near reactor relevant pressures, confinement times, and temperatures. In other words, in terms of physics performance, the tokamak has met nearly all the requirements for a reactor and it is expected that a next generation experiment (e.g. ITER, DEMO, JT-60SA) will close the remaining gaps.
The tokamak is an axisymmetric torus with a large toroidal magnetic field, a moderate plasma pressure and a relatively small toroidal current. It is presently the leading candidate to become the world's first fusion reactor, a status earned by virtue of its excellent physics performance. Specifically, the achieved values of $p\tau_E$ (Lawson parameter, where p is the pressure and τ_E is the confinement time) at high temperature in a tokamak exceed those of any of other concepts. Because of its performance, there is a large number of major tokamak experimental facilities operating, or being constructed, in the international fusion program.

A schematic diagram of a tokamak is shown in figure (4.1). Observe that there are four basic magnet systems in the tokamak:

- the toroidal field coils, which produce the large toroidal field;
- the ohmic transformer, which induces the toroidal plasma current required for equilibrium and ohmic heating;
- the vertical field system, which is required for toroidal force balance;
- the shaping coils, which produce a non-circular cross section to improve MHD stability limits and alleviate plasma-wall impurity problems.

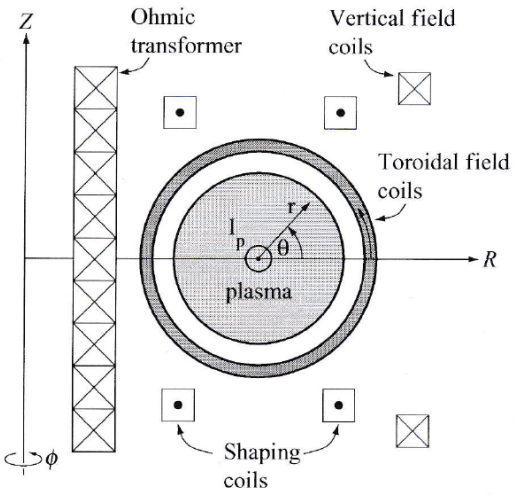

Figure 4.1: *The magnetic field configuartion of a Tokamak*, [45].

Typical operation of a tokamak discharge starts with the establishment of a large steady toroidal magnetic field. Next, neutral gas is injected into the vacuum chamber and often pre-ionized. The transformer induced toroidal current is then ramped up to its maximum value and maintained for the "flat top" portion of the pulse. During flat top operation external heating power in the form of RF or neutral beams is applied to the plasma.

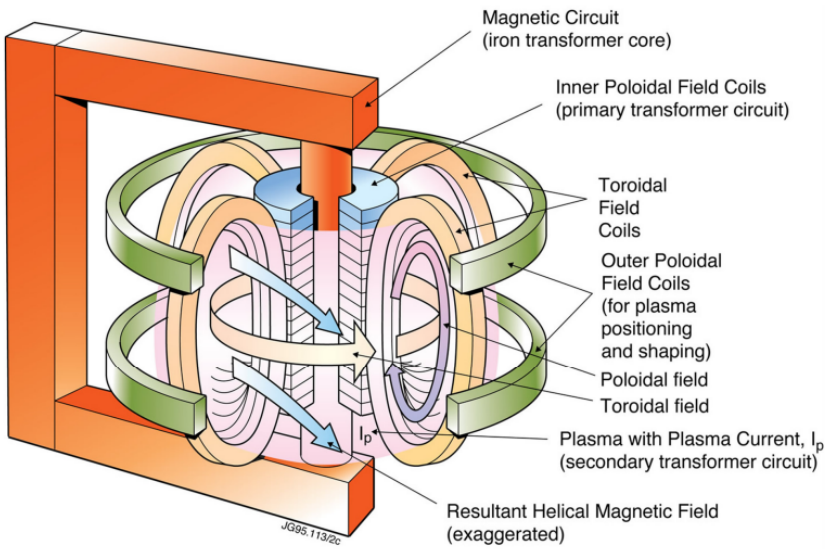

Figure 4.2: *The magnetic field configuartion of a Tokamak.*

The magnitude of the external power is usually substantially greater than that of the ohmic power. Most of the interesting experimental plasma physic occurs during the flat top period.

In terms of reactor desirability, the tokamak has a number of advantages and a few problems. The main advantages are associated with good physics performance. The large toroidal field and correspondingly large edge safety factor (a quantity connected to MHD stability) lead to finite values of MHD stable β (a quantity connected to the radial pressure balance provided by the fields in magnetic fusion configurations) without a conducting wall and to reasonably high experimental values of the energy confinement time

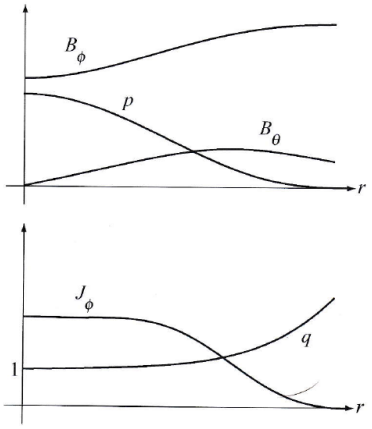

Figure 4.3: *Typical profiles in a Tokamak in the large-aspect-ratio limit* $\frac{R_0}{a} \to \infty$, [45].

τ_E; good confinement allows the plasma to heat up to high temperatures using only a moderate amount of external heating.

There are several problems facing the tokamak. First, the need for a large toroidal magnetic field increases the technological complexity and cost of the reactor. Most of the alternative concepts have been designed to alleviate this problem by utilizing a small external toroidal magnetic field, which in turn leads to a small edge safety factor. Philosophically, these concepts are trading off more difficult plasma physics for simpler reactor technology. Tokamak reactor designs have shown that high toroidal magnetic fields are certainly achievable from a practical engineering point of view - it is just that it would be technologically simpler end economically less expensive if such a large field were not required.

The second main issue arises because a reactor will almost certainly need to operate as steady state device. This requirement is incompatible with an ohmic transformer, which cannot inductively drive a DC current for an indefinite period time. Some form of external current drive is required. In general, the methods of external current drive involve costly and high-technology power sources, such as microwaves or neural beams. Furthermore, current-drive efficiency is not very high - the number of input watts per output ampere is large. The net result is that if too much current needs to be driven, power balance becomes unfavourable and the economics become unattractive.

Fortunately, in a tokamak there is a transport-driven toroidal current, known as the "boot-strap current". This current arises naturally, and does not require any external sources. Depending upon the pressure and magnetic field profiles, the bootstrap current can provide between virtually none and 95% of the total current.

The present consensus in the fusion community is that 75% or more of the current needs to be provided by external current drive. A further complication is that achieving a high bootstrap fraction requires a high β, whose value invariably lies above the no-wall β limit. Thus, high bootstrap tokamaks will likely need to stabilize the resistive wall mode.

The second problem facing the tokamak can be summarised as follows. A successful tokamak must achieve a high-β, high-bootstrap-fraction plasma that can be sustained in steady state with only a small amount of external current drive and no ohmic transformer. This is one of the main plasma physics missions of future research.

Finally, the importance of satisfying the MHD β limit against external balloning-kink modes must be re-emphasized. When this criterion is violated experimentally there is almost always a catastrophic collapse of the plasma pressure and current. Such events are appropriately called "major disruptions". They must be avoided in large experiments and reactors since the large transient forces developed can cause actual physical damage to the structure.

The conclusion is that it is important to accurately know the MHD β stability limit against ballooning-kink modes and to learn how to operate as close to the limit as possible to maximize performance.

Consider now variations on the basic tokamak. The first variation discussed involves elongation and

triangularity of the plasma cross section increases the β limit against low-n ballooning-kink modes. There is, however, a practical limit to the maximum achievable elongations greater than a factor of height/width ~ 2.
The next variation discussed concerns operation in the "advantage tokamak" (AT) regime. It is AT operation that is intended to address the main plasma physics issue discussed above. In AT operation the profiles are externally adjusted to produce a hollow toroidal current density and high β_p (a quantity connected to the radial pressure balance provided by the poloidal magnetic field), the right combination to generate the large bootstrap current essential for minimizing the current-drive requirements. Profile control is accomplished experimentally by means of programming the time dependence of the plasma current and the radial and time dependence of the external heating sources. The MHD that arises here is that for a large bootstrap current, the ballooning-kink β limit without a perfectly conducting wall is invariably violated and the resulting resistive wall mode must be feedback stabilized. It is possible to determine exactly how close the wall must be to make the transition from an ideal mode to a resistive wall mode in order for feedback stabilization to be a practical possibility.

4.2 JT-60SA

JT-60SA is a joint international project involving Japan and Europe for the construction and operation of a new tokamak intended to prepare and support ITER operation. The mission of the JT-60SA Tokamak, which will be built in Japan, is to contribute to the early realization of fusion energy in support and supplement of the ITER program. The JT-60SA project is part of the broader approach for fusion energy. "SA", standing for “super advanced”, refers to the use of Superconducting Coils Magnets and to the study of advanced modes in plasma operation. The SCM system includes Toroidal and Poloidal Field Coils. In addition the machine features a number of normal conducting coils: Fast Plasma Control Coils, Resistive Wall Mode Control Coils and Error Field Correction Coils, [38]. First plasmas are foresee in 2016.

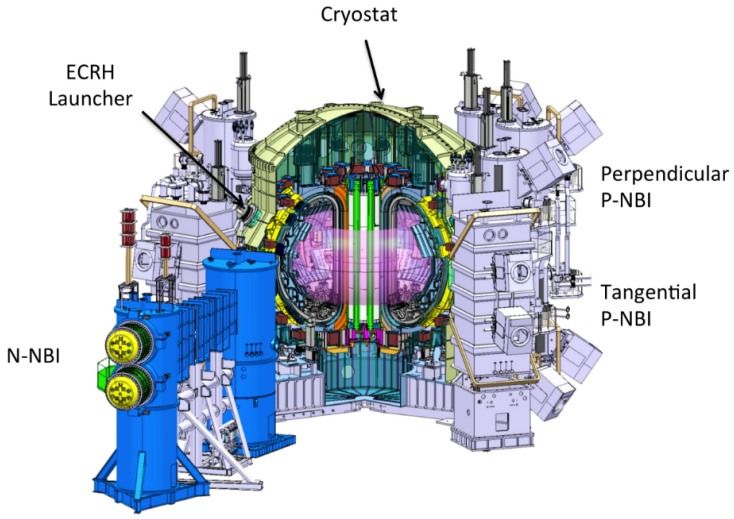

Figure 4.4: *JT-60SA device*, [47].

This device is intended to play a key role to prepare and accompany the ITER programme in the prospect of DEMO. The design of an early DEMO will very likely start before ITER D-T campaigns and for that reason important information will have to come from existing devices.
About the geometrical features, JT-60SA is a tokamak with major radius $R = 2.96m$ and minor radius $a = 1.18m$, aspect ratio $A = \frac{R}{a} = 2.5m$ which is intended to complement similar existing and near term international efforts.
With plasma current capabilities up to $5.5[MA]$ (at $B_t = 2.25[T]$) and an envisaged heating power of up

to 41[MW] it will operate in DD, aiming at reaching break-even equivalent regimes. Final goal of the JT-60SA research program is to prove the integration of all the requirements needed in a high-performance DEMO scenario, having as main reference a low-aspect ratio, high performance, steady state DEMO prototype.
The JT-60SA device is capable of confining break-even-equivalent class high-temperature deuterium plasmas lasting for a duration (typically 100s) longer than the time scales characterizing key plasma process, such as current diffusion and particle recycling, using superconducting toroidal and poloidal field coils. The device should also pursue fully non-inductive steady-state operations with high values of the plasma pressure exceeding the no-wall ideal MHD stability limits. The target regimes of JT-60SA are shown in figure (4.5).

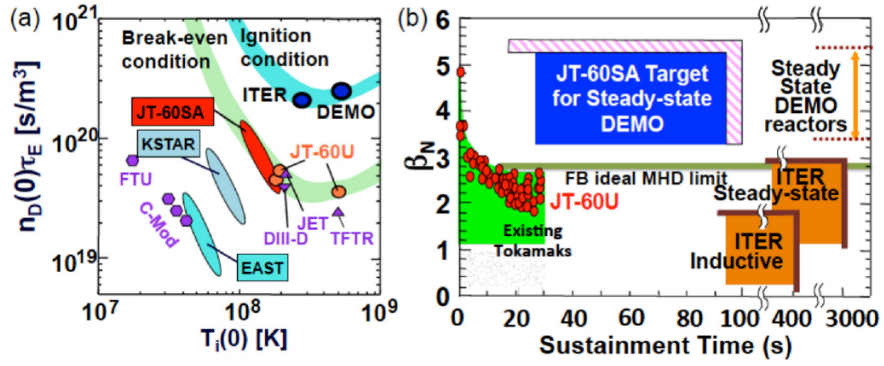

Figure 4.5: *Target regimes of JT-60SA*, [47].

The JT-60SA experiments should explore ITER and DEMO-relevant plasma regimes in terms of non-dimensional plasma parameters at high densities in the range of $1 \times 10^{20}\ m^{-3}$. In order to satisfy these requirements, the JT-60SA device has been designed to realize a wide range of diverted plasma equilibrium configurations covering a high plasma shaping factor (S $\approx$ 7) and low aspect ratio (A $\approx$ 2.5) with a sufficient inductive plasma current flattop duration. Compared with the JT-60U device, the plasma elongation is high ($k_x \approx 1.9$) simultaneously with high plasma triangularities ($\delta_x = 0.4 - 0.5$) at high plasma currents.
The shape parameter of JT-60SA is equivalent to that of the Slim-CS DEMO which has the highest shape parameter among the DEMO designs. The major radius of JT-60SA is about half of ITER and the Slim CS DEMO.
The plasma size of JT-60SA locates between ITER and other non-circular cross-section superconducting tokamaks. An integrated knowledge of these super conducting tokamaks, JT-60SA and ITER will establish a reliable nuclear fusion science and technology basis for DEMO. Typical parameters of JT-60SA are shown in the table of figure (4.6).

The maximum plasma currents are 5.5[MA] in a low aspect ratio configuration and 4.6[MA] in the ITER-shaped configuration. Inductive operations at $I_p = 5.5[MA]$ with a flat top duration of up to 100s is possible with the available flux of $\approx 9[Wb]$. The heating and current drive system will provide 34[MW] of neutral beam injection (10[MW] of 500[keV]$N - NB + 24[MW]$ of 85[keV]$P - NB$) and 7[MW] of 110[GHz] + 138[GHz] dual frequency ECRF.
The divertor target is designed to be water-cooled in order to handle the expected heat flux up to 15$[\frac{MW}{m^2}]$ for up to 100s.
With these capabilities, JT-60SA allows explorations in ITER- and DEMO- relevant plasma regimes in terms of the non-dimensional parameters.
In DEMO reactors, we need to sustain high values of the energy confinement improvement factor, the normalized beta β_N, the bootstrap current fraction, the non-inductively driven current fraction, the plasma density normalized to the Greenwald density, the fuel purity, and radiation power simultaneously in steady-state. However, such a high "integrated performance" has never been achieved. The most important goal of JT-60SA for DEMO is to demonstrate and sustain such integrated performance.

Parameters	#2 Full Ip Inductive 41MW	#4-1 ITER-like-Shape Inductive 34MW	#4-2 Advanced inductive (hybrid) 37MW	#5-1 High βN Full CD 37MW	#5-2 High βN Full CD 31MW
Plasma current, I_P (MA)	5.5	4.6	3.5	2.3	2.1
Toroidal magnetic field, B_T (T)	2.25	2.28	2.28	1.72	1.62
Major radius, R_P (m)	2.96	2.93	2.93	2.97	2.96
Minor radius, a (m)	1.18	1.14	1.14	1.11	1.12
Aspect ratio, A	2.5	2.6	2.6	2.7	2.6
Elongation, κx, κ_{95}	1.87, 1.72	1.81, 1.70	1.80, 1.72	1.90, 1.83	1.91, 1.84
Triangularity, δx, δ_{95}	0.50, 0.40	0.41, 0.33	0.41, 0.34	0.47, 0.42	0.45, 0.41
Safety factor, q_{95}	3.0	3.2	4.4	5.8	6.0
Shape Parameter (=q_{95}Ip/(aBt))	6.3	5.7	5.9	7.0	7.0
Plasma Volume (m3)	131	122	122	124	124
Heating Power, Pheat (MW)	41	34	37	37	31
Temperature (Vol-ave.), <Ti>,<Te> (keV)	6.3, 6.3	3.7, 3.7	3.7, 3.7	3.4, 3.3	3.1, 2.9
Electron Density, Vol-ave. (E20/m3)	0.56	0.81	0.62	0.42	0.43
Stored Energy (Thermal, Fast ion) (MJ)	22.2, 4.0	18.0, 1.5	13.4, 2.1	8.4, 2.7	8.1, 1.7
Thermal Energy Confinement Time τE(s)	0.54	0.52	0.36	0.23	0.25
Current DiffusionTime (s)	32.7	15.2	14.6	12.6	10.8
Assumed Confinement improvement, HHy2	1.3	1.1	1.2	1.3	1.38
Normalized beta, β_N	3.1	2.8	3.0	4.3	4.3
Bootstrap current fraction, fBS	0.28	0.3	0.4	0.68	0.79
Non inductive CD fraction, fCD	0.5	0.43	0.58	1	1
Normalized density, ne/ nGW	0.5	0.8	0.8	0.85	1.0

Figure 4.6: *Typical Parametrs of JT-60SA*, [47].

JT-60SA allows exploitations of fully non-inductive steady-state operations with $10[MW]/500[keV]$ tangential N-NBCD and $7[MW]$ of ECCD. The expected plasma current for high β_N (=4.3) fully non-inductively current driven operation is $2.3[MA]$ with $P_{in} = 37[MW]$ with the assumed HH = 1.3.

JT-60SA research project complements ITER in all areas of fusion plasma development necessary to decide DEMO construction. For this purpose, the JT-60SA Research Plan has been organized to complete the main mission of JT-60SA before the end of DEMO construction design.
The most important goal of JT-60SA is, by collaborating with ITER, to decide the practically acceptable DEMO plasma design including practical and reliable plasma control schemes suitable for a power plant. The DEMO design reference for JT-60SA is an "economically attractive steady state" reactor and the target values for the key plasma parameters has been set as shown in figure (4.7).

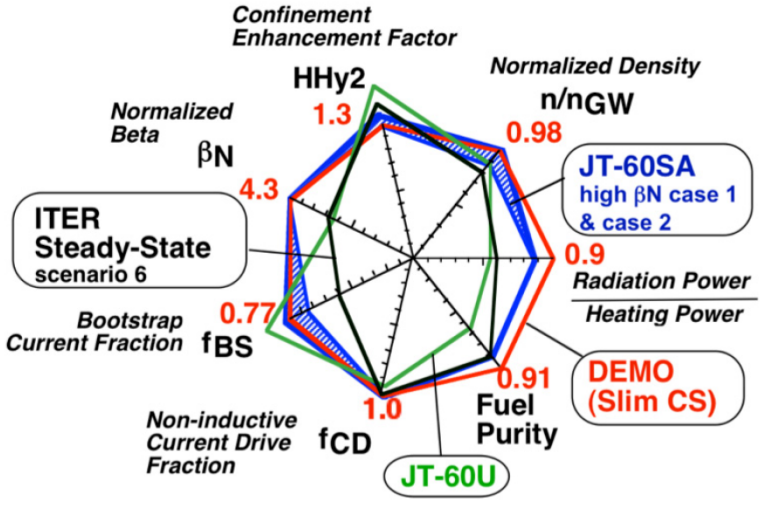

Figure 4.7: *Typical Parametrs of JT-60SA*, [47].

However, the JT-60SA research plan has to treat the "DEMO regime" as a spectrum spreading around the reference. It should be also noted that DEMO needs to have realistic control margin. If JT-60SA cannot reach the reference values, we have to reduce the DEMO design parameters. In turn, if JT-60SA can demonstrate higher values, we can design a more copact DEMO reactor. However, if JT-60SA finds that the control margin is unrealistically small, we have to keep the present reference values. It should be emphasized that, for such decision making of DEMO plasma parameters, we have to consider "practically, reliability and economy". Evaluation of DEMO plasma regime in terms of safety and availability as a power plant is also needed. The important role of JT-60SA is to provided data sets sufficient for these evaluations. The key research elements are:

- Extension of operation boundaries above ITER;
- Demonstration of high integrated performance;
- Development of plasma control schemes;
- Decision of DEMO design parameters.

In exploring these subjects, collaborative studies with modelling simulation, fusion engineering, and ITER are indispensable.

4.2.1 JT-60SA, Toroidal Field Coil

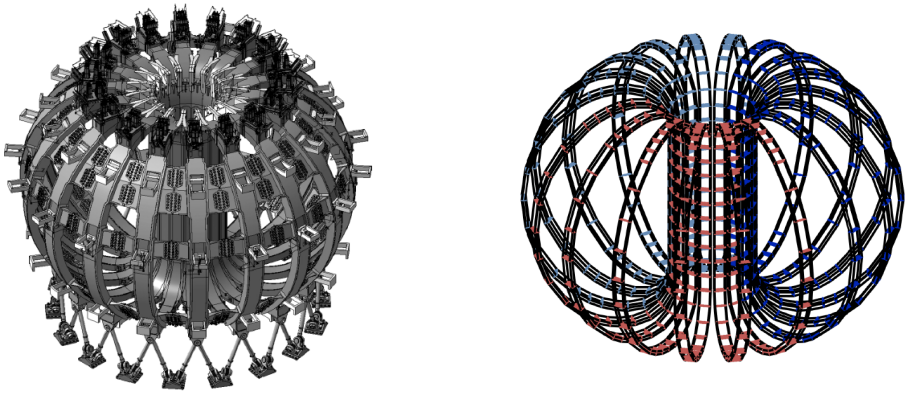

Figure 4.8: *Model and representation of the 18 Torodal Field Coils, the coils are grouped in 3 blocks of 6 coils and each coil is made by 72 turns modelled by filament wires (Right figure).*

The Toroidal Field Coils system is composed by 18 coils grouped in three sections interconnected through three quench protection circuits. The converter AC/DC has to provide a current of 25.7 $[kA]$ at 80 $[V_{DC}]$ and it is composed by six-pulse, unidirectional thyristor bridge. The coils system is protected against overvoltages, fault to ground and from quench by different systems of control and protection, [36].

Each one of the 18 coils is composed by 72 loops which geometry is reported in [39] and it is shown in figure (4.8). Furthermore, the connection scheme of the turns is proposed in figure (4.9).

Each loop is composed by an internal conductor coil divided in 324 superconducting strands (made by Niobium-Titanium) plus 162 cooper strands of 0.81 mm diameter each, [37].
This arrangement provides a void fraction of approximately 32%, with a Cu/not-Cu ratio comprised between 1.6 and 1.9. This corresponds to a total mass of 33.4 t of superconducting strand for the whole TF magnet.

Being crossed by a nominal current of 25.7$[kA]$, the conductor is cooled by a forced flow of supercritical helium having a nominal mass flow rate of 4 $[g/s]$. The dimensions of the section of the internal conductor are $18 \times 22mm$.
Each superconductor is surrounded by the jacket, a stainless steel conductor with thickness of $2mm$ that

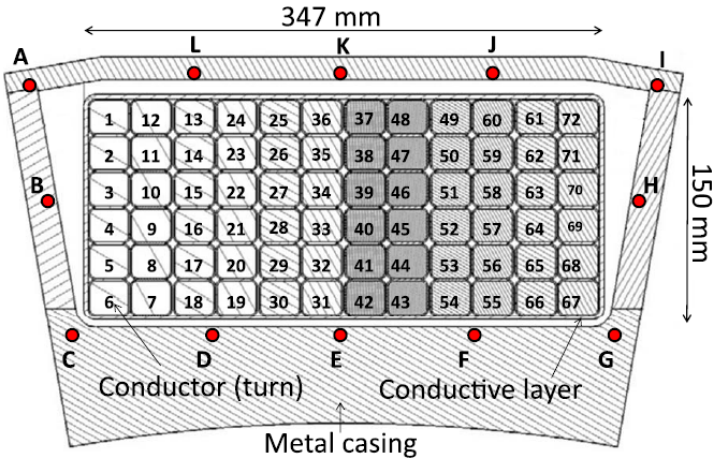

Figure 4.9: *Connection sheme of 72 turns.*

follows the internal conductor along the development of the coil.
Each winding pack of the Toroidal Filed magnet of JT-60SA consists of 72 conducting turns arranged in 6 double pancakes, as shown in figure (4.9). The insulation between each coil is guaranteed by a half-overlapped glass fiber tape, that has a relative permittivity of about 5.
The six pancakes that subdivided the 72 turns are surrounded by a conducting layer ($3mm$ thickness) that has a high resistivity (shown in figure (4.9)).

The geometrical shape of the turns is shown in figure (4.10) and it is described in [39]. Figure (4.10) represents the higher part of the "guide loop": a non-physical loop virtually collocated in the center of the 6 pancakes. Its geometrical data allows to construct all the geometry of the 72 turns by doing some geometric operation.

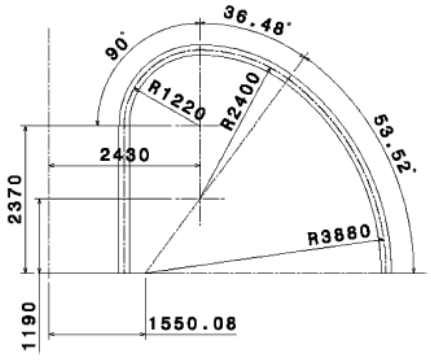

Figure 4.10: *Geometry of "guide loop", [mm], [39].*

The winding pack is inserted in a stainless steel casing which dimensions are reported in [37] and in figure (4.9). The casing is grounded by a resistance of 0.1 Ω, connected in a point and it is also connected to the layer.
The casing has the function of mechanical support for the winding packs and for two other coil systems, namely the Equilibrium Field coils and the Central Solenoid (CS) segments, which are also resting on the Toroidal Field casing, connected at specific positions.
The thickness of the casing varies from $20mm$ to $90mm$ and for our purpose we have considered a simplified geometry for the model of the object.

In this chapter we want to present how we have modelled the Toroidal field coils, in order to study

the electromagnetic behaviour of the machine at different frequencies.

4.3 PEEC filament model

About the first modelling approach, we have decided to use the filamentary PEEC-Code, considering only the superconductors coils and neglecting the presence of jacket, layer and casing. In figure (4.8) are represented all the 18×72 turns, but we have considered only one or six coils in most of our simulations.

4.3.1 Toroidal Field Coils

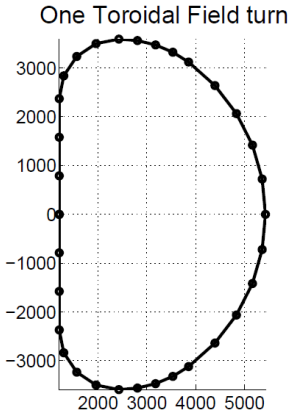

Figure 4.11: *Discretization of one Toroidal Field turn for filamentary code, dimensions in* $[mm]$.

In this subsection we want to show the results obtained from the analysis of one Toroidal Field Coil in terms of self and mutual inductance of the 72 loops, the impedance seen from the voltage sources and the distribution of nodal potentials and branch currents along the conductors.

The turns have been modelled like closed on its self from a geometric point of view but, from the standpoint of the electrical equivalent circuit, short lumped sides have been inserted to have the correct connection between the turns (see the connection scheme in figure (4.9)).

In figure (4.11) is reported the discretization of one turn with 31 PEEC capacitive nodes and 30 PEEC inductive sides.

The radius of the filament is $9mm$ and the coils have been powered considering two voltage sources connected to the start node of the first loop and the infinity node, for the first generator, and, to the end node of the last loop and the infinity node for the second generator. In this way we have constrained the potential of the first and of the end node of the object.

The start and end nodes of each turn are electrically different but they geometrically overlap in the origin of figure (4.11).

The first result obtained from PEEC filamentary code that we want to show is the value of the self and mutual inductance of the coils reported in figure (4.12). As we can see, the values of self inductance of the turns vary from 1.978 $10^{-5}[H]$, for the smaller ones (like the turn 6 in the connection scheme), to 2.076 $10^{-5}[H]$, for the bigger ones (like turn 1 in the connection scheme).

The values of mutual inductance between the first loop and the other 71 show that the magnetic coupling is higher for the turns 2 and 12, which are the closest to turn 1.

These results can be compared to the values reported in [38]. In this paper is given a value of the self-inductance varying from 18.6 $[\mu H]$ to 19.3 $[\mu H]$, from the smaller to the bigger turn.

These values have been evaluated with a finite element model and the differences may be due to the using of a too simplified model for the representation of the turns, that are considered with a circular cross section, in contrast with the reality.

The inductances have been evaluated by considering the relative matrix blocks of the global **L** matrix

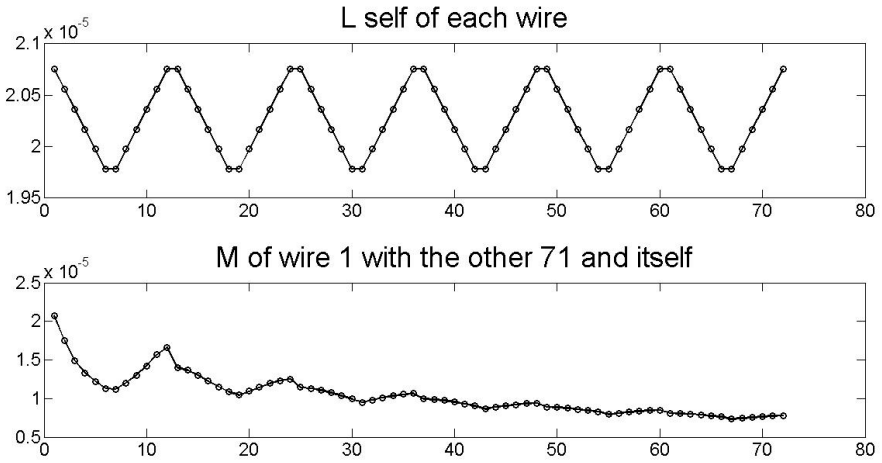

Figure 4.12: *Self Inductance of the 72 turns and Mutual Inductance between turn-1 and the others 71 turns of a Toroidal Field Coil.*

of the coils. It is also possible to extract the value of the self inductance of the entire coil (made by 72 turns) by summing all the entrances of $\mathbf{L}$ matrix. The reached value of $0.0633[H]$ can be also obtained by dividing the imaginary part of the impedance by ω, when the frequency is lower enough for neglecting the capacitive effects.

In the table below are reported the values of self inductance for a turn, a single turn, one coil and 6 coils.

Table, Self Inductance for TF Coils of JT60-SA

Considered Turns	Self Inductance $[H]$
1 Turn	$2.1957 \cdot 10^{-5}$
72 Turns, One Coils	0.0633
6 Coils	0.7178

In a similar way it is possible to evaluate the Maxwell Capacitance Matrix, [42], between two turns by inverting the corresponding block matrices of the $\mathbf{P}_{global}$ matrix of the coil.
In order to obtain the matrix of capacitance between two turns (turn i and j) we have to extract from the $\mathbf{P}_{global}$ matrix the 4 matrix blocks related to the partial coefficients of potential of elements of turn i with itself, of turn j with itself, turn i with j and vice versa.
By doing this, we can construct the local matrix of partial coefficients of potential, which can be inverted in order to reach the local capacitance matrix between the two turns. By summing all together the entrances of the four block matrices we can obtain the Maxwell capacitance matrix of two turns. We report here the Maxwell Capacitance Matrix, relative to two radially adjacent turns:

$$\mathbf{C}_M = \begin{bmatrix} 5.7702 \cdot 10^{-10} & -5.0413 \cdot 10^{-10} \\ -5.0413 \cdot 10^{-10} & 5.7299 \cdot 10^{-10} \end{bmatrix} \tag{4.1}$$

In figure (4.13) is shown the trend of off-diagonal terms (negated) of Maxwell Capacitance Matrix, related to the first turn and all the others.

As second result, we want to show the values of anti-resonance peak obtained from the simulation in the frequency domain of only one turn, one coils and six coils connected in series. The values are reported in the tabular.

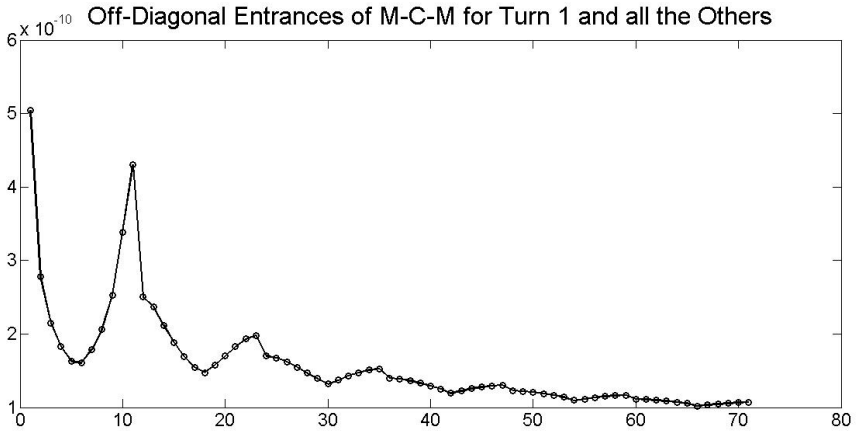

Figure 4.13: *Negated off-diagonal entrances of Maxwell Capacitance Matrix for turn 1 with all the others.*

Table, Anti-Resonance peak for TF Coils of JT60-SA

Considered Turns	Anti-Resonance Frequency [Hz]
1 Turn	$7.735 \cdot 10^6$
72 Turns, One Coils	$3.865 \cdot 10^4$
6 Coils	$1.233 \cdot 10^4$

The impedance of the coil has been evaluated by the ratio between the difference of potential of the nodes where the voltage sources are connected and the current that flow in these appended sides.

4.4 PEEC volume model

Coil Model

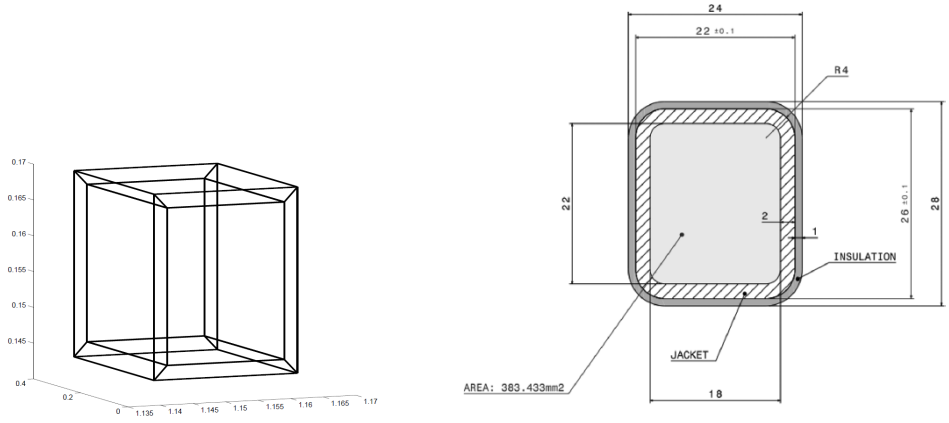

Figure 4.14: *Superconductor and Jacket, model not in scale. Left: PEEC model. Right: Representation.*

In this section we explain how we have modelled the Toroidal Field Coils of JT-60SA for the PEEC-Volume method. As opposed to filamentary model, using hexahedral elements instead filaments, it has been possible to consider a more accurate model for the machine, considering also the jacket and the casing.

In this model the jacket and the internal superconductor have been modelled like a single heterogeneous object that we have considered such as a single turn.
All the objects considered in the model -the turns (made by the internal superconductor an the external jacket) and the casing- have been divided in the same number of elements along the development of the turns in poloidal direction, while it is possible to decide independently the number of radial subdivisions for each object.

About the superconductor we have decided to consider it with a single element for the cross section just because, how previously said, the internal conductor is made by 324 superconducting strands and 162 copper strands wrapped each other, so we can consider a uniform distribution of current in the cross section.

The jacket always follows the superconductor and it is modelled by four hexahedra that envelop the internal superconductor, as shown in figure (4.14). The four parts of the jacket can also be divided in more hexahedra along the radial direction, in this way we can take into consideration also the current distribution along the thickness.

In our model the geometry of the casing has been simplified compared to the real shape of the object shown in (4.9). The adopted geometry is shown in figure (4.15), where the dimension are: $0.235 \times 0.470m$ for the external profile, $0.165 \times 0.36m$ for the internal profile, $0.20m$ for the smaller thickness, $0.55m$ for the lower and upper thickness (related to the figure) and $0.50m$ for the thickness on the right.

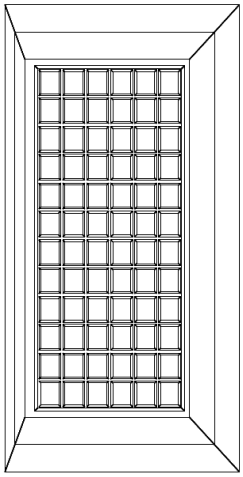

Figure 4.15: *Semplified geometry used for the model of the casing; PEEC Model.*

The casing can be divided in a certain number of elements along the radial direction. In figure (4.15) the object has been divided in two elements along the radial direction while in the poloidal direction (non-visible in the figure) it has been discretized by the same number of elements used for the superconductor and jacket.

Inductance Evaluation for the Superconductor

In analogy with what we have done for the filamentary model, we want to report the obtained results in terms of self and mutual inductance of the turns.

First, we have considered only the superconductor by neglecting the presence of the jacket, in this way it is possible to make comparisons with the results obtained by the filamentary model. With this considered model the values of inductance have been easily extrapolated directly by the inductance matrix **L**.

The values of self and mutual inductance (between the first turn and all the others) are shown in figure (4.16). The values have been reached for a coarse and for an accurate discretization of the turns (see figure (4.17)).

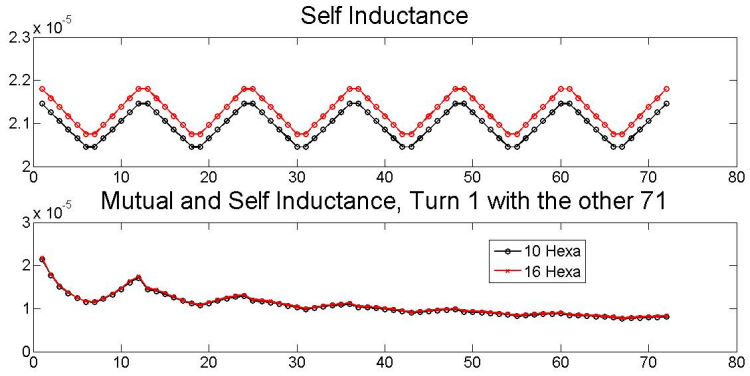

Figure 4.16: *Self and Mutual Inductance of the turns of Toroidal Field Coils, JT-60SA.*

Furthermore, in order to make some consideration about the effect of the quality of the discretization we report in the table below the obtained values for the self inductance of the first turn modelled with different number of hexahedra.

Table, Self Inductance Evaluation, Effect of disretization

Number of *nodal hexahedra*	Self Inductance [H]
42	$2.2138 \cdot 10^{-5}$
26	$2.2061 \cdot 10^{-5}$
16	$2.1800 \cdot 10^{-5}$
10	$2.1456 \cdot 10^{-5}$

All the values have been obtained by using a first order of Gauss-Legendre integration in all the the three directions, which implies to use 8 points for the numerical evaluation of the integrals.

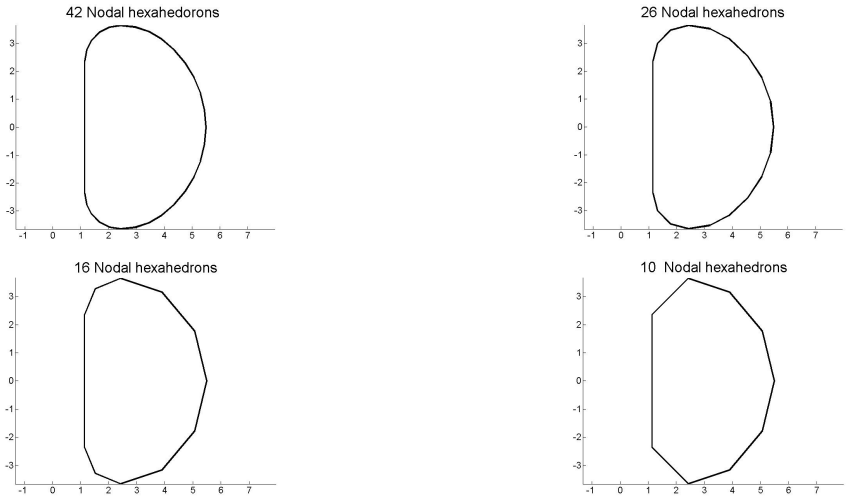

Figure 4.17: *Different distretizations for the turns of the Toroidal Field Coil of JT-60SA; PEEC Model.*

Self Inductance Evaluation of a Turn, Superconductor and Jacket

Now we want to consider the turn composed by the superconductor enveloped by the jacket, and evaluate the self inductance for this kind of object.

In this subsection we consider two types of discretization for the turns: the first with 48 *nodal hexahedra* for the superconductor and only one element in the radial direction for the jacket; the second with 134 *nodal hexahedorns* for the superconductor and two elements in the radial direction of the jacket.

The jacket is made by stainless-steel that has a resistivity of about $75 \cdot 10^{-8}[\Omega m]$ at room temperature but, in this particular application, the object is directly connected to the superconductor which is cooled to a temperature of about $2K$, so its resistivity is lower and approximately equal to $50 \cdot 10^{-8}[\Omega m]$.

For this kind of object the self inductance can be estimated by the evaluation of the impedance seen from the voltage sources.

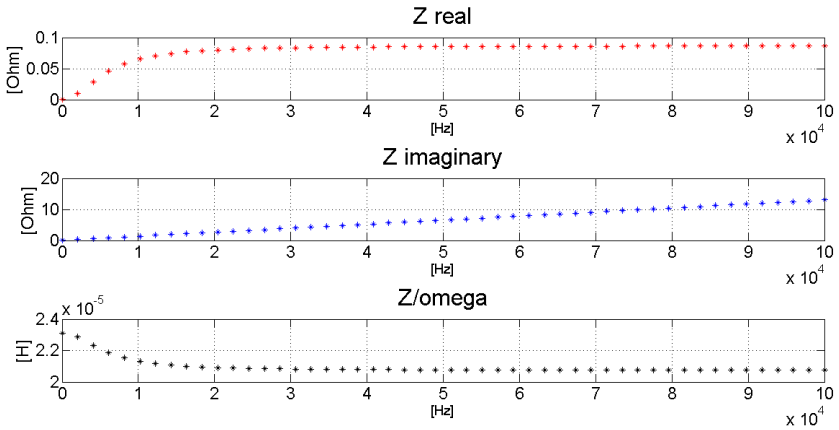

Figure 4.18: *Impedance of one turn (superconductor and jacket) with the frequency.*

In our model the turns are powered by 5 voltage sources, that impose the value of the potential for the start nodal hexahedron of the super conductor and for the four nodal hexahedra of the jacket, which envelope the nodal hexahedron of the superconductor. These voltage sources are connected to the object and to the infinity node. They impose a value of the potential of the "start" nodes of the turns equal to 1 $[V]$.
There are other 5 voltage sources that impose a negative value of -1 $[V]$ to the "end" nodes of the turns. If the jacket is divided by more than one element in the radial direction, it becomes necessary to insert a higher number of voltage sources in order to impose the value of the potential to all the start nodes of the turns (for example, if the jacket is divided by two elements in the radial direction, we will use 9 voltage sources for the start nodes and 9 voltage sources for the end nodes).

In figure (4.19) is shown the trend of the real and imaginary part of the impedance of one turn (considering the superconductor and the jacket) and the estimated value of the "inductance" evaluated as $\frac{Z_i}{\omega}$, where $Z = Z_r + jZ_i$, this and the following results are related to the first type of discretization considered.

As we can see, the estimated value of the inductance appears to be equal to $2.312 \cdot 10^{-5}[H]$ for the low frequency of $1[Hz]$ and it stabilizes at a value of $2.075 \cdot 10^{-5}[H]$ for the higher frequency.

Furthermore, the value of the real part of the impedance (related to the resistivity of the jacket) appears to be nulls for the low frequency and it rises and stabilizes with the increasing of frequency. This trend can be explained considering that with the growth of the frequency the impedance related to the superconductor side elements rises, so the current starts to flow in all the section formed by the superconductor and the jacket.

For the second discretization the values of real and imaginary part of the impedance are very similar to the results obtained by the first discretization. The estimated values of self inductance varies from $2.317 \cdot 10^{-5}[H]$, for the low frequency, to $2.079 \cdot 10^{-5}[H]$, for the higher frequency, while the real part of the impedance rises until a value slightly higher than $0.1[\Omega]$.

Self Inductance Evaluation of the Toroidal Field Coil, Superconductor and Jacket

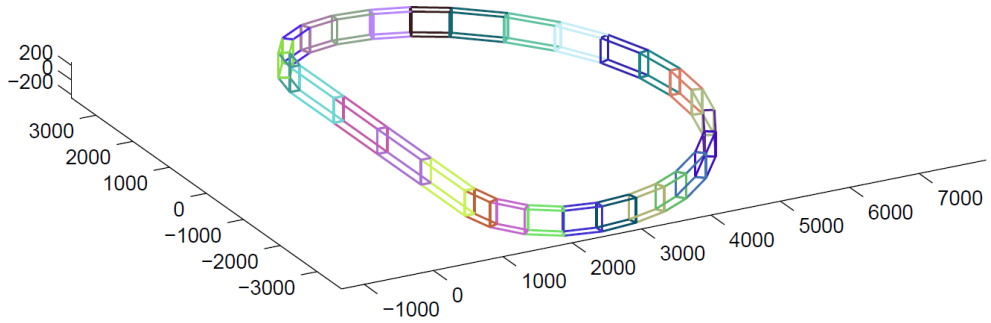

Figure 4.19: *PEEC model of a Toroidal Field Coil of JT-60SA, representation of contour lines* .

In this subsection we show the obtained results concerning the estimation of the self inductance of the Toroidal Field Coil of JT-60SA, obviously considering all the 72 turns made by superconductor and jacket.
For reason related to computational cost it was not possible to use a very fine discretization of the turns and we have considered the jacket with a single element in radial direction. If we had considered more elements the number of *side* and *nodal hexahedra* would have enormously increased, so also the size and the time to compute **L** and **P** matrix would have been very high.
Furthermore, also the time for the inversion of the system (necessary to reach the value of current flowing in the side elements) would have been considerable.
For these reasons we have first considered each turn discretized by 16 *nodal hexahedra* along the toroidal direction of the turns. The estimated inductance has been evaluated for these frequencies: 100, 550 and 1000 $[Hz]$. The reached value of the inductance is 0.0627 $[H]$ for all the three frequencies.
Other analyses have been done by considering different number of hexahedra for the discretization of the turns, the obtained results have been quite similar.

Current Distribution in a turn, effect of frequency and discretization

In this subsection we want to discuss the effect of the frequency and discretization in the current distribution of a turn. For reasons which will clarified latter we consider only a turn (considering superconductor and jacket).

Considering figure (4.10), we can say that each turn (divided in two symmetric parts) is formed by a vertical part 2.37 m long, a circular part of an angle of 90°, a second circular part of an an angle of 36.48°and a last circular part of an an angle of 53.52°. The first straight, from a geometrical point of view, could be represented by a singular hexadron along the main direction while the other circular parts required more elements in order to guarantee a good approximation of the real shape of the turn. Besides the geometrical point of view, it is also necessary to consider the physical aspects concerning the discretization. The turn is made by an internal superconductor (represented by a singular hexahedron) and by the jacket that has a more thin thickness than the superconductor.
The jacket is modelled by four hexahedra that surround the superconductor (in the radial direction). From the point of view of the *electrical equivalent circuit*, the object can be represented as shown in figure (4.20).

The inductor (1) represents the *side hexahedra* of the internal superconductor, which connects two *nodal hexahedra* (SC_1 and SC_2) along the toroidal direction. There is no resistance in this branch because of the superconducting material.
The impedance (4) and (7) represent the *side hexahedra* that connect the *nodal hexahedra* of the jacket in the same toroidal position of SC_1 and SC_2. For simplicity and clarity only two of the four arrays of *nodal hexahedra* that surround the superconductor have been considered.

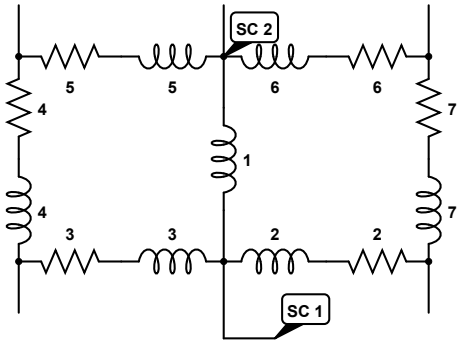

Figure 4.20: *Equivalent circuit related to a part of a turn of Toroidal Field Coil of JT-60SA.*

The impedances (2), (3), (5) and (6) represent the *side hexahedra* which connect the *nodal hexahedra* of the superconductor and the jacket.
Once again, for simplicity and clarity the voltage sources related to electric and magnetic couplings have not been represented.
In general, at least a very fine disretization is used, the vertical sides (1), (4) and (7) represent *side hexahedra* longer than the ones represented by sides (2), (3), (5) and (6), because of the geometrical dimensions of the turn.
This involves that the impedance of these branches can be bigger than the others, especially with the frequency increase.
This produces a non-realistic behaviour of the electrical equivalent circuit: the current tends to flow through "horizontal" sides rather than side (1) (which is made by superconducting material). This effect is shown in figures (4.21) and (4.22).

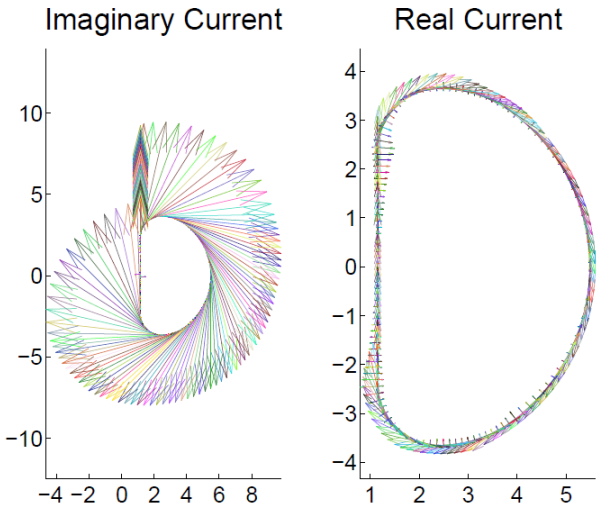

Figure 4.21: *Current distribution in a turn, effect of the discretization, fine.*

Figures (4.21) and (4.22) show qualitatively the effect discussed above. The two currents distribution shown in (4.22) have been obtained for a coarse discretization of the turn (16 *nodal hexahedra* in the toroidal direction). This involves that the impedances of sides which connect superconductor and jacket are smaller that the ones which connect two *nodal hexahedra* of the superconductor, so the current tends

to flow through these sides rather than the superconductor.
The results reported in the figures are related to a frequency of 1000 $[Hz]$. Obviously, this effect is heavily dependent to the frequency because, with the fall of the frequency, the purely imaginary impedance of the branches related to the superconductor decreases.

This effect, due to a combination of discretization and frequency value, obliges to study accurately the number of elements chosen to model the geometry. In particular, mostly with the increase of the frequency, it is necessary to use a finer discretization in order to avoid the phenomenon discussed above. This implies to use a huge number of elements if we are considering all the 72 turns of the Toroidal Field Coil (and also the casing and the layer) and this could be a problem for a computational cost point of view.

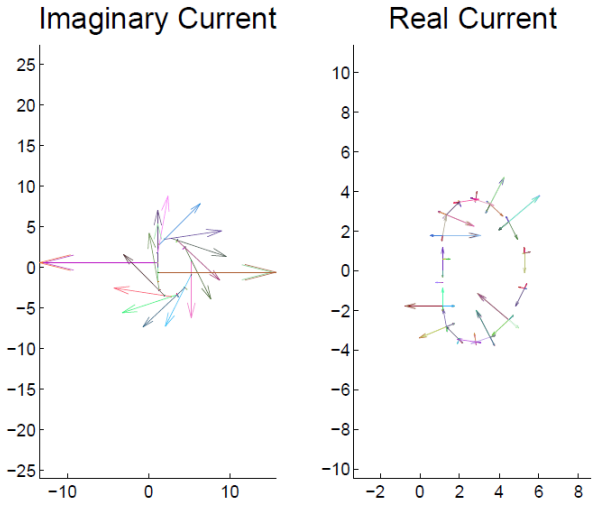

Figure 4.22: *Current distribution in a turn, effect of the discretization, coarse.*

The time required for the composition of **P** and **L** matrices grows quadratically with the increasing of the number of *nodal* and *side* elements.
Some technique can be used in order to reduce the computation cost and the time required for the simulation.
First, **P** and **L** matrix are always symmetric matrices so it is not necessary to compute all the entrances but it is enough to evaluate only the half.
Secondly, it is possible to parallelize the part of the code designed to the evaluation of the coefficients.
Obviously the performance depends also on the programming language used. In this thesis work the code has been written in MATLAB, which offers a "comfortable" ambient of programming but it doesn't give good performances when big nested cycles of iterations are used (as the ones carried out to fill **P** and **L** matrices, which require a double iteration on the *nodal* and *side* elements).
For this reason this part of the code has been rewritten in FORTRAN language, which gives better performance respect MATLAB for these kind of problems.
By adopting all the strategies here discussed, a speed-up factor of 10000 has been reached compared to the first version of the code.
Another considerable aspect is the time required for the system inversion, that also grows quadratically with the increase of the system dimension.
To reduce the time required for the inversion it is possible to adopt a reduced system, such as the one reported in (2.35). By using a "reduced system" it is possible to dramatically reduce the dimension of the system, so also the time required for its inversion, but some post-processing is required to obtain the node potentials.
Another possibility is to use some "sparsification" technique, as the one based on *Hierarchical Matrix* theory ($\mathcal{H}$-matrix), [48], [49].

The theory of $\mathcal{H}$-matrices leads to consider a matrix with a more performing data structure compared to the usual way to consider it. By adopting this theory, it is possible to store and perform algebraic calculations (like matrix inversion) with full matrices, saving memory and computational time.
Since P.E.E.C. method requires to treat very full matrices, the theory of $\mathcal{H}$-matrices appears to be very attractive in order to reduce the computational cost required by the system inversion, mostly if analyses in the frequency and time domain are demands.

Anti-Resonance Peak

In this subsection we are going to report the obtained results in term of Anti-Resonance Peak.
The values of frequencies for which the anti-resonance peak appears are reported in Table "Anti-Resonance Frequencies" and the analyses have been done by considering different parts of the machine.

Table, Anti-Resonance frequencies

Considered Turns	Anti-Resonance Frequency [Hz]
1 Turn	$7.325 \cdot 10^6$
12 Turns	$5.350 \cdot 10^4$
72 Turns	$1.922 \cdot 10^4$
72 Turns and Casing	$\approx 2 \cdot 10^4$

The obtained results are influenced by the effect of the disctretization discussed in the previously subsection. With the increase of the number of the considered turns the dimension of the matrices increase and also the time and computational cost. For this reason, with the increase of the number of loops considered in the model, a more coarse discretization has been used.
This obviously affects the results; in order to have a more accurate model of the coils or to consider more than one TF coil, it is necessary to have a more performing code and/or computer.
For the aim of this thesis this has not been required but for further analyses this problem has to be taken into account.

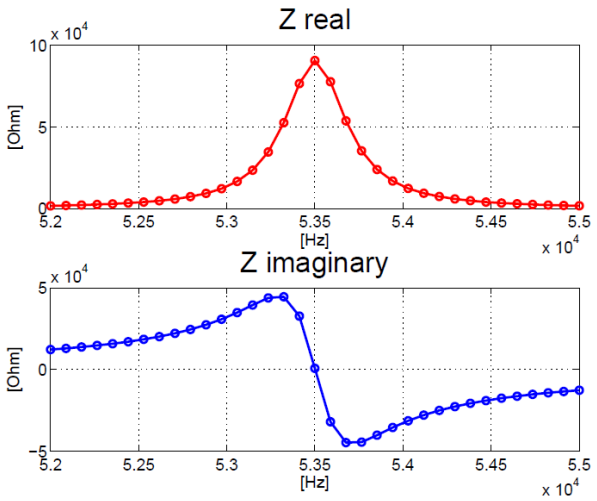

Figure 4.23: *Anti-resonance 12 turns of Toroidal Field Coil of JT-60SA, in empty space.*

In figure (4.23) is shown the anti-resonance peak obtained by the analysis of 12 turns of *Toroidal Field Coil* of JT-60SA. The turns have been considered in empty space.
Each turn, considering the upper part shown in figure (4.10), has been discretized by 7 elements for the vertical stretch, 6 elements for the first circular stretch, 3 elements for the second circular stretch and 7 elements for the last circular stretch. So, each turn has been discretized by 46 *nodal hexahedra* along the poloidal direction so, considering jacket and superconductor, each turn has been divided in 230 elements,

for a total number of 2760 *nodal hexahedra*, that is also the dimension of **P** matrix.
Indeed, the number of *side hexahedra* is 7116 while the **L** matrix is 7129×7129, considering also the appended side (loads and voltage sources).
With these dimensions of the matrices the time needed for the creation of the matrices and the time required for the inversion of the system are still reasonable.

Indeed, in figure (4.24) is shown the impedance in anti-resonance condition for 72 turns (one Toroidal Field Coil) of JT-60SA.
For this study the turns have been divided in $3+3+2+3$ elements, respectively related to the 4 stretches which form the half upper part of the turn (see figure (4.10)).
By doing this each turn has been discretized by 22 *nodal hexahedra* in poloidal direction for an overall number of *nodal elements* of 7920 (considering the presence of the superconductor and jacket).
The overall number of *side hexahedra* has been 20242 plus 365 appended sides (loads and voltage sources).

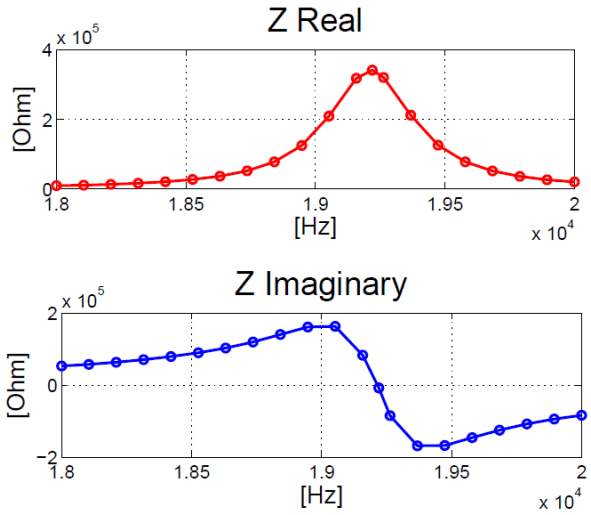

Figure 4.24: *Anti-resonance 72 turns of Toroidal Field Coil of JT-60SA, in empty space.*

The anti-resonance value of $1.922 \cdot 10^4$ $[Hz]$ is close to the value obtained by a research team working in Germany for "Fusion for Energy", their results cannot be shown in this thesis because under NDA (Non-Disclosure Agreement).
In general, it was not possible to compare the results obtained by PEEC code with the ones obtained by this research team because our model has not been able to consider the presence of the dielectric as opposed to the commercial software used by the "Fusion for Energy" team.
Future investigations are foreseen in order to consider also the presence of the dielectric (see the next subsection).

4.4.1 Inclusion of Dielectric Material

The main problem concerning the modelling of the Toroidal Field Coil of JT-60SA is related to the presence of the dielectric ($\varepsilon_r \approx 5$) between the turns, layer and casing.
The presence of this dielectric material obviously influences the electric couplings between the elements so, in order to have a correct model of the machine, its presence must to be considered. The right way to do this it is to include dielectric cells into the PEEC model, shortly introduced in the (1.4.2).
This kind of cells have not been considered in this thesis work and also in literature they have not been treated enough yet.
In order to consider the presence of the electric material, for some analyses (like the one which has given the last result of Table "Anti-Resonance frequencies") some rough operation has been done for the entrances of **P** matrix, but this approach has not give satisfactory results.

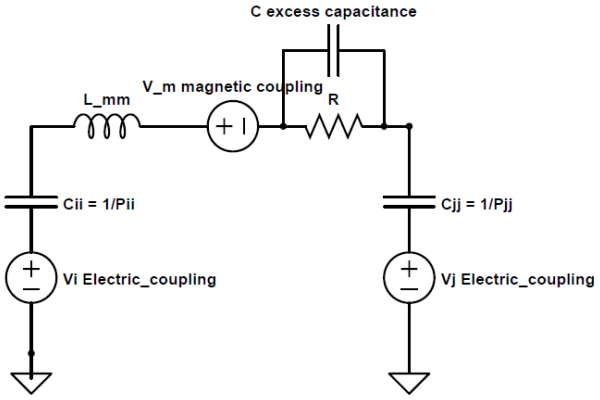

Figure 4.25: *Dielectric cell.*

By adding these cells to the code, the system to solve must be changed. Considering figure (4.25) and neglecting for the moment the presence of the excess capacitance, we have that the impedance between the nodes can be written in matrix form as: $\mathbf{Z} = \mathbf{R} + j\omega\mathbf{L}$, where $\mathbf{R}$ and $\mathbf{L}$ are the resistance and inductance matrix respectively. By adding the excess capacitance the *matrix impedance* $\mathbf{Z}$ becomes as shown in (4.2).

$$\begin{aligned} \mathbf{Z} &= \frac{\mathbf{R}\mathbf{X}_C^2}{\mathbf{R}^2 + \mathbf{X}_C^2} - j\frac{\mathbf{R}^2\mathbf{X}_C}{\mathbf{R}^2 + \mathbf{X}_C^2} + j\mathbf{X}_L \\ \mathbf{X}_C &= \frac{1}{\omega\mathbf{C}_{ex}} \\ \mathbf{X}_L &= \omega\mathbf{L} \end{aligned} \tag{4.2}$$

where $\mathbf{C}_{ex}$ is the diagonal matrix containing the excess capacitance coefficients of the dielectric cells.

The formulation has been obtained by considering the equivalent impedance of the dipole related to the parallel of the resistance and the "excess capacitance" in figure (4.25).

For conductor cells the excess capacitance is null, so the related X_C has infinite value and $\mathbf{Z}$ becomes: $\mathbf{Z} = \mathbf{R} + j\omega\mathbf{L}$.

For ideal dielectric cells, that have infinite resistivity, the expression of $\mathbf{Z}$ becomes: $\mathbf{Z} = -j\mathbf{X}_C + j\omega\mathbf{L}$.

So, if in the model are present these two kinds of cells, the $\mathbf{Z}$ matrix can be evaluated as $\mathbf{Z} = \mathbf{R\&C} + j\omega\mathbf{L}$, where $\mathbf{R\&C}$ is a diagonal matrix that has real entrances equal to the partial resistance for conductors cells and imaginary and negative entrances for dielectric cells.

So the system to be solved becomes in general:

$$\begin{bmatrix} \mathbf{A}^T & \mathbf{Z} \\ j\omega\mathbf{1}^\star & -\mathbf{PA} \end{bmatrix} \begin{bmatrix} \mathbf{V} \\ \mathbf{I} \end{bmatrix} = \begin{bmatrix} \mathbf{Vs} \\ \mathbf{PIs} \end{bmatrix} \tag{4.3}$$

A "real" dielectric cell can be modelled in a PEEC method as the one shown in figure (4.25).

It is often difficult to know the resistivity value of a dielectric material but usually this value is so high that the presence of the resistance in the PEEC model of the dielectric cell can be neglected.

This reasoning it is not applicable for the self and mutual inductance, just because also the displacement currents, that flow in the dielectric cells, produce the magnetic vector potential $\vec{A}$, so the magnetic coupling with these cells, in theory, must to be considered.

Then, the rows of the $\mathbf{L}$ matrix related to these dielectric cells are full rows, so the inclusion of the dielectric cells in the PEEC-Code could burden the computational cost for the analysis in the frequency domain of the TF coils of JT-60SA.

On the other hand, it is possible to consider a simplified model for the dielectric cells: even if the magnetic

coupling with the currents flowing in the dielectric material cannot be in general ignored, we have to say that the displacement currents that flow in the dielectric cells will be considerable only for high frequency values. By doing this observation and considering that the frequency values required by the analysis in the frequency domain of JT-60SA are not so high, we can neglect the presence of self and mutual partial inductances for these cells. Then, the partial dielectric cells can be modelled simply with a partial capacitance.
With this simplification the global system becomes however larger than the one related to the method which doesn't take into account the presence of the dielectric material, but the rows of **L** matrix related to the dielectric cells will have null entrances. Therefore, by adopting this simplification, it will be possible to save time and computational cost during the assembly of the **L** matrix (that is the one that requires more time) and also during the inversion of the system, that appears more sparse.

4.4.2 Future Studies on JT-60SA with PEEC method

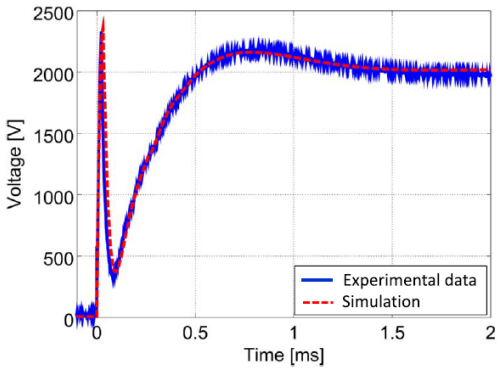

Figure 4.26: *Voltage appearing across quench protection circuits during operation with nominal current.*

With the implemented codes it has been possible to study the machine without considering the presence of the dielectric material.
This limitation of the code can be overcome in future by adding the dielectric cells, which require some more studies.
With the addition of these cells it will be necessary to discretize also the space interposed between the turns, the layer and the casing. This will make more complicated the geometry and also the model; furthermore, it will be needed more elements in order to discretize also the dielectric material, so the matrices will become larger.
On the other hand, with the inclusion of dielectric cells in the method, it will be possible to have a precise model of the machine and this will allow to study more accurately the behaviour of the machine.

Another interesting study that could be performed is the simulation of the discharge of the 6 Toroidal Field Coils in the quench protection circuit.
In order to test the model, a valid benchmark is to compare the voltage wave appearing across quench protection circuit during the discharge in the P.E.E.C. model of the machine with the one shown in figure (4.26).
In figure (4.26) the experimental data are compared with the ones obtained with a Spice-model of the machine reported in [38]. In order to perform this simulation it is necessary to study the discharge in the time domain.
A simplified model of quench protection circuit is shown in figure (4.27). As we can see, in the electric circuit a diode is present. Its presence requires to implement a theta method (or another kind of time domain study method) which allows to consider this kind of circuit elements.
The implementation of these features in the P.E.E.C. Volume-Code will allow to study general problems,

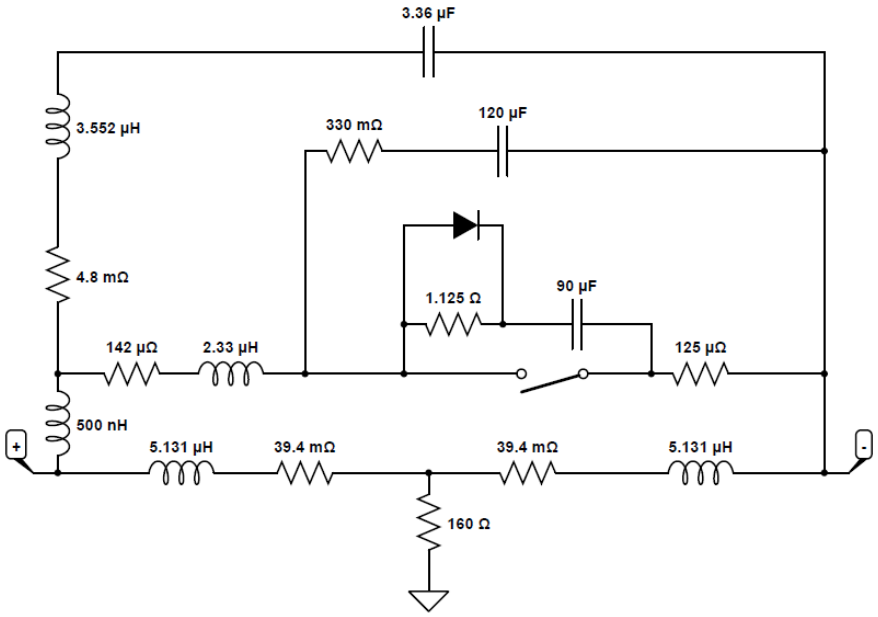

Figure 4.27: *Simplified model of Quench Protection Circuit.*

such as the discharge of the TF coils of JT-60SA in a electric circuit which contains non-linear elements. Furthermore, by applying a good discretization to the machine it will be possible to analyse the potential distribution along the turns of the machine and possibly foresee potentially dangerous phenomena for the insulation during fast discharges of the coils.

Another interesting study concerning the model is the effective electromagnetic relation between the internal superconductor and the jacket. In the developed model these two objects have been considered as a single structure made by two different materials.
In reality a "contact resistance" is probably present between the two elements and its inclusion in the model could be beneficial in terms of computational cost.
Indeed, by adding these appended sides between the *nodal hexahedra* of the jacket and superconductor, the problem concerning the disctretization and the current distribution discussed in subsection (4.4) might diminish, so a minor number of elements could be require for the analyses.

Conclusions and Future Research

P.E.E.C. method appears very attractive for frequency and time domain analyses of electromagnetic devices because of its capability to consider modelled objects and lumped circuit elements in the same electrical equivalent circuit.
In other hand, because of its relative youth, there are still some topics which require future researches, in order to make P.E.E.C. method more general, efficient and performing.
The topics identified during this thesis are:

- *Dielectrics*; The insertion of dielectrics cells in the method. This argument has already been treated in literature but some investigation must to been done in order to deepen this topic;
- *Planar P.E.E.C.*; In this thesis a "filament" and a volume P.E.E.C. code have been developed. It will be interesting to implement also a "planar" P.E.E.C. code which allows to study problems where the skin effect produces a current distribution mostly in the boundary of the objects. Furthermore, a general code which can consider filament, planar and volume cells could be very attractive;
- *External Electric Field*; In this thesis the inclusion of external electric field has not been considered but, in a more sophisticated code, this feature could be considered in order to have a more general instrument;
- *Coefficients*; It is necessary to investigate in more general approaches for the evaluation of the partial coefficients (mostly for the partial inductances). A general method should allow to compute "exactly" the partial coefficient for non-orthogonal cells while in this thesis an error is introduced when the volume elements are general hexahedra instead of parallelepipeds;
- *Sparsification*; The possibility to juxtapose a *sparsification* method (as the one based on the theory of $\mathcal{H}$-matrix) appears to be very useful in order to reduce the time and the computational cost required by the inversion of big and full systems deriving from the study of complex and electrically large electromagnetic devices with the P.E.E.C. method.

Regarding the study of fusion reactors magnets, such as the Toroidal Field Coils of JT-60SA, P.E.E.C. method has been initially chosen because, from the first informations about the harmonic frequencies of the voltage wave which appears across quench protection circuits operation (figure 4.26)), it seemed that the effect of propagation time had to be considered.
Then, during the thesis work, with the development of the information and the comprehension of the problem, this has been refuted and probably, also because of the presence of the dielectric material which requires to complicate the PEEC model, a code based on FEM-BEM (Finite Element Method & Boundary Element Method) could have been more suitable for this kind of devices.
On the other hand, the possibility to study modelled objects and lumped elements in the same system makes the PEEC method attractive for the study of the discharge of these particular inductors in quench protection circuits. So, future research concerning simplified PEEC method (as the one proposed in the discussion of subsection (4.4.1)) could make the method even more attractive and competitive also for different analyses for the fusion electromagnetic devices.
About that, some investigation will be presented in two contributions, [50], [51].

Appendix A

Code Scheme, Volume

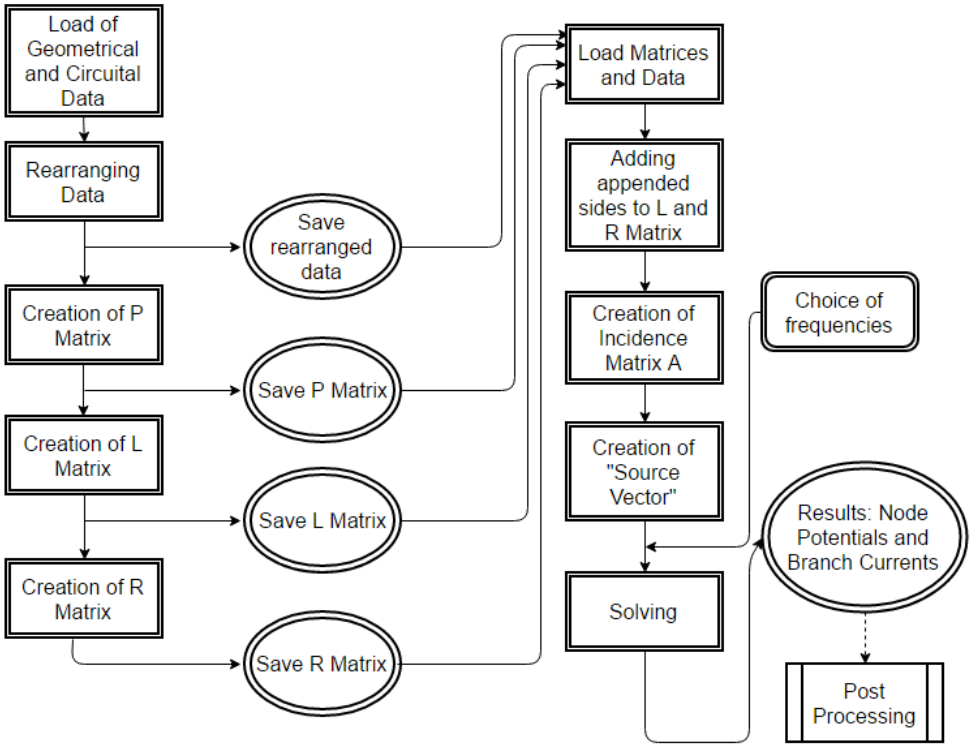

Figure A.1: *Matrices Creator and Solver for P.E.E.C. Volume Code.*

The geometrical data are given in terms of **G**, **C**, **D** matrices and the coordinates of points are collected in a $N_P \times 3$ matrix, where N_P is the number of points.
Matrix **G** is a $N_l \times N_P$ sparse matrix: for each row (each side) there is a -1 in the start node and 1 in the end node; N_l is the number of sides.
Matrix **C** is a $N_S \times N_l$ sparse matrix: for each surface (each row) there is a 1 or a -1 depending on the chosen direction of the related face-normal; N_S is the number of faces.
Matrix **D** is a $N_v \times N_s$ sparse matrix: for each row (each volume) there is a 1 for the faces having outgoing normal respect the volume and -1 for the faces having incoming normal into the volume; N_v is the number of volumes.
Circuital data refer to the appended sides: loads and voltage sources. Each appended side is determined by:

- the resistance value;
- the self inductance value;
- the ID of the "start" *nodal hexahedron* (0 if "infinity node");
- the ID of the "end" *nodal hexahedron* (0 if "infinity node");
- the ID of the face of the "start" *nodal hexahedron* which the appended element is connected (0 if we want to consider also this face like "free face")
- the ID of the face of the "end" *nodal hexahedron* which the appended element is connected (0 if we want to consider also this face like "free face")
- the value of the potential (only for the voltage sources)

Other data are the resistivity of the materials considered in the model and possible current sources that for the P.E.E.C. method are not considered as appended sides but only as current injected in the circuit nodes.
Geometrical data are rearranged in order to determine the geometrical points for each *nodal hexahedron* and *side hexahedron*.
Furthermore, for every *nodal hexahedron* the six IDs of the faces which compose the element are determined; each face is considered as "free" or "shared": the shared faces are neglecting from the evaluation of the partial coefficients of potential.
P matrix and **L** matrix are created by doing a double iteration on elements (*nodal hexahedra* for **P** matrix and *side hexahedra* for **L** matrix), **R** matrix is created by a single iteration on *side hexahedra*. Afterwards, the matrices are saved.
"Solver Code" first loads the matrices and the data, then it completes the **L** and **R** matrices by adding the appended sides (Loads and Voltage Sources), then Incidence Matrix **A** and the "Source Vector" are created.
During the "Solving phase" the system is created considering the frequency value; this phase is iterated for each value of frequency chosen.
Results in terms of Node Potentials and Branch Currents are obtained. Post-processing can be used in order to obtain the electromagnetic fields, equivalent impedance etc.

Appendix B

Inclusion of Dielectric Cells

In this appendix we want to show the results concerning the extension of the code to the dielectrics cells. This work has been done during the last part of the thesis, so this topic has been inserted only in this appendix, while in the rest of the thesis the dielectric cells have not been considered.

The analyses and validations have been done considering parallel-plate capacitor with square surfaces and this geometry has been also considered as example for this appendix.
The geometry considered is the following: the two parallel-square plates are $5 \times 5 \times 10^{-9}$ $[m]$ and the distance between the two plates is $10^{-5}[m]$. The thickness of the plates is negligible compared with the other geometry entities, in this way the 4 lateral surfaces of the two plates give a negligible capacitive effect respect the other two parallel surfaces 5×5 $[m]$.
The distance between the two surfaces is also very small in order to minimize the edge effects. With this geometry the well known equation for the capacitance (B.1) gives as result: $2.2135 \cdot 10^{-5}[F]$.

$$C = \varepsilon_0 \frac{S}{d} \tag{B.1}$$

where S is the area of the the parallel surface (25 $[m^2]$ for this case) and d is the distance between the two surfaces (10^{-5} $[m]$ for this case).

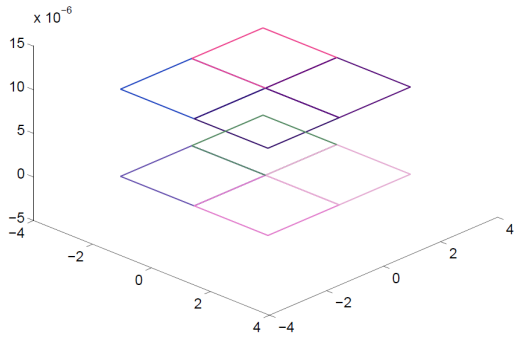

Figure B.1: *Parallel-plate Capacitor, PEEC-Volume-Code Model.*

Instead, PEEC Volume-Code gives as result $2.2137 \cdot 10^{-5}[F]$. The capacitance value has been obtained by applying two current sources to the two *nodal hexahedra* which form the two conducting plates, then the capacitance value has been extracted from the impedance evaluated as $Z = \frac{I}{\Delta V} = \frac{1}{j\omega C}$, where ΔV is the difference of potential between the two *nodal hexahedra* related to the two conducting plates.
The two external faces of the two plates have been removed from the "free faces" of the two plates, in order to consider the electric coupling of the only two "internal" parallel surfaces and allow the comparison with equation (B.1).

The evaluation has been done also by dividing the plate in 2×2 *nodal hexahedra* (as shown in figure (B.1)), each one supplied by a current source and the result has been the same.

Afterwards, the capacitance of the same parallel-plate capacitor has been evaluated considering the space between the two conducting plates filled by a dielectric material of relative permittivity equal to 5. For this analysis the geometry has been modelled as an array of *nodal hexahedra* where the first and the last one are related to the conducting plates and the others discretize the dielectric material.

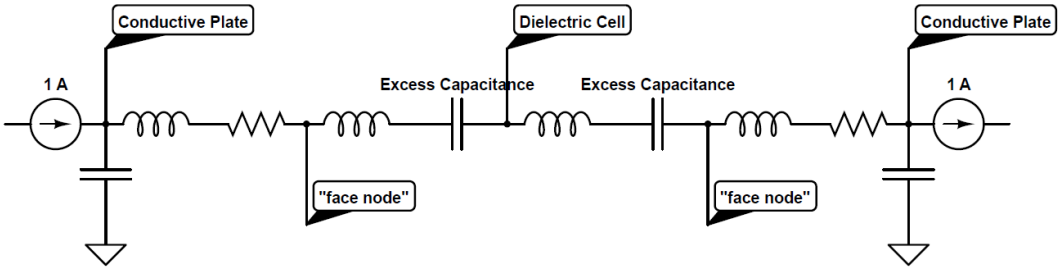

Figure B.2: *Parallel-plate Capacitor with dielectric, Electrical Equivalent Circuit.*

From the point of view of the electric equivalent circuit, we can refer to figure (B.2) which represents a model with a single nodal hexahedron for the dielectric material. For simplicity the generators concerning the electric and magnetic coupling between the partial elements have not been represented in the figure. As we can see from the electric circuit, the dielectric cells have not the pseudo capacitance just because the two faces which they share with the two plates have been considered belonging to the conducting plates. Then, in general, the entrances of the rows and the columns of the **P** matrix related to the dielectric cells are nulls.
The main difference respect the PEEC-Code without the dielectric cell is due to the fact that the faces shared by a dielectric and a conducting cell must be considered as "shared faces" and also "free faces" belonging to the conducting nodal cell.
For our purpose we have decided to model the "dielectric sides" with the partial inductances (self and mutual) and with the (self) partial excess-capacitance, but in general also a partial resistance in parallel with the excess-capacitance can be considered, in order to model "real" dielectric materials.
In general the partial inductance coefficients must be considered because also the displacement currents which flow in the dielectric cells produce the Magnetic Vector Potential $\vec{A}$, so also the magnetic coupling with these currents must be considered.

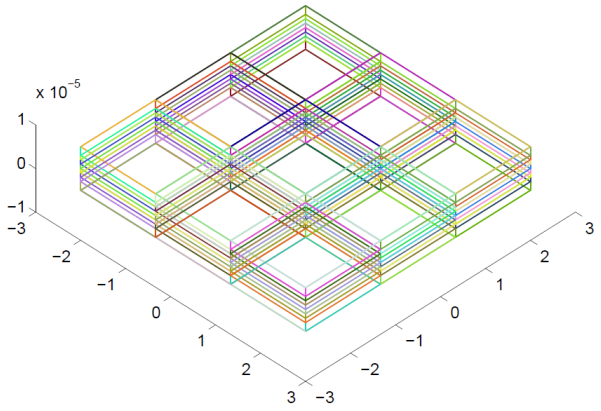

Figure B.3: *Parallel-plate Capacitor with Dielectric modelled by* $3 \times 3 \times 10$ *nodal hexahedra.*

For problems where the frequency is relatively low, the current flowing in the dielectric cells is very limited (so also the magnetic coupling with these cells is negligible), then for large electromagnetic

devices, which work at "low" frequency, the dielectric cells should be modelled neglecting the inductance coefficients. By doing this simplification it is possible to save time during the creation of $\mathbf{L}$ matrix and during the system inversion, because the system appears "more sparse".
The capacitance value extracted by the PEEC-Code extended to the dielectric cells gives as results: $1.1068 \cdot 10^{-4}[F]$, which is five times bigger than the capacitance of the capacitor in empty space.

The same analysis has be done also increasing the number of cells which discretize the dielectric materials and the results have been the same.
Furthermore, the geometry has been modelled as shown in figure (B.3) where the structures is discretized by $3 \times 3 \times 10$ *nodal hexahedra*. Once again the capacitance value has been the same.

The final validation has been done considering the series of two parallel-plate capacitors. Each capacitor has the same geometric entities of the one already described and the dielectric permittivity of the first dielectric material is 5 while the second one is 7.
Form the circuit theory we have that the equivalent capacitance of two capacitors connected in series is given by $C_{eq} = \frac{C_1 C_2}{C_1 + C_2}$.
For our problem C_1 and C_2 are given by: $C_1 = \varepsilon_{r_1} C$ and $C_2 = \varepsilon_{r_2} C$, while C is given by (B.1) and its value is $2.2135 \cdot 10^{-5}$.
So C_{eq} is equal to $C_{eq} = \frac{5 \cdot 7}{5+7} C = 6.4562 \cdot 10^{-5}$ $[F]$. The value of the equivalent capacitance extracted with the PEEC-Code has been: $C_{eq\ PEEC} = 6.4561 \cdot 10^{-5}$ $[F]$.

Bibliography

[1] A. E. Ruehli, *Equivalent Circuit Models for Three Dimensional Multiconductor System*, IEEE Transactions on Mircowave Theory and Techniques, MTT-22(3):216-221,MY 1966.

[2] A. E. Ruehli, *Survey of computer-aided electrical analysis of integrated circuit interconnections*, IBM Journal of Research and Development, 23(6):626-639, November 1979.

[3] H. Heeb, A. E. Ruehli, *Three-Dimensional Interconnected Analysis Using Partial Element Equivalent Circuits*, IEEE Transaction on Circuit and Systems, 38(11):974-981, November 1979.

[4] J. Ekman, *Electromagnetic Modeling Using the Partial Element Equivalent Circuit Method*, EISLAB, Dept. of Computer Science and Electrical Engineering Lulea University of Technology, Lulea, Sweden.

[5] J. Ekman, *Simplified PEEC Models for PCB Stuctures and Comparison to Experimental Data.*

[6] J. Ekman, *Experimental Verification of PEEC Based Electric Field Simulation.*

[7] J. Ekman, *Integral Order Selection Rules for a full wave PEEC Solver.*

[8] J. Ekman, *Nonorthogonal PEEC Formulation for Time- and Frequency- Domain EM and Circuit Modeling.*

[9] J. Ekman, *A comparative study of PEEC circuit elements computation.*

[10] J. Ekman, *3D PEEC Capacitance Calculation.*

[11] Clayton R. Paul, *INDUCTANCE, Loop and partial.*

[12] Edward B. Rosa, *THE SELF AND MUTUAL INDUCTANCES OF LINEAR CONDUCTORS.*

[13] A.Musing and J. W. Kolar, *Efficient Partial Element Calculation and the Extension to Cylindrical Elements for th PEEC Method*, Power Electronic System Laboratory, ETH Zurich.

[14] F. Barozzi, F. Gasparini, *FONDAMENTI DI ELETTOTECNICA, elettromagnetismo*, UTET.

[15] Clayton R. Paul, *COMPATIBILITÁ ELETTROMAGNETICA, Concetti fondamentali di elettromagnetismo, Applicazioni progettuali*, HOEPLI.

[16] Frederick W. Grover, *Inductance Calculations*, Dover Phoenix Editions.

[17] E. Durand, *ÉLCTROSTATIQUE, 2 PROBLÊMES GÉNÉRAUX CONDUCTEURS.*

[18] Laxmikant K. Urankar, *Vector potential and Magnetic Field of Current-Carrying Finite Arc Segment in Analytical Form, Part 1: Filament Approximation.*

[19] Massimo Fabbri, *Magnetic Flux Density and Vector Potential of Uniform Polyheadral Sources*, Department of Electrical Engineering, University of Bologna.

[20] Roberto D. Graglia, *On the Numerical Integration of the Linear Shape Functions Times the £-D Green's Functions or its Gradient on a Plane Triangle.*

[21] A. Musing, J. Ekman and J.W. Kolar, *Efficient Calculation of Non-Orthogonal Partial Elements for the PEEC Method.*

[22] Martin Ludwig Zitzmann, *Fast and Efficient Methods for Circuit-based Automotive EMC Simulation.*

[23] Clayton R. Paul, *ANALYSIS OF MULTICONDUCTOR TRANSMISSION LINE.*

[24] Yu. Ya. Iossel', E. S. Kochanov and M. G. Strunskiy, *THE CALCULATION OF ELECTRICAL CAPACITANCE.*

[25] Tufano Luigi, *Il metodo "Partial Element Equivalent Circuit" per la modellizzazione elettromagnetica di interconessioni e packaging elettronico*,University of Napoli "Federico 2_{nd}".

[26] A. E. Ruehli, *Inductance Calculation in a Complex in a Complex Integrated Circuit Environment.*

[27] J. Ekman, *MNA Circuit Equations for the PEEC Method using Coupled Current Sources.*

[28] Fabio Freschi, *Fast Block-Solution of PEEC Equations*, Department of Energy, Politecnico di Torino, Italy.

[29] G. Antonini, A. Orlandi, J. Ekman, *Full-Wave Time Domain PEEC FOrmulation Using a Modified Nodal Analysis Approach.*

[30] G. Antonini, A. Orlandi, A. E. Ruehli *Analytical Integration of Quasi-Static Potential Integrals on Nonorthogonal Complanar Quadrilaterals for the PEEC Method.*

[31] Antonio Paolucci, *LEZIONI DI TRASMISSIONE DELL'ENERGIA ELETTRICA*, cleup.

[32] E. Vialardi, G. Akoun *A PEEC-Based Methodology and hybrid code for analysis of 3D irregular interconnects.*

[33] Z. F. Song, F. Dai, D. L. Su, S. G. Xie, F. Duval *Reduced PEEC Modeling of wire-groung structures using a selective mesh approach.*

[34] Nenghong Xia and Y. Du, *Volume and Sourface Elements-Based PEEC for Magnetic Plate Shielding at Low Frequency.*

[35] Lorenzo Codecasa, Ruben Specogna, Francesco Trevisan, *A new set of basis functions for the discrete geometry approach.*

[36] A.Coletti, O. Baulaigue, P. Cara, R. Coletti, A. Ferro E. Gaio, M. Matsukawa, L. Novello, M. Santinelli, K. Shimada, F. Starace T. Terakado, K. Yamauchi, JT-60SA power supply system, Fusion Engineering and Design.

[37] V. Tomarchio, P. Barabaschi, A. Cucchiaro, P. Decool, A. Della Corte, A. Di Zenobio, D. Dugle, L.Meunier, L. Muzzi, M. Nannini, M. Peyrot, G. Phillips, A. Pizzuto, C. Portafaix, L. Reccia, K. Yoshida and L. Zani, *Design of the JT-60SA Superconducting Toroidal Field Magnet.*

[38] L. Novello, P. Cara, A. Coletti E. Gaio, A. Maistrello, M. Matsukawa, G. Phillips, V. Tomarchio and K. Yamauchi, *Analysis of Maximum Voltage Transient of JT-60SA Toroidal Field Coils in Case of Fast Discharge.*

[39] M. Nannini, C. Portafaix, P. Decool, N. Dolgetta, L. Zani and P. Barabaschi, *Mechanical Analysis of the JT-60SA TF Coils.*

[40] S. Pissanetzky, *Comments on analytical computation of magnetic vector potential from tetrahedral conductors*, IEEE Trans. Magn., vol 29, no. 2, pp. 1282-1283, Mar. 1993.

[41] Menno E. Verbeek, *Partial Element Equivalent Circuit (PEEC) models for on-chip passives and iterconnects.*

[42] E. Di Lorenzo, FastFieldSolvers, *The Maxwell Capacitance Matrix.*

[43] Roger F. Harrington, *Field Computation by Moment Methods.*

[44] Giulio Antonini, *The partial Element Equivalent Circuit Method for EMI, EMC and SI Analysis.*

[45] Jeffry Freidberg, *Plasma Physics and Fusion Energy*, Cambridge.

[46] P. Barabaschi, T. Bolzonella, G. Giruzzi, S. Ishida , Y. Kamada, K. Lackner, G. Matsunaga, T. Nakano, F. P. Orsitto, K. Shinohara, T. Suzuki, H. Urano, M. Yoshida, and the JT-60SA team: JT-60SA EU- Home Team, Fusion for Energy, Boltzmannstr 2, Garching 85748, Germany; Associazione EURATOM-ENEA, Consorzio RFX, corso Stati Uniti 4, 35127 Padova, Italy; CEA, IRFM, 13108 St Paul-Lez-Durance, France; JT-60SA Project Team, 801-1 Mukoyama, Naka, Ibaraki 311-0193, Japan; JT-60SA JA-Home Team, 801-1 Mukoyama, Naka, Ibaraki, 311-0193 Japan; Max-Plank Institut für Plasmaphysic, EURATOM Association, 85748 Garching, Germany; Associazione EUROTOM-ENEA, CR ENEA Frascati, C. P. 65, 00044 Frascati, Rome, Italy, *JT-60SA scientific programme toward ITER and DEMO*.

[47] JT-60SA Research Unit, JA Home Team: JAEA, JA Contributors, EU Home Team, EU Contributors, *JT-60SA Research Plan, Research Objectives and Strategy, Version 3.3* 2016 March, JT-60SA Research Unit.

[48] Mario Bebendorf, *Hierarchical Matrices, A Means to Efficiently Solve Elliptic Boudary value Problems*, Lecture Notes in Computational Science and Engineering, 2008.

[49] S. Börm, L. Grasedyck and W. Hackbusch, *Introduction to hierarchical matrices with applications*, Engineering Analysis with Boundary Elements, 27(5):405-422, 2003.

[50] Riccardo Torchio, Paolo Bettini, *PEEC-based analysis of complex fusion magnets during fast voltage transients with H-matrix compression*, CEFC 2016.

[51] Riccardo Torchio, Piergiorgio Alotto, Paolo Bettini, Federico Moro, *Analysis of complex fusion magnets with a PEEC-based approach*, IGTE 2016.

[52] Paul Baumgartner, Thomas Bauernfeind, Werner, Renhart, Oszkar Biro, Riccardo Torchio, *Limitations of the Pattern Multiplication Technique for Uniformly Spaced Linear Antenna Arrays*, CobCom 2016.

[53] Thomas Bauernfeind, Paul Baumgartner, Oszkár Bíró, Christian Magele, Kurt Preis, Riccardo Torchio, *PEEC-Based Multi-Objective Synthesis of Non-Uniformly Spaced Linear Antenna Arrays*, CEFC 2016.